FIELD SIMULATION OF WASTE IMPOUNDMENT SEEPAGE IN THE VADOSE ZONE: SITE CHARACTERIZATION AND ONE-DIMENSIONAL ANALYTICAL MODELING

by

Alva Marie Parsons

Submitted in Partial Fulfillment of
the Requirements for the Degree of
Master of Science in Hydrology

New Mexico Institute of Mining and Technology
Socorro, New Mexico

August, 1988

ABSTRACT

A field experiment west of New Mexico Tech campus was conducted to simulate seepage from a lined impoundment into a stratified soil in a semi-arid climate. Water was applied through a drip irrigation system at a flux rate of approximately $1x10^{-5}$ cm/sec over a 10m x 10m surface. The flux is about 100 times less than the mean saturated hydraulic conductivity of the soil profile. Moisture movement was monitored with neutron logging equipment and tensiometers in the 30m x 30m field site to depths up to 9 meters.

Extensive site characterization to determine the geologic and hydrologic properties of the field site was accomplished through destructive split spoon and soil core (100 cc) samples collected during monitoring equipment installation. The profile is stratified and heterogeneous, consisting of two major facies types. Red brown silty sand and pebbles of the piedmont slope facies derived from Socorro Peak directly to the west overlie well sorted, tan, fine to coarse sands of ancestral Rio Grande River origin. There are two major cobble horizons within the piedmont slope facies which have a strong control on moisture movement. Laboratory analyses were performed to find saturated/unsaturated hydraulic properties of the soil profile.

Field observations of the wetting front movement indicate that stratification tends to inhibit downward vertical moisture movement, enhancing lateral spreading effects. After 60 days of infiltration, the wetting front had progressed 6 meters vertically and 2 to 3 meters laterally away from the edge of the irrigation system.

The McWhorter and Nelson one-dimensional analytical solution (1979) was applied to wetting front movement directly below the irrigation system. The stratified soil profile was represented by one-, two-, and five-layered systems of homogeneous isotropic layers. The McWhorter and Nelson model was modified to account for stratification and used to predict the depth to the wetting front for the three conceptual models. The analytical model predicts the wetting front very well for about the first 20 days of infiltration compared to field results for one, two and five layers. At late time the McWhorter and Nelson model overpredicts the depth to the front by as much as 50%.

The analytical model results imply that one-dimensional flow dominates at early time during infiltration. After the wetting front has advanced through significant textural differences, vertical inhibition of the moisture movement occurs. At late time multi-dimensional flow components such as lateral spreading have more pronounced effect on moisture movement. It is not appropriate to use a one-dimensional flow model to predict observations in a multi-dimensional flow system.

TABLE OF CONTENTS

Table of Contents--Continued

Table of Contents--Continued

Table of Contents--Continued

LIST OF ILLUSTRATIONS

List of Illustrations---Continued

List of Illustrations---Continued

List of Illustrations---Continued

LIST OF TABLES

ACKNOWLEDGEMENTS

Much thanks is due to my advisor, Dan Stephens, who introduced me to the field of vadose zone hydrology. His guidance in the course of the last three years of research is appreciated. Also, thank you to the other faculty at New Mexico Tech who helped make my graduate studies a worthwhile experience.

This research has been funded by the U.S. Bureau of Mines Generic Waste and Recovery Center. It funded me as well as numerous undergrad student workers. Student workers have spent hours of drudgery doing site set-up, monitoring, lab work and data entry. Special thanks to Robert Mace for his "industrial music" in the lab, and Bob Friesen for excellent drafting work.

The cooperative working atmosphere at school is due to the support and friendship of fellow graduate students. Many hours were spent bouncing ideas off the heads of Warren Cox, Bob Knowlton, and others. The social imagination of Swen, Marcy, Bruce, Barb, Cindy, Gary, Greg and other hydro folks made the stay in Socorro enjoyable.

I have been lucky enough to have my parents' support in my educational endeavors, both financial and otherwise. How many times has Dad asked about the latest published paper? And finally, here's to my field partner, Earl Mattson, who decided if we could work on the same research project together for two years, we would always get along together.

1. INTRODUCTION

Mill tailings comprise a mixture of crushed host rock as well as fluids and chemicals used to extract ore. In the past, many tailings disposal impoundments were unlined and seepage of the original fluids entered aquifers. Abandoned tailings piles may generate leachate from infiltrated precipitation over long periods of time.

Current federal regulations require mill operators to demonstrate that there will be no seepage discharge from tailings impoundments which could impact water resources. This forces operators to use synthetic and clay liners or cap materials to inhibit seepage. Seepage which may escape either through unexpected leaks in the synthetic liner or through anticipated slow release from clay liners undoubtedly will be transported through porous material which is only partially saturated with liquid.

Predicting the pathway and travel time for seepage to move from an impoundment through unsaturated material toward the groundwater can be quite difficult. This is partially attributed to difficulties in properly characterizing hydraulic properties of unsaturated material (Larson and Stephens, 1985) and its inherent spatial variability (Yeh and Gelhar, 1983). It is also due to inherent weaknesses in some predictive transport models.

Often the models do not reproduce observed behavior, although they have a sound physical basis. For example, analytic fluid flow models applied to field results generally assume one-dimensional vertical flow (e.g. McWhorter and Nelson, 1979; Klute and Heerman, 1978). However, recent theories, laboratory and field evidence suggest that spatial heterogeneity in hydraulic properties causes infiltration over large areas to follow multi-dimensional pathways through the vadose zone.

Multi-dimensional flow often arises due to anisotropy. Theoretically, lateral spreading is enhanced where seepage occurs into dry material (Mualem, 1984), as shown in the laboratory by Stephens and Heerman (1988). Crosby and others (1968, 1971) concluded that pollutants from a septic tank drain field in glacial outwash deposits of the Spokane Valley, Washington, are dispersed laterally due to low soil moisture content and large capillary forces.

The importance of lateral flow components is amplified greatly by the presence of stratification which creates sharp contrasts in texture between adjacent strata. Stratification tends to inhibit the downward movement of seepage. Miller and Gardner (1962) conducted a vertical column infiltration laboratory experiment in layered soil. They showed that for a fine over coarse material, the wetting front was inhibited until enough water accumulated at the interface for the tension to be low enough to allow movement into the underlying coarser material. The degree of inhibition was increased when the pore

sizes in the lower layer were increased. Showing similar results, Palmquist and Johnson (1962) executed a laboratory tank experiment consisting of five layers of different diameter glass beads. Infiltrating water initially moved away from the source at nearly equal horizontal and vertical velocities. Upon reaching a coarser layer, downward movement stopped and lateral spreading occurred.

Similar results have been observed in the field. Miller (1963) described the importance of lateral flow components on moisture retention beneath irrigation test plots (approximately 3m x 3m) where the profile contains a fine over coarse textured layer. In Hanford, Washington, Routson and others (1979) investigated leakage from a radioactive storage tank into stratified glacial fluvial deposits, finding that seepage occurred to a greater extent in the horizontal than vertical direction. Johnson and others (1981) observed similar phenomena due to leachate migration from a landfill in silty sand to coarse sand and gravel in the Mississippi River Lowland of Illinois.

We are conducting a field experiment to simulate seepage into a stratified soil from a lined impoundment to demonstrate the importance of lateral movement of seepage and the capability of models to predict seepage in the vadose zone. Water is applied through a drip irrigation system at a constant flux which is approximately 100-fold less than the average saturated hydraulic conductivity of the soil profile. Water movement through the profile is monitored with tensiometers and neutron

logging equipment. Movement of a pulse of soluble bromide tracer is traced by porous cup samplers.

We will compare our field results with existing analytical one- and two-dimensional models and multi-dimensional saturated-unsaturated numerical models. A controlled field experiment of this type has not been performed to date (Stephens and others, 1984). Our results should be useful for calibrating or validating the predictive capabilities of numerous multi-dimensional flow and transport numerical codes under field conditions. The specific objectives of my study are to:

1) Characterize the geologic and hydraulic properties of the soil profile;
2) Compare the observed moisture movement in the field to hydrogeologic field controls; and
3) Compare one-dimensional analytic solution predictions for depth to the wetting front (McWhorter and Nelson, 1979) to field observations in a stratified soil profile.

A detailed description of the experiment design, equipment calibration, and a two-dimensional analytic model analysis (Warrick, 1974) is found in a companion report (Mattson, 1988).

The field experiment site is located west of the New Mexico Tech campus in Socorro, New Mexico, about 120 km south of Albuquerque (Figure 1) in a semi-arid environment. The area receives about 20 cm of precipitation per year and the gross annual lake precipitation is about 178 cm. The site is situated

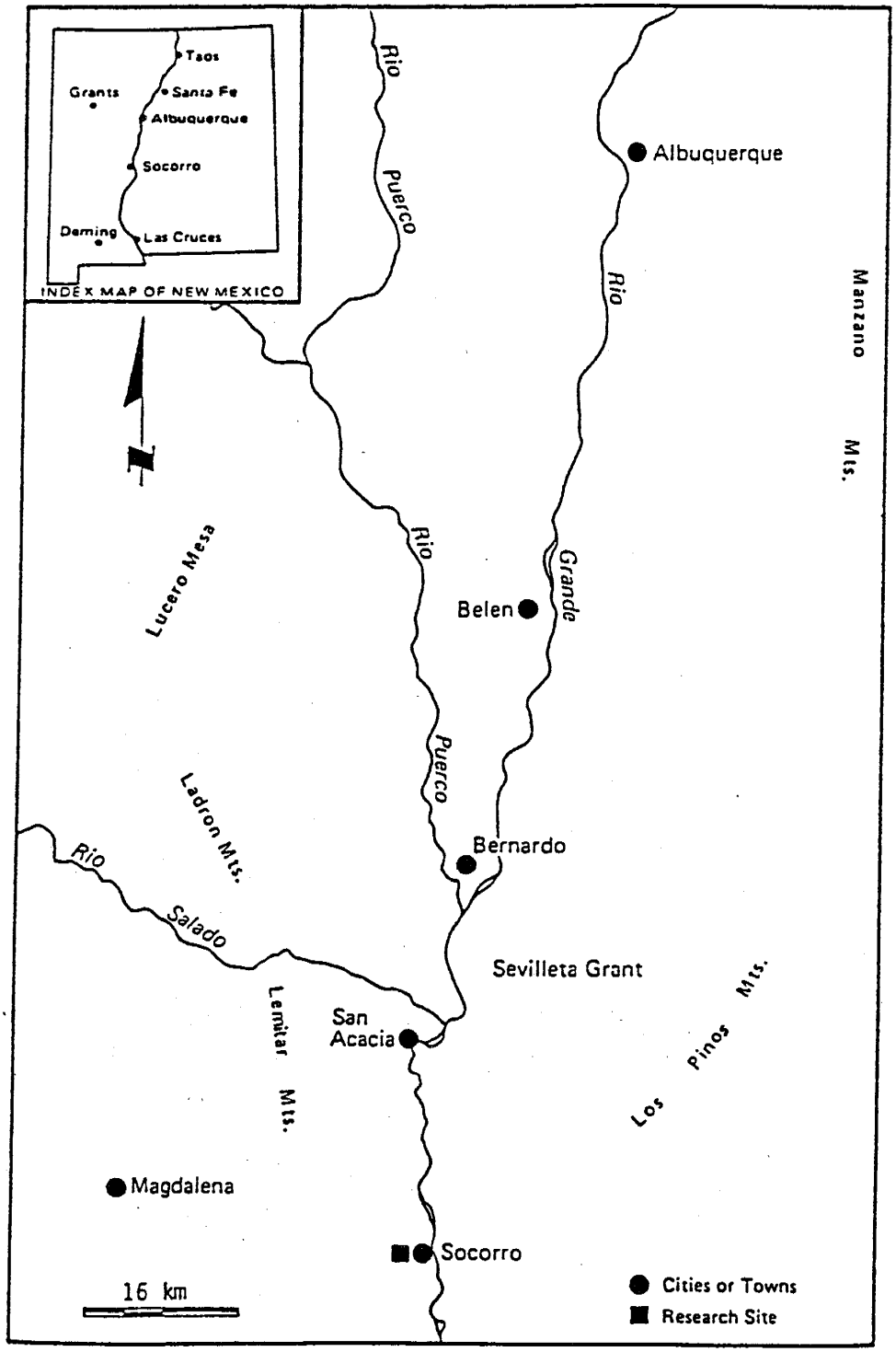

Figure 1. Index map.

in an east-west trending arroyo; T3S, R1W. Since 1963, this wash has been blocked off by a north-south trending flood control dike located just 40 meters west of our study area. Vegetation in the arroyo is very sparse, consisting of scattered sage and grasses. The New Mexico Tech golf course, directly to the east of the field site, is irrigated for most of the year. The field site itself has never been previously irrigated; and depth to water is about 24 meters.

2. METHODS OF ANALYSIS

The one-dimensional wetting front movement observed in the field for the first 60 days of infiltration is compared to the McWhorter and Nelson analytical model (1979) predictions for depth to the wetting front. McWhorter and Nelson's one-dimensional model is easy to use and requires minimal data collection. Such a simplified one-dimensional approach will help determine whether the conceptual models of the soil profile characteristics are adequate before more complicated analytical and numerical models are applied in two- and more dimensions.

This section presents the theory of vertical moisture movement in a stratified soil profile. The McWhorter and Nelson model is derived, previous comparisons of the model results to numerical simulations discussed, and modifications to the model which account for stratification are explained in the following section.

2.1. THEORY OF VERTICAL MOISTURE MOVEMENT IN STRATIFIED SOIL

Darcy's law for flow restricted to the vertical direction, Z, is:

$$q = -K(1 + d\psi/dZ) \qquad (1)$$

where q is the flux, K the hydraulic conductivity, and ψ the

pressure head. If the flux is less than the saturated hydraulic conductivity of the soil, unsaturated flow conditions exist.

Under unsaturated flow conditions, stratification of different textured soils has a strong effect on the downward vertical movement of moisture. For one reason, the moisture retention curve is dependent on the soil texture (Figure 2). The greater the clay content, in general, the greater the water content at any particular negative pressure. When the soil is sandy, the pores are larger and more uniform so that at a given pressure the large pores empty, leaving only a small amount of water (Hillel, 1980a). For another reason, under static conditions the negative pressure head at points above the water table is equal to the elevation:

$$Z = \psi/\rho_w g \qquad (2)$$

where Z is the elevation, ψ the pressure head, ρ_w the density of water and g the gravitational constant (Figure 3). Thus, for static water in the vadose zone, the negative pressure head is continuous and independent of the porous solid (McWhorter and Sunada, 1977). In a layered profile, the pressure head is continuous across textural boundaries, thereby forcing a discontinuity in moisture content (Bear, 1972) (Figure 4).

Two different textural combinations are possible in a two-layered soil profile. When a coarse layer of higher saturated hydraulic conductivity overlies a less conductive finer-textured layer, the wetting front advance is controlled by the upper layer until it reaches the textural boundary. After entering the fine

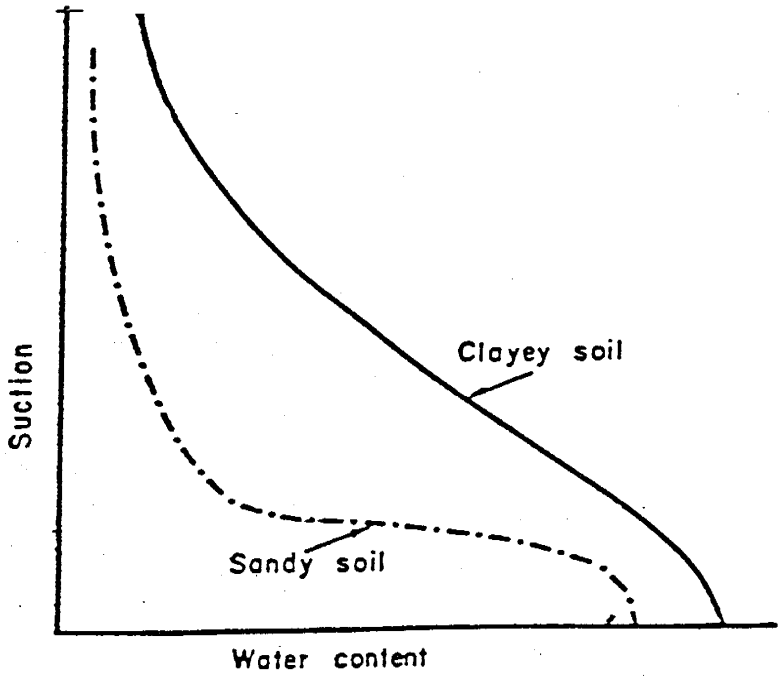

Figure 2. The effect of texture on the moisture retention relationship (from Hillel, 1980a).

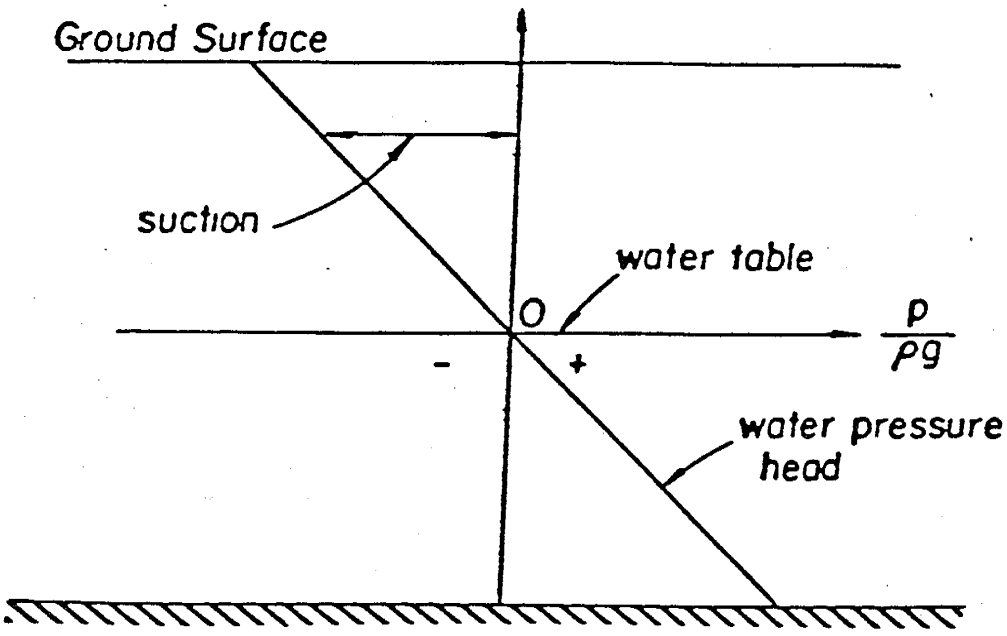

Figure 3. The distribution of pressure head in static subsurface water (from McWhorter and Sunada, 1977).

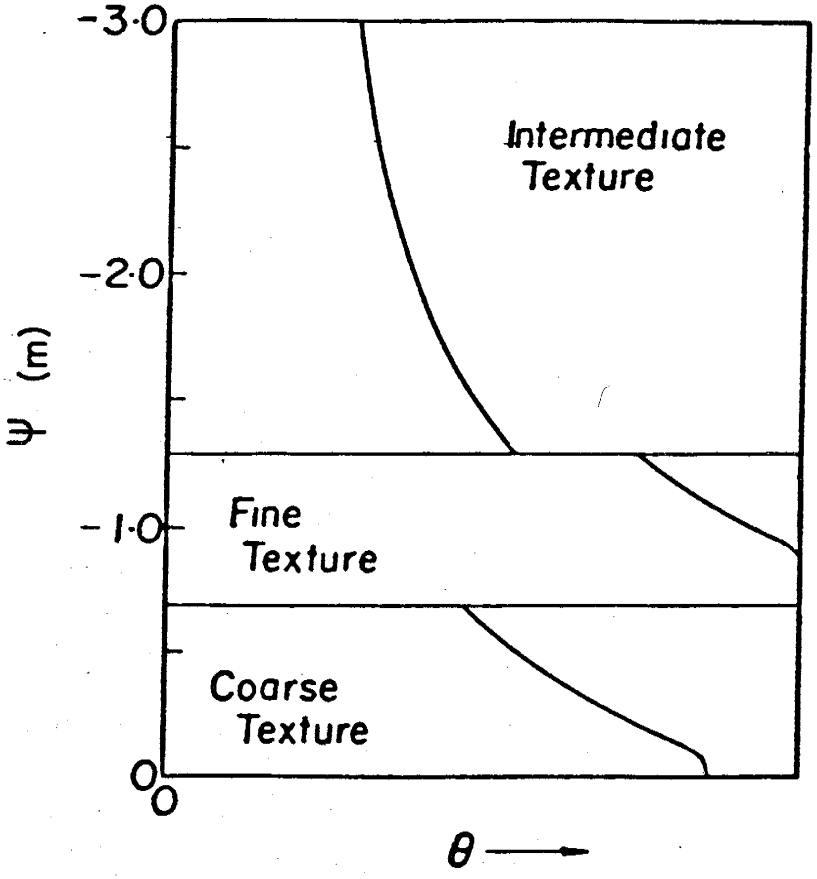

Figure 4. Moisture content distribution in a stratified soil (modified from McWhorter and Sunada, 1977).

layer, the rate of wetting front advance decreases to the conductivity of the underlying layer. Over a long time period, it is the layer of least conductivity which controls the process (Hillel, 1980b). For the opposite case of a fine layer over a coarse layer, at first the advance of the wetting front is controlled by the upper fine layer. However, as water reaches the interface above the coarse layer, the advance of the wetting front may be impeded as observed in laboratory experiments by Miller and Gardner (1962). The pressure head at the wetting front above the interface is too small to permit entry into the larger pores of the underlying coarse layer. The advance of the wetting front is impeded until the pressure head at the interface increases to the water-entry pressure head of the coarse material (Figure 5). Increased pressure may correspond with a possible increase in moisture content as illustrated by a laboratory experiment described by Aylor and Parlange (1973). The moisture may also move laterally above the coarse layer at this time as observed by Palmquist and Johnson (1962).

2.2. PREVIOUS WORK

The Green and Ampt equation (1911) was derived for one-dimensional infiltration under a ponded surface by treating the isotropic soil profile as a bundle of capillary tubes. In the Green and Ampt approach, there is a zone of constant hydraulic conductivity and moisture content within the wetted zone. The

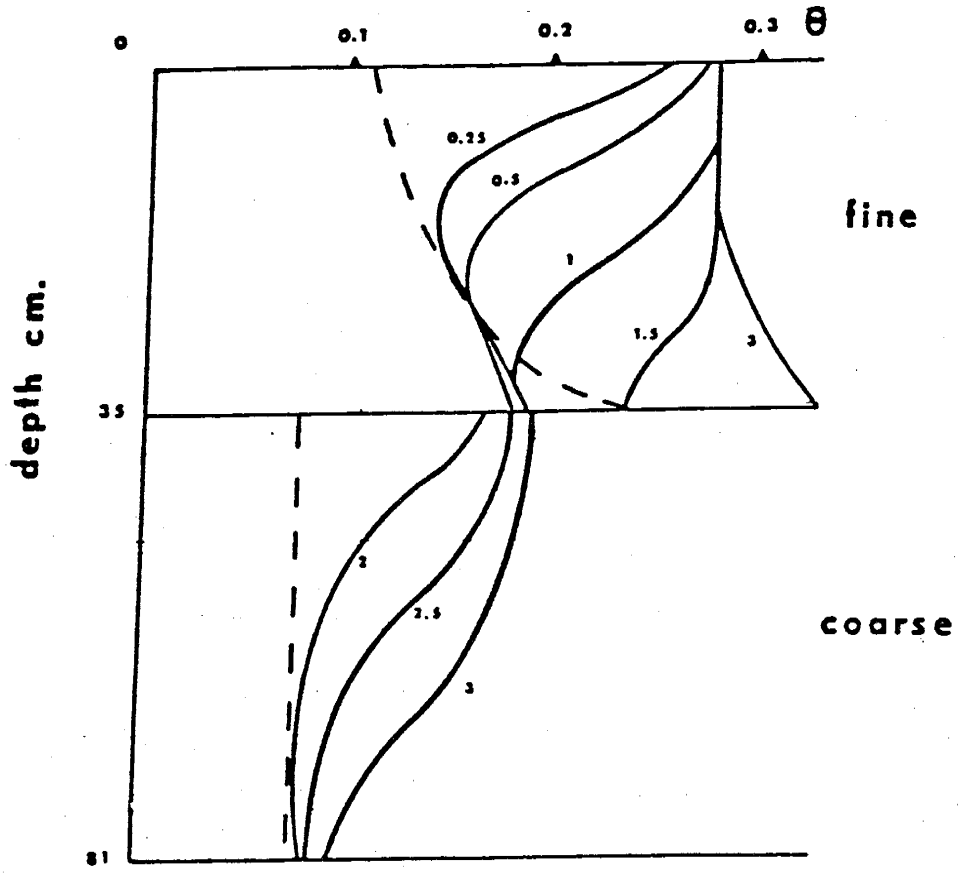

Figure 5. The numerical calculation for vertical infiltration into a stratified soil. Dashed lines show initial volumetric moisture content and solid lines show soil moisture profiles. The numbers correspond to time in hours (from Aylor and Parlange, 1973).

wetting front is viewed as a plane separating a uniformly wetted infiltrated zone from the unwetted zone.

Recently, several researchers have utilized Green and Ampt's model for application in stratified and nonuniform soils. An approximate Green and Ampt model was developed for a stratified soil with steady-state infiltration at the upper boundary and a water table located at the lower boundary (Zaslavsky, 1964; Bybordi, 1968; Childs and Bybordi, 1969). The water table at our field site is located at about 24 meters depth. Bybordi's (1968) datum elevation is the water table, with pressure head decreasing with distance up from the datum. Hence, it is not feasible to apply his model to our field experiment due to very large calculated pressure heads. Childs and Bybordi (1969) assume the lower layer has a lower conductivity, which is not true at our field site. Bouwer (1969) presented a tabular procedure to calculate the relationship between accumulated infiltration and time in soil with nonuniform hydraulic conductivity and water content. Bouwer's model assumes that either the hydraulic conductivity decreases with depth or the change in moisture content decreases with depth. Neither condition occurs in the soil profile at our site. Additionally, modifications in the Green and Ampt model have been made to accommodate transient conditions in the topsoil (Hillel and Gardner, 1970; Chu and others, 1986).

Several studies have been reported in which the Green and Ampt model is compared to measured data (Asseed and

Schwartzendruber, 1975; Idike and others, 1980; Moore and Eigel, 1981). The Green and Ampt model predicts infiltration rates fairly well, but generally fails to predict moisture content distributions in the profile, due to the simplifying assumption of piston-type flow inherent in the equation derivation (Moore and Eigel, 1981).

McWhorter and Nelson (1979) developed a one-dimensional predictive model to estimate the seepage rate from tailings impoundments into unsaturated material when the floor of the impoundment is several meters above the water table. Their model assumes a constant flux boundary condition occurs at the foot of the impoundment liner and allows saturated or unsaturated vertical seepage from the liner to occur. These conditions apply to conditions at our field site. The McWhorter and Nelson model is used to predict the depth to the wetting front beneath the center of our field site for the first 60 days of infiltration. The following section describes the model and its derivation.

2.2.1. McWhorter and Nelson Model

The McWhorter and Nelson model views seepage from beneath the impoundment as taking place in three different stages. The first stage describes the wetting front advance downward through partially saturated foundation material. The seepage occurs either as saturated or unsaturated flow. After the seepage reaches an impervious layer or the water table, a groundwater mound will develop and rise toward the impoundment during the second stage. Finally, the third stage occurs if the groundwater

mound establishes contact with the impoundment and saturated flow takes place.

Several assumptions are made which simplify the model computations. The strata are assumed to be uniform and isotropic. Capillarity is only accounted for by the existence of a negative pressure head below the liner corresponding to some moisture content which is less than the porosity of the impoundment liner. Only one-dimensional vertical flow is allowed, thereby eliminating lateral spreading of moisture which tends to occur in stratified profiles. The effects of lateral variation of aquifer hydraulic conductivity is neglected as well as the tendency for the hydraulic conductivity of earthen liners to change with time.

Seepage described by the first stage of the McWhorter and Nelson model occurs at our field site. Infiltration of seepage produces a wetting front which moves downward through time. The wetting front is the transition zone where the water content changes from an initial volumetric moisture content, θ_i, ahead of the front to a final moisture content, θ_f, behind the front (Figure 6). This conceptual model is based on the infiltration theory of Green and Ampt (1911).

Unsaturated vertical flow through porous media may be described by Richard's equation:

$$\text{div}[K \text{ grad}(\psi+z)] = \partial\theta/\partial t \qquad (3)$$

where div is the divergence operator, K the effective hydraulic conductivity, grad the gradient operator, ψ the pressure head,

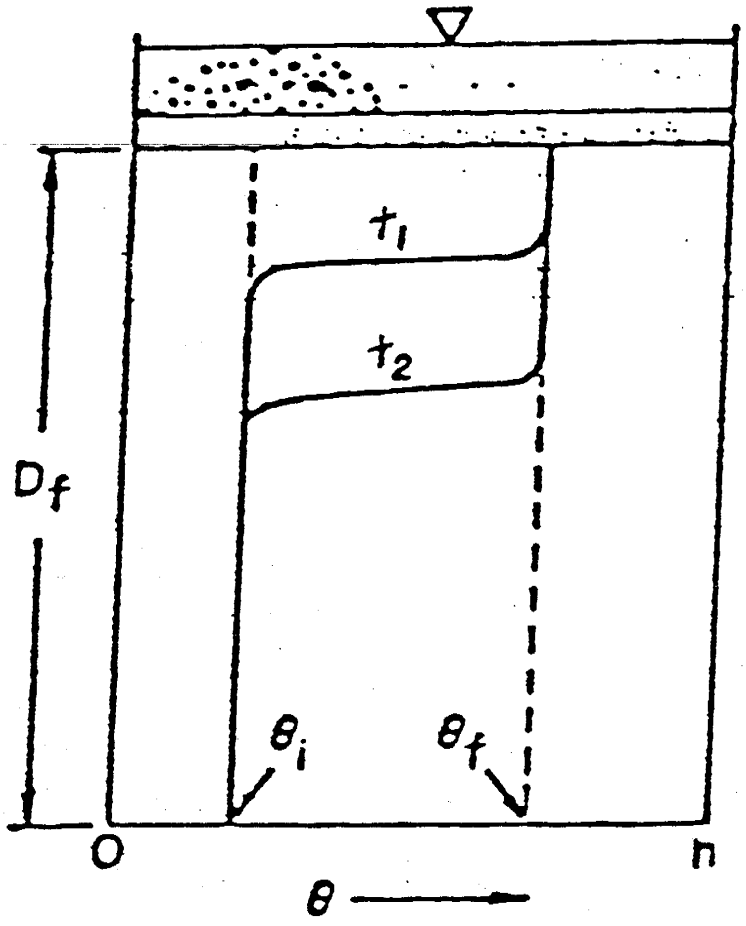

Figure 6. Schematic distribution of volumetric moisture content during the first stage of infiltration from an impoundment. θ_i is initial moisture content and θ_f is final moisture content (from McWhorter and Nelson, 1979).

and z the elevation head. During the first stage of seepage in McWhorter and Nelson's model, idealized one-dimensional infiltration occurs from a constant flux upper boundary, the liner. Parlange (1972) developed an approximate solution to Richard's equation (3) for a constant flux boundary. His solution for the time variation of the volumetric water content at the top of the foundation material is:

$$t = \int [K(d\psi/d\theta)/q(q - K)]d\theta \qquad (4)$$

where

$$K = K_s[(\theta-\theta_r)/(n-\theta_r)]^{\{(2+3\lambda)/\lambda\}} \qquad (5)$$

where K_s is the saturated hydraulic conductivity of the foundation material, θ_r is the residual moisture content, n is the porosity, and λ is the pore size distribution index (Brooks and Corey, 1966). Assuming (q - K) approaches zero, a unit hydraulic gradient occurs where pressure gradients are zero and gravity is the sole driving force. At large time when $K(\theta_f)$ is equal to the flux, q, then from equation 5 the final moisture content can be predicted by:

$$\theta_f = (n - \theta_r)(q/K_s)^{\lambda/(2+3\lambda)} + \theta_r \qquad (6)$$

Once the final moisture content immediately beneath the impoundment liner is predicted, the depth to the wetting front at a particular time is calculated by a mass balance equation:

$$z_{wf} = q*t/(\theta_f-\theta_i) \qquad (7)$$

where parameters have been previously defined. It then follows that the rate of change in wetting front position is:

$$dz_{wf}/dt = q/(\theta_f-\theta_i) \qquad (8)$$

The pore size distribution index, λ, describes the capillary properties and is related to the slope of the $\log\theta$-$\log\psi$ curve. It is determined by the method of Brooks and Corey (1964). Measured laboratory values for λ range from greater than zero to 7.8 (Brooks and Corey, 1966). λ is large for a material having a narrow range of pore sizes and small in materials with a wide pore size distribution.

2.2.2. Analytical and Numerical Model Comparison

Siegel and Stephens (1980) evaluated the reliability of the McWhorter and Nelson approach by comparing it to the results of a numerical solution which was not subject to the same limitations as the analytical solution. Axisymmetric numerical simulations were run to calculate seepage from a 20 meter diameter pond lined by a material having one hundredth the saturated hydraulic conductivity of the underlying foundation material. Siegel and Stephens found that for isotropic conditions, the McWhorter and Nelson analytical model predictions for the depth to the wetting front are nearly identical to results obtained using the numerical model (Table 1). However when the McWhorter and Nelson model was applied under anisotropic conditions, the analytical model underestimated the depth to the wetting front by as much as 80% compared to numerical simulation results. The numerical code is considered to produce the "true" wetting front location because it allows lateral spreading to occur in the unsaturated zone, and evapotranspiration to take place adjacent to the pond.

The results reported by Siegel and Stephens have important

Soil	Wetting front location below the liner at the pond center, meters.			
	Analytical	Numerical		
	(One-D)	Isotropic	Anisotropy=8	Anisotropy=20
GE3 silt loam	9.39	9.19	6.91	5.18
Sandstone	11.66	11.33	8.60	6.38

Table 1. McWhorter and Nelson analytic model predictions compared to numerical results for the wetting front location below the center of the pond after one year (from Siegel and Stephens, 1980).

implications for our study. The McWhorter and Nelson model is accurate under isotropic conditions, based on good agreement with numerical simulations. However, they observed poor performance of the analytical model under anisotropic conditions. The stratified profile at our field site may be considered to possess effective anisotropic properties.

2.3. MCWHORTER AND NELSON MODEL MODIFICATIONS

For the purpose of simplicity, McWhorter and Nelson assume that seepage occurs into uniform isotropic media. Yet the soil profile at our field site is stratified. As previously discussed, stratification affects the vertical movement of seepage.

In order to account for changes in hydrologic properties inherent in a stratified profile, the McWhorter and Nelson model was modified to account for different homogeneous isotropic layers. A computer program MNM.FOR (Appendix M2) was written which solves for the final moisture content immediately beneath the impoundment liner (equation 6) and then calculates the depth to the wetting front (equation 7). The code will accommodate the hydrologic properties of an unlimited number of layers. The prescribed flux rate can be changed according to the given flux rate which occurred at that time.

For example, in a two layer system, the program calculates the final moisture content in the first layer (equation 6). Next,

the depth to the wetting front is solved at time, t, (equation 7) using hydrologic properties of the first layer. Depth to the wetting front is successively calculated for increased values of time. When the front enters the second layer at time, t, a different final moisture content is calculated by using hydrologic properties of the second layer (equation 6). It is assumed that the initial moisture content in front of the wetting front and the final moisture content behind the front instantaneously changes to that of the second layer. The t^{th} calculation for the depth to the wetting front is then recalculated using the final moisture content of the second layer in equation 7. Calculations continue for depth to the wetting front in the second layer until the wetting front reaches a prescribed maximum depth.

3. GEOLOGY

The experimental field site is located in the eastern-most part of the Basin and Range Province, within the Rio Grande Depression which extends from central Colorado south to El Paso, Texas (Figure 7). In central New Mexico, the Rio Grande River flows through a series of north-south trending structural basins which are underlain by Tertiary rocks and bordered in most places by highlands of older rocks.

The field site is underlain by alluvial sediments of the Santa Fe Group. This section describes the geology of the Santa Fe Group, emphasizing the Sierra Ladrones Formation, the upper subdivision within the Santa Fe Group in central New Mexico. A geologic history of the Socorro Peak area is presented. Subsurface geologic features of the field site and outcrops with similar characteristics are described.

3.1 BACKGROUND

Based on a reconnaissance study, Hayden (1869) referred to poorly consolidated basin fill sediments north of Santa Fe, New Mexico as the Santa Fe "marls" (see Bryan, 1938). During the early 1900's, the main body of sedimentary deposits of the Rio Grande depression, from the north end of the San Luis Valley to

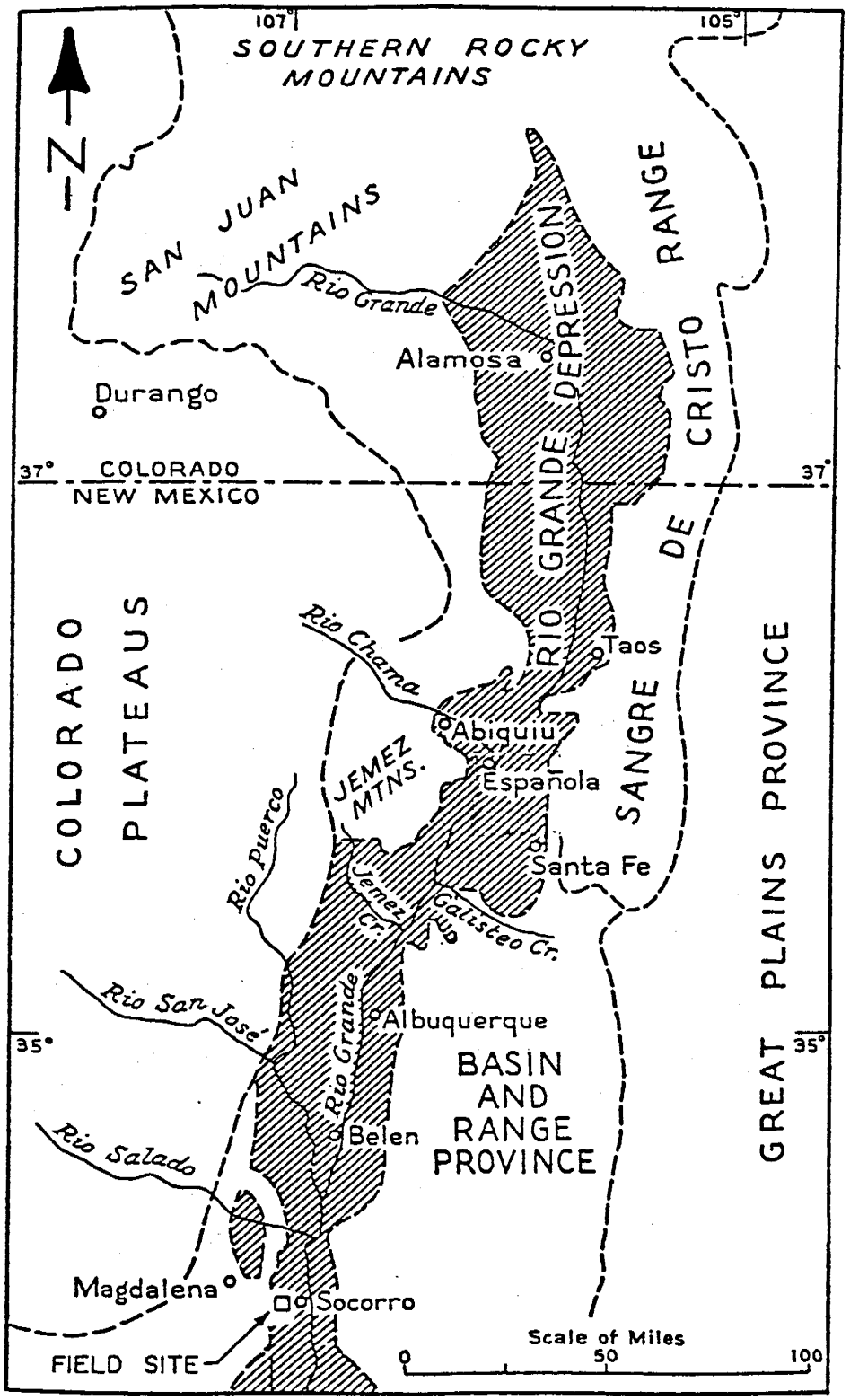

Figure 7. Northern Rio Grande Depression (from Denny, 1940).

and beyond El Paso, were considered to be the same general age, and belong to the Santa Fe Formation (Bryan, 1938). Later, Baldwin (1963) proposed that the Santa Fe Formation should carry group status. Today, most geologists agree that the Santa Fe deposits are a group and should include essentially all basin filling materials related to the Rio Grande rift ranging in age from Miocene to middle Pleistocene (Baldwin, 1963; Hawley and others, 1969; Machette, 1978; Chamberlain, 1980). Its broad usage is an advantage in areas where the basin fill is not or cannot be subdivided (Baldwin, 1963).

Machette (1978) mapped the San Acacia Quadrangle, about 20 km north of the experimental field site, and subsequently redefined the Santa Fe Group in central New Mexico. He suggested dividing the Santa Fe deposits into an upper and lower unit; the Sierra Ladrones Formation and Popotosa Formation respectively. Machette reported the upper Santa Fe unit, ". . . of early Pliocene to middle Pleistocene age is here named for the Sierra Ladrones (low foothills of the Ladron Mountains) and consists of alluvial fan, piedmont slope, alluvial flat, flood plain, and axial stream deposits, and locally derived basalt flows," (Machette, 1978). These units had previously been called the Santa Fe Formation in San Acacia (Denny, 1940). The Popotosa Formation had not been included in the Santa Fe Group before this time and represents the lower Santa Fe deposit in central New Mexico. The Popotosa Formation consists of several intertongueing facies of bolson

deposits including fanglomerates, gysiferous playa beds, and piedmont slope deposits (Machette, 1978).

The Sierra Ladrones Formation, found in its type locality in San Acacia, can be correlated with the upper buff member and part of the middle red member of the Santa Fe Formation of Bryan and McCann (1937) near Albuquerque (see Baldwin, 1956), and in the Rio Puerco area (Wright, 1946). The formation is broadly equivalent to the Camp Rice Formation in southern New Mexico (Hawley and others, 1969). The axial stream deposits, also known as ancestral deposits of the Rio Grande, are the main characteristic to distinguish the valley-fill sequence of the Sierra Ladrones Formation from the underlying Popotosa closed basin deposits. Debrine and others (1963) mapped ancestral sand deposits across the Rio Grande River, east of Socorro. They found a grey, well-sorted sand and gravel unit composed of materials derived from sources to the north. The bed of ancestral river deposits was dated as upper Pliocene by a fossil mastodon jaw found by Needham in 1936 (Debrine and others, 1963). Ancestral Rio Grande sands form a continuous stratum in the subsurface of the Rio Grande Valley between the type locality in San Acacia and Socorro (Chamberlain, 1980). The sands crop out fairly continuously along the course of the present Rio Grande River from as far north as Santa Fe to south of El Paso, Texas. (Bachman and Mehnert, 1978).

Chamberlain (1980) divides the Sierra Ladrones Formation into three sedimentary facies in the Socorro Peak area just west

of Socorro. They are a mud and silt facies (Tslo) and a fluvial sand facies (Tslf) of the ancestral Rio Grande River, and a piedmont slope facies (Tslp) derived from adjacent mountain ranges (Figure 8). In the Socorro Peak area, the Sierra Ladrones Formation lies in angular unconformity over the upper Popotosa Formation. The Sierra Ladrones Formation grades upward from alluvial flat mud and silts into lower axial stream sand deposits. The sands interfinger with the upper overlapping piedmont slope reddish brown sandstones and fanglomerates (Machette, 1978). The top of the formation is placed at the base of thin veneers of gravelly alluvium which rest on piedmont surfaces cut across strata of Popotosa and Sierra Ladrones Formation. Thickness and extent of the Sierra Ladrones deposits are predominantly controlled by varying amounts of erosion across tilted fault blocks. The thickest Sierra Ladrones exposure crops out in Nogal Canyon where 350 meters of strata can be observed. The exact thickness in the Socorro Basin east of Socorro Peak is unknown, but it may be significantly greater than 350 meters (Chamberlain, 1980).

Much of the eastern slopes of Socorro Peak are covered by a thin mantle of surficial deposits of Quaternary age consisting of alluvial fan and piedmont slope deposits, resting unconformably on broad pediment surfaces, landslide deposits, colluvium, and young alluvium in arroyo floors, valley bottoms, and low drainages.

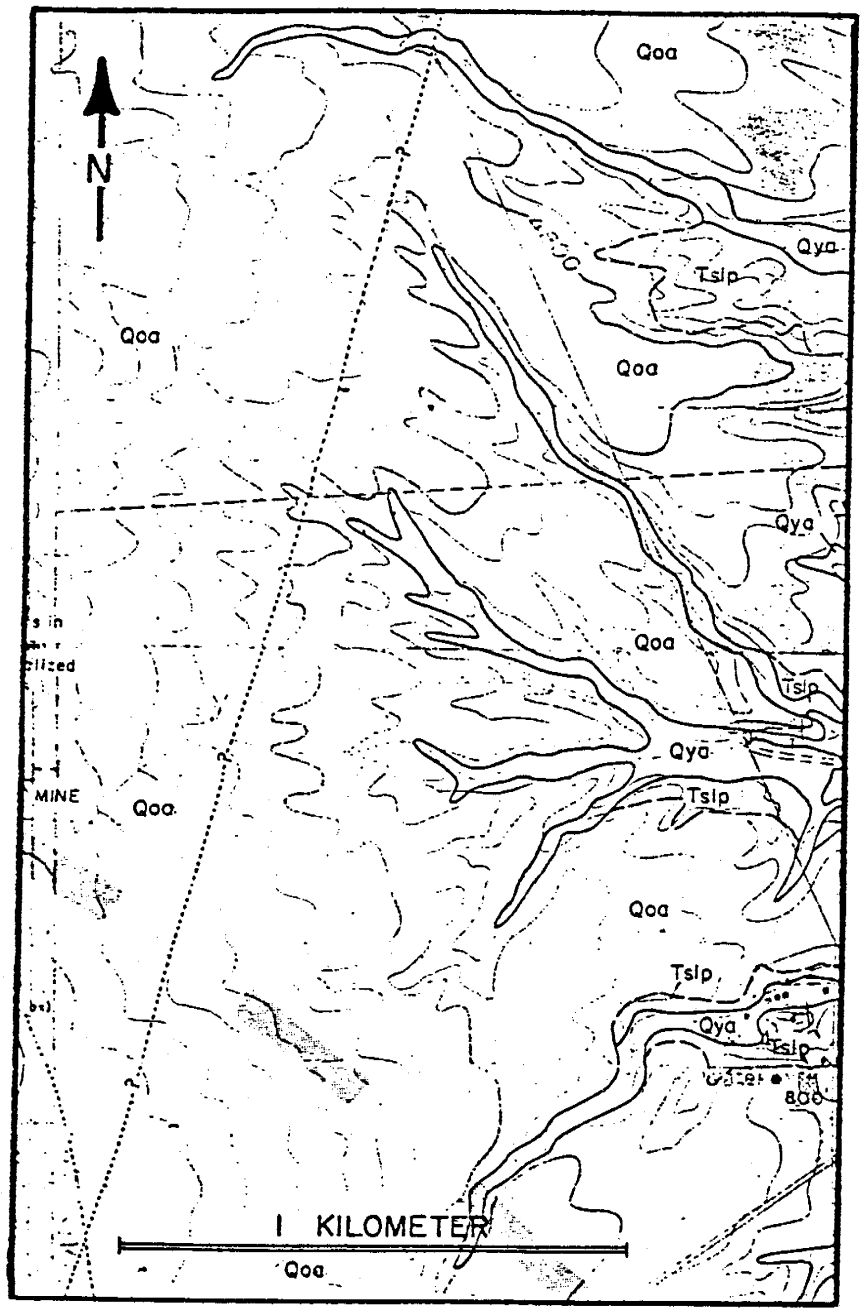

APPROXIMATE FI
SITE LOCATION

Figure 8. Geology mapped by Chamberlain (1980) west of the field site. Qoa = terraces and piedmont surfaces, Qya = entrenched arroyos, Tslp = piedmont slope facies.

3.2 HISTORY

Following the Mesozoic Period, Laramide events formed highlands to the west and northeast of the Socorro area. A period of highland erosion and deposition in a broad sedimentary basin occurred during the Eocene (53.5 - 37.5 m.y.a.), followed by mid-Tertiary volcanic activity (DeBrine and others, 1963). From 26 to 7 m.y.a., (Miocene time), a large basin extended from the Gallinas Range on the west to the Laramide highlands east of the Rio Grande, and from the northern Ladron Mountains to the Magdalena and Chupadera Mountains in the south (Figure 9).

Several thousand feet of alluvial fan, piedmont slope, fluvial and playa deposits known as Popotosa Formation accumulated within the basin. The lowest portions of the basin persisted in a north trending area along the present Chupadera, Socorro, and Lemitar mountains where 244-762 meters of uniform gypsiferous clays were deposited in a playa environment. Rhyolytic magmas rose and extended over the thick clay deposits from 12 to 7 m.y.a. Chemical and petrographic data suggest that a very large geothermal system existed at this time (Chapin and others, 1978).

Sometime after 7 m.y. and before 4 m.y. ago, the Popotosa basin had been disrupted by extensional forces breaking it into fault block uplifts and grabens (Chapin and others, 1978). A combination of rifting and contemporaneous epirogenic uplifting of the southern Rocky Mountains and adjacent areas can explain

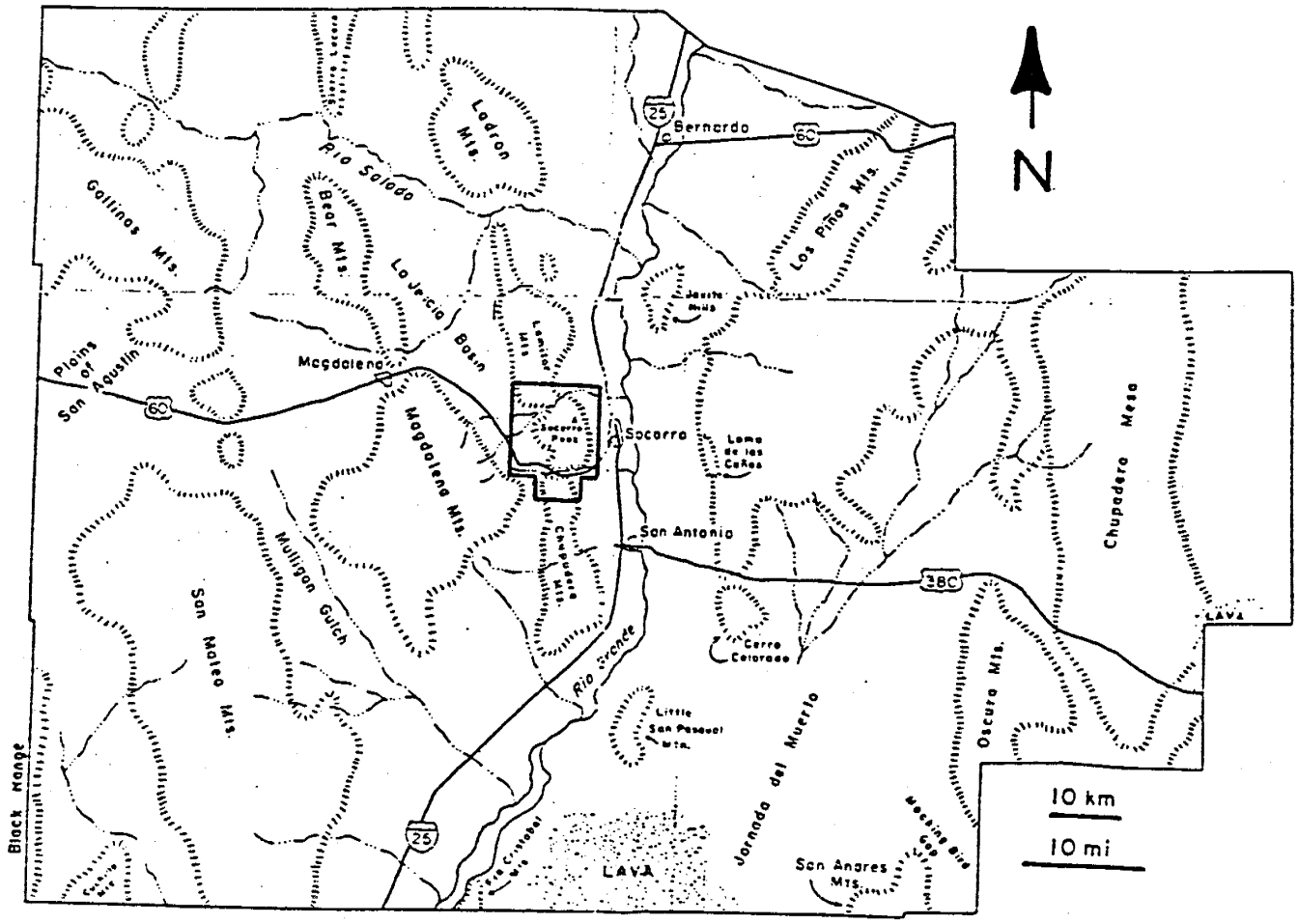

Figure 9. Index map of Socorro County. Chamberlain's (1980) study area is outlined in the Socorro Peak vicinity.

the development of modern mountain ranges in the Socorro area at this time (Chamberlain, 1980). Extensive pediment surfaces were carved across uplifted and tilted Popotosa beds and older rocks. Most of the alluvial fans were depositing material into the Socorro basin on the east, forming part of the lower Sierra Ladrones Formation. Concurrently, the regional drainage system integrated the Rio Grande River into the Socorro basin. The river flowed along the eastern edge of the basin from San Acacia to San Antonio (DeBrine, 1963). Broad, gently sloping pediment plains graded into the tan well-sorted, arkosic sands and muddy overbank facies of the ancestral river (Figure 10). As regional uplifting occurred, an eastward prograding wedge of piedmont slope gravels shed by the developing western mountain front caused the ancestral Rio Grande to retreat to the east, burying the older fluvial sands in the Socorro basin.

Early Sierra Ladrones facies do not indicate the presence of significant relief where the modern Lemitar, Socorro, and Chupadera mountains now exist; however, the coarsening upward sequence of mud, silt, sands, and gravels of this formation indicate an increase in topographical relief since late Miocene or early Pliocene time (approximately 4-7 m.y.a). Younger Sierra Ladrones piedmont slope gravels can be directly related to modern topography (Chamberlain, 1980).

The Rio Grande system was internally drained until the capture of the ancestral Rio Grande at El Paso in middle Pleistocene time (300,000-500,000 y.a.) (Kottlowski, 1958). This

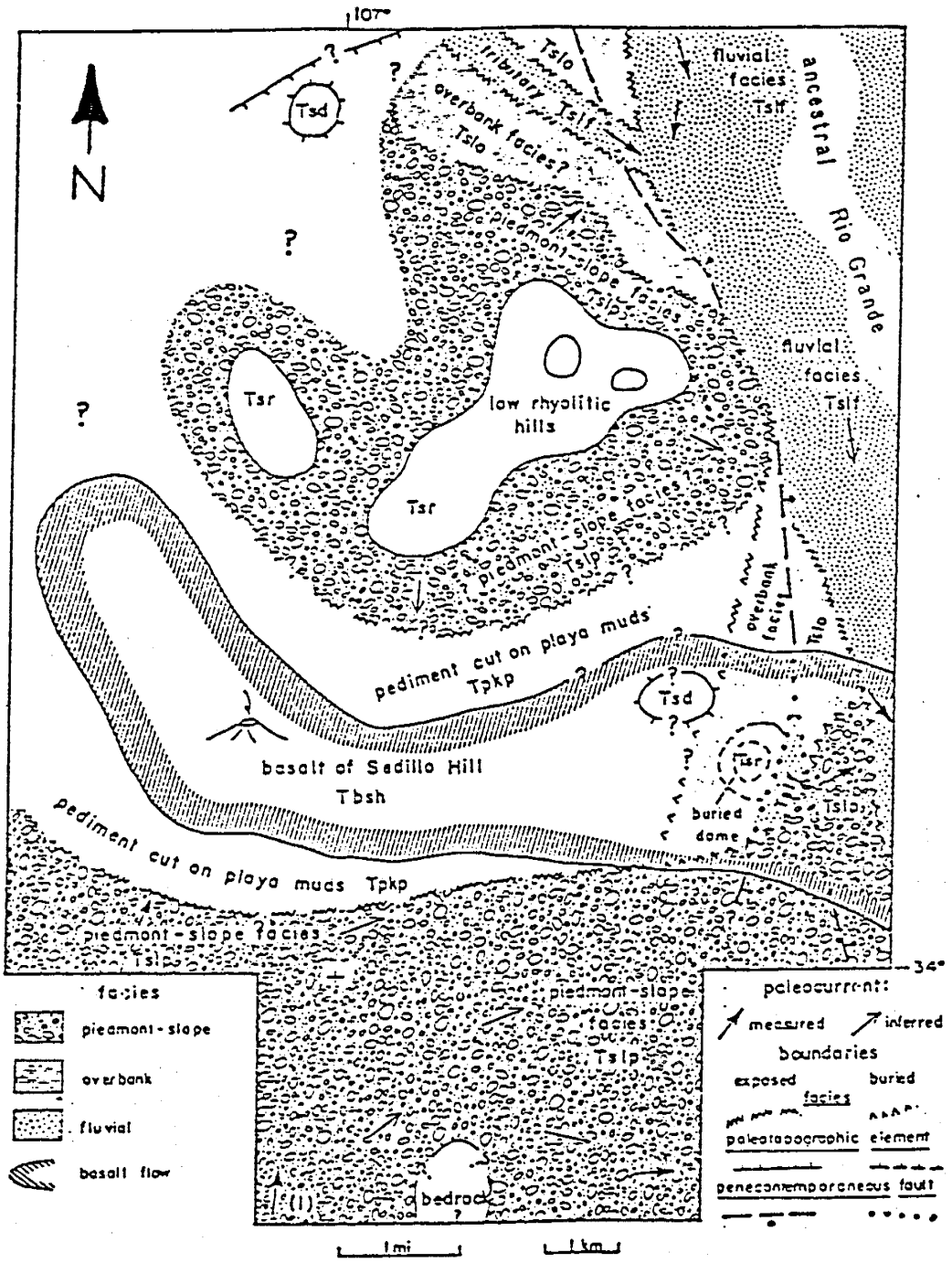

Figure 10. Paleogeologic map of the Socorro Peak area in middle Pliocene time summarizing relationships of the lower Sierra Ladrones Formation (from Chamberlain, 1980). Chamberlain's study area location indicated previously (Figure 9).

event lowered the river's baselevel throughout its course, creating deep entrenchment into earlier deposits. The highest outcrops of the ancestral Rio Grande surfaces in the Socorro area are about 180 meters above the present floodplain, due to entrenchment and localized effects of rifting (Chapin and others, 1978).

Quaternary cycles of erosion and deposition correspond with the stage of recent glaciations (Chamberlain, 1980). These events are evident in the stepped landscape of broad piedmont surfaces (Qoa), terraces (Qoa), and entrenched arroyos (Qya) in the Socorro area (Figure 8).

3.3. SUBSURFACE FEATURES

Two distinct facies of the Sierra Ladrones Formation are found beneath the 30m x 30m field site. The soil profile is stratified, consisting of an upper zone of red brown silty sands and pebbles interbedded with cobbles, and a lower zone of clean, tan fine sand and fine to coarse sands and pebbles. Clay lenses of undetermined extent are present throughout both zones. The underlying tan sands represent Chamberlain's (1980) ancient Rio Grande fluvial sand facies (Tslf), while the red brown silty sands and pebbles are piedmont slope facies (Tslp) derived from the Socorro Range to the west (Figure 10).

As pointed out by Chamberlain (1980), the alluvial fan piedmont slope gravels in the Socorro Basin are thought to have

prograded eastward as Socorro Peak grew, thus burying the ancestral Rio Grande sands and forcing the channel eastward. Accordingly, there may be a transition zone between the two facies types present three to four and a half meters below the field site, between two cobble horizons. In the west part of our site, poorly sorted, red brown sand, silt and pebbles interfinger with well sorted, tan, fine sands and silty clays to the east. This deposition sequence suggests that cobbles were washed from western highlands. Subsequently the ancestral Rio Grande River encroached into the field site one last time, leaving fine sand and silty clay deposits before the piedmont slope deposits forced the river to the east.

3.4. FIELD MAPPING

Several outcrops exhibiting similar characteristics to the field site profile can be found in arroyos south and west of the study area (Figure 11). Additionally, a trench was excavated west of the field site.

3.4.1. Trench

In December, 1985, New Mexico Tech Physical Plant crews excavated a trench for burying garbage. Their trench, about 3.5 meters wide and 0.5 to 2.0 meters deep, extended along the western border of the study area. Directly after excavation, several vertical sections were described.

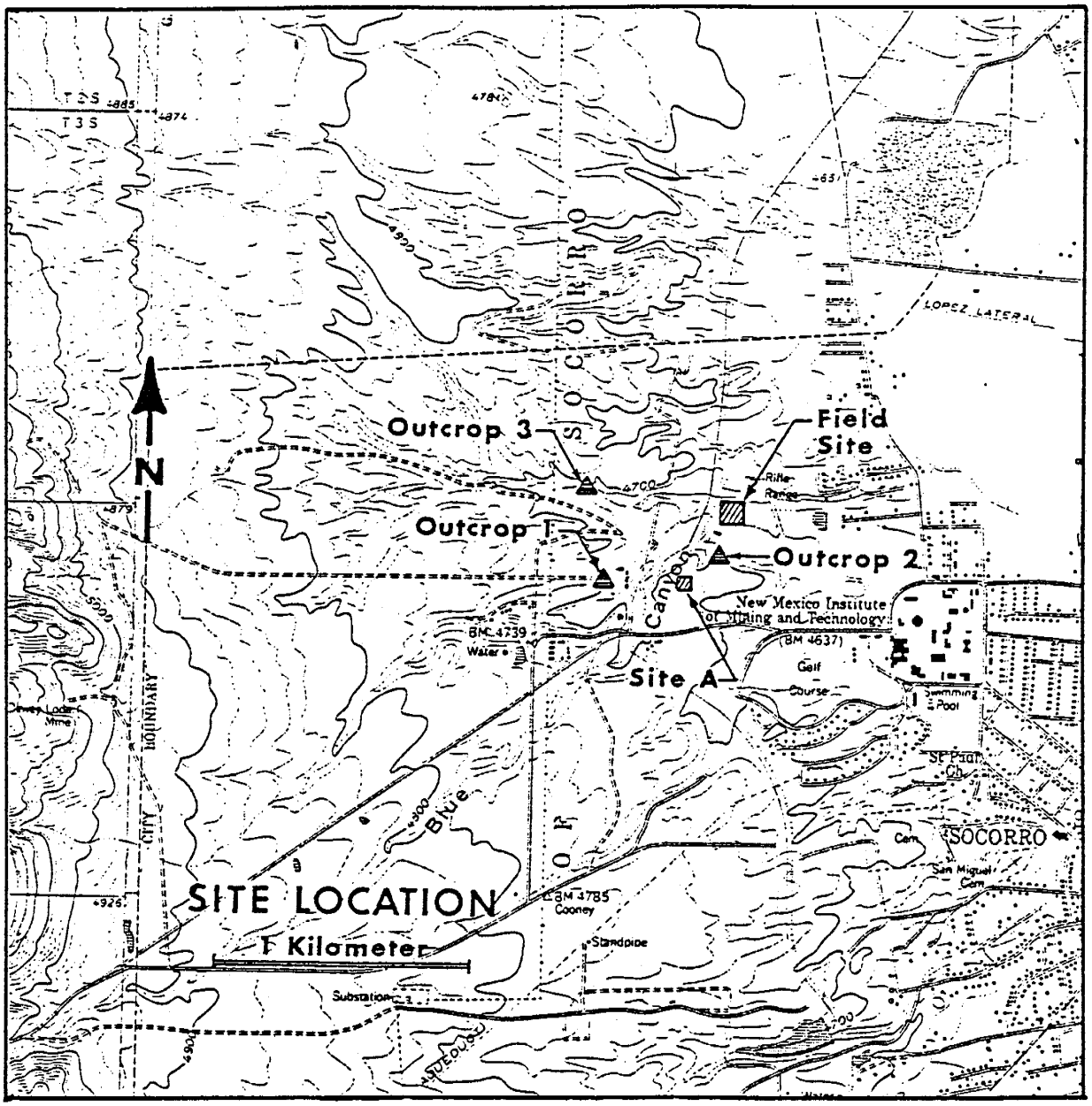

Figure 11. Site location map.

Some of the small scale features within the piedmont slope facies observed on the trench wall are mapped on four vertical sections located five meters apart (Figure 12). They show some of the small scale features within the upper meter of the soil profile. Two major soil textures are present; fine to coarse sands and pebbles overlying fine sand, silt, and clay. The upper unit is about a meter thick, and layers within this horizon range from 10 to 40 cm thick. Several fining upward sequences consisting of gravel to fine sand and silt were observed to range in thickness from 2 to 20 cm. Most of the lenses and small scale layering features do not correlate laterally over distances exceeding five meters, although the major zones do. It is assumed that some of the same characteristics are also present in the deeper piedmont slope facies.

3.4.2. Outcrop 1

Outcrop 1, located 550 meters southwest of the field site, shows continuous fine and coarse layering from 30 to 80 cm thick in the piedmont slope facies. Major divisions in texture are laterally continuous for meters across the outcrops. Within each dominant horizon, there are finer layers similar to those described in the trench excavated near the field site. Similar characteristics are observed at Outcrop 3 (Figure 13) to the north of Outcrop 1 (Figure 11).

Large scale bedding thicknesses within the fluvial facies are not exposed. Small scale sedimentary structures observed in

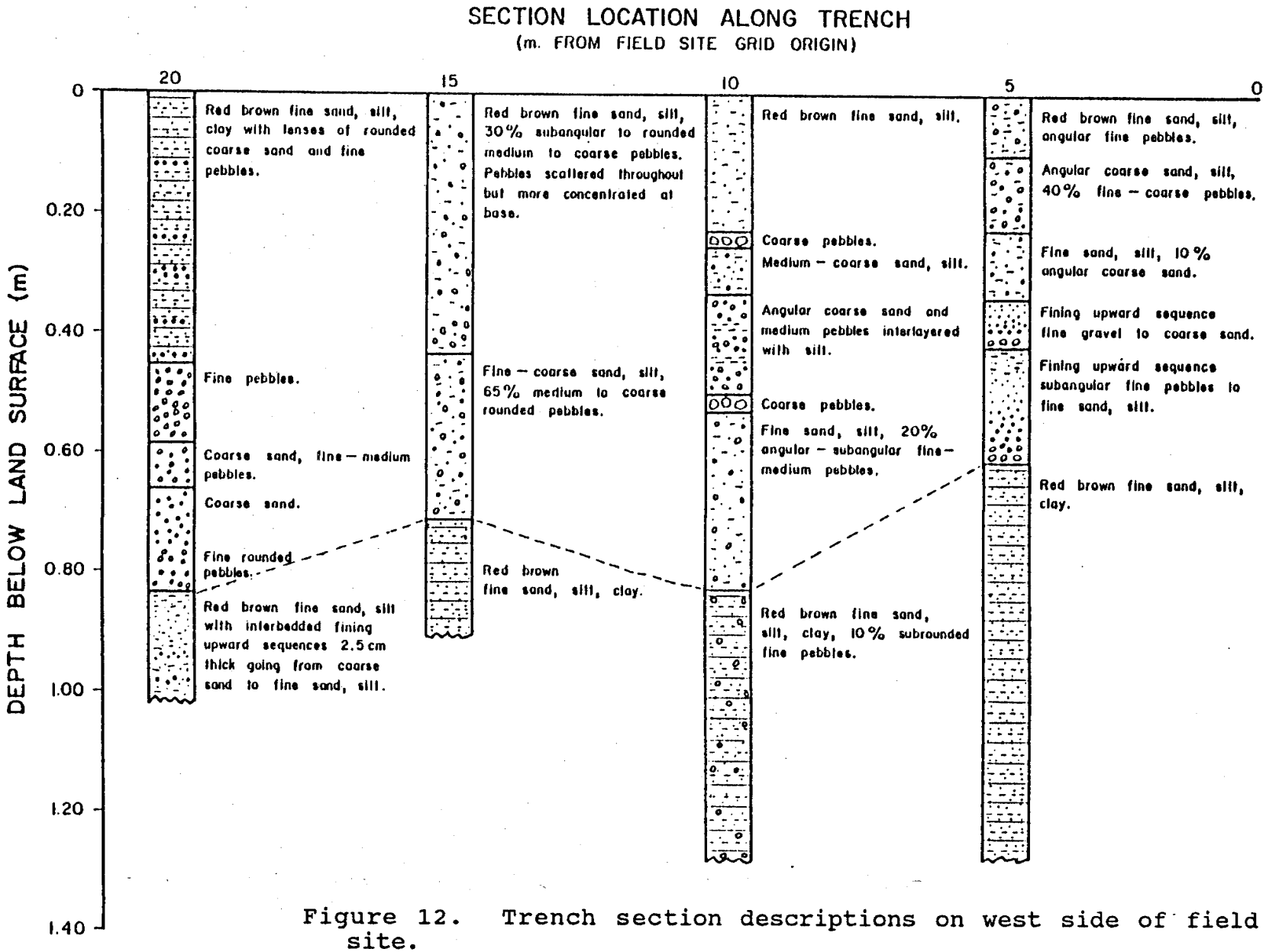

Figure 12. Trench section descriptions on west side of field site.

Figure 13. Lateral continuity of strata in the piedmont slope facies at Outcrop 3 located west of the field site.

this facies include channels up to 2.0 meters wide and 0.5 meters deep, and cross-bedding millimeters to centimeters thick.

Outcrop 1 exposes the interface between the upper piedmont slope material and lower fluvial sands. The contact is sharp and conformable, but varies by several meters in elevation due to channels and other irregularities (Figure 14).

3.4.3. Outcrop 2

Outcrop 2 (Figure 11), located 193 meters south of the field site in the same arroyo has a very distinct cobble/boulder horizon. Outcrop 2 is in the piedmont slope facies and has a dense horizon 1.5 to 2.5 meters thick composed of rounded cobbles and boulders ranging from 2 to 50 cm diameter. The cobbles and boulders are surrounded by a matrix consisting of red brown, fine to coarse sand, silt, and fine pebbles. This cobble/boulder horizon is composed of about 30% boulders, 40% cobbles, and 30% matrix.

3.4.4. Piedmont Slope Facies and Fluvial Sand Facies Contact

The contact between the piedmont slope facies and fluvial sand facies is conformable (Chamberlain, 1980) and sharply defined (Figure 14). Outcrop 1 is the only example of the piedmont slope and fluvial sand facies contact observed near the field site.

The elevation of the contact between the piedmont slope facies and fluvial sands is determined for three localities: the field site, Site A, and Outcrop 1. At the field site the average piedmont slope and fluvial sand contact is about 1412.0 MASL (5.4 meters below datum), based on surveying results and depth to

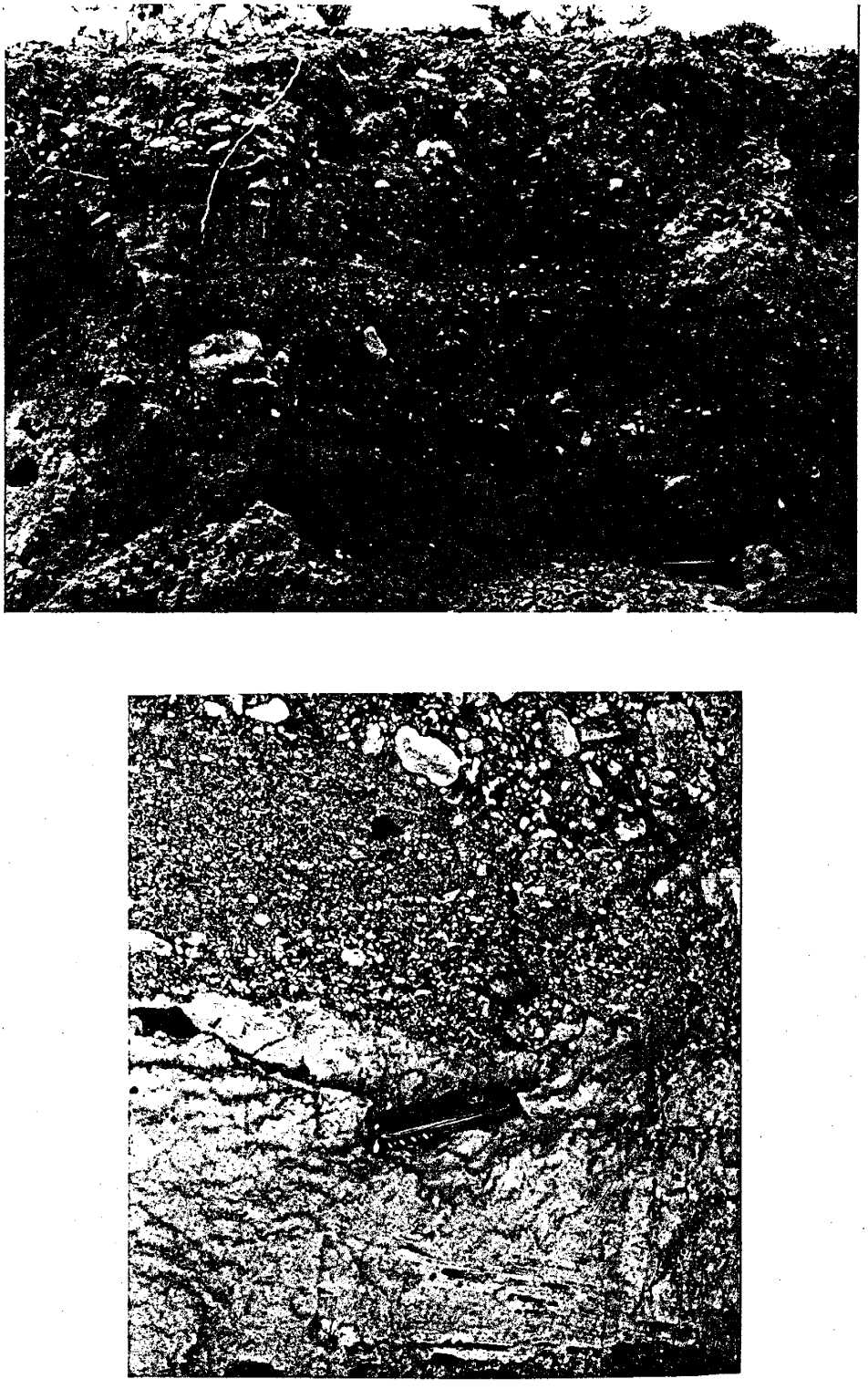

Figure 14. Contact between the piedmont slope facies and fluvial sand facies at Outcrop 1 located southwest of the field site.

cobble zones determined while drilling. The contact is assumed to be directly below the lower cobble zone, disregarding the possible transitional zone discussed in Section 3.3. In 1984, a test borehole was drilled as a preliminary step in preparing the proposal for this field study. The borehole location, referred to as Site A, is found about 250 meters southwest of the field site (Figure 11). The location where the borehole drilling took place has been bulldozed and leveled. Consequently, an exact borehole location was not determined. The approximate elevation of the top of the Site A borehole was estimated using surveying equipment. According to the drill log, tan fluvial sands were encountered at 15.5 meters depth below the ground surface (Betson, 1984), or 1412.5 MASL. The contact elevation between the piedmont slope facies and fluvial sand facies exposed at Outcrop 1 was estimated to be 1412.5 MASL by horizontal siting with a brunton compass from Site A to Outcrop 1.

The slope of the surface between the two facies can be determined using the three-point approach applied in structural geology (Ragan, 1973). Calculated from the three different contact locations and elevations, the average attitude of the contact between the piedmont slope facies and fluvial sand facies in the area near the field site is strike N32E, dip 4.5 SE.

Locally the contact between the piedmont slope facies and fluvial sands is irregular. Prior to the piedmont slope facies deposition, arroyos were created in the ancestral fluvial sands during epirogenic uplift (Chamberlain, pers. comm., 1985).

Within the 30m x 30m area at the field site, the contact appears to dip slightly to the northeast (Figures 17,18). At Outcrop 1 the contact elevation varies by 1 to 3 meters due to the irregular fluvial sand surface. Also, the contact observed at Outcrop 1 is not exposed at an outcrop of similar elevation about 80 meters north of Outcrop 1 despite apparent horizontal continuity of bedding planes and no indication of faulting.

Based on a general correlation of the two facies to nearby outcrops, experiment results at the field site could realistically be extrapolated to nearby locations with similar textured material. A direct correlation of the piedmont slope facies and fluvial sand facies contact from one location to another is not easy because the two facies are known to interfinger (Chamberlain, pers. comm., 1985). Regardless to the irregularity of the piedmont slope and fluvial sand facies contact over large distances, the bedding structure of the piedmont slope facies is visually similar at Outcrops 1, 2, and 3. A comparable observation in the fluvial sand facies is not possible.

3.4.5. Cobble Zone Correlation

The elevation of a cobble and boulder zone exposed in Outcrop 2 was estimated to be 1430 MASL using a 7.5 minute series topographic map (scale 1:24000). Outcrop 2 is located directly southwest of the field site, along the same strike as the piedmont slope facies and fluvial sand facies contact at the field site.

A possibility exists for the cobble zone located at Outcrop 2 to be directly correlated with the lower cobble zone at the

field site. For a direct correlation between the cobble zones at both localities, it is necessary for the zones to be at equal elevations assuming deposition on a uniform surface. Both cobble zones at the field site are about 17 meters below the cobbles and boulders noted in Outcrop 2. It may be that the cobble zones at the two localities are directly correlated but deposited at different elevations. Regardless to a direct correlation, it is highly likely that the cobble zones beneath the field site have similar properties to the cobble zone observed in Outcrop 2.

4. HYDROGEOLOGIC SITE CHARACTERIZATION

Hydrogeologic site characterization includes determining the geologic and hydraulic properties of the soil profile. The following section provides details on sample collection, geology and correlations to nearby outcrops, laboratory analyses to determine hydraulic properties, soil profile characterization based on laboratory results, and methods to apply hydrogeologic data in analytic models.

4.1 SAMPLING PROCEDURES

Due to the stoney nature of the soil, when installing monitoring equipment in the field area a Mobil B-52 auger drill rig was used to drill 20.3 cm (8") boreholes. Split spoon samples and soil core samples (100 cc) were collected from neutron access tube and tensiometer boreholes, and brought to the laboratory for analysis. The neutron access tube and tensiometer boreholes are found at each monitoring station. The monitoring station locations are based on a plan view X-Y coordinate system with the origin located at the southwest corner of the field site (Figure 15).

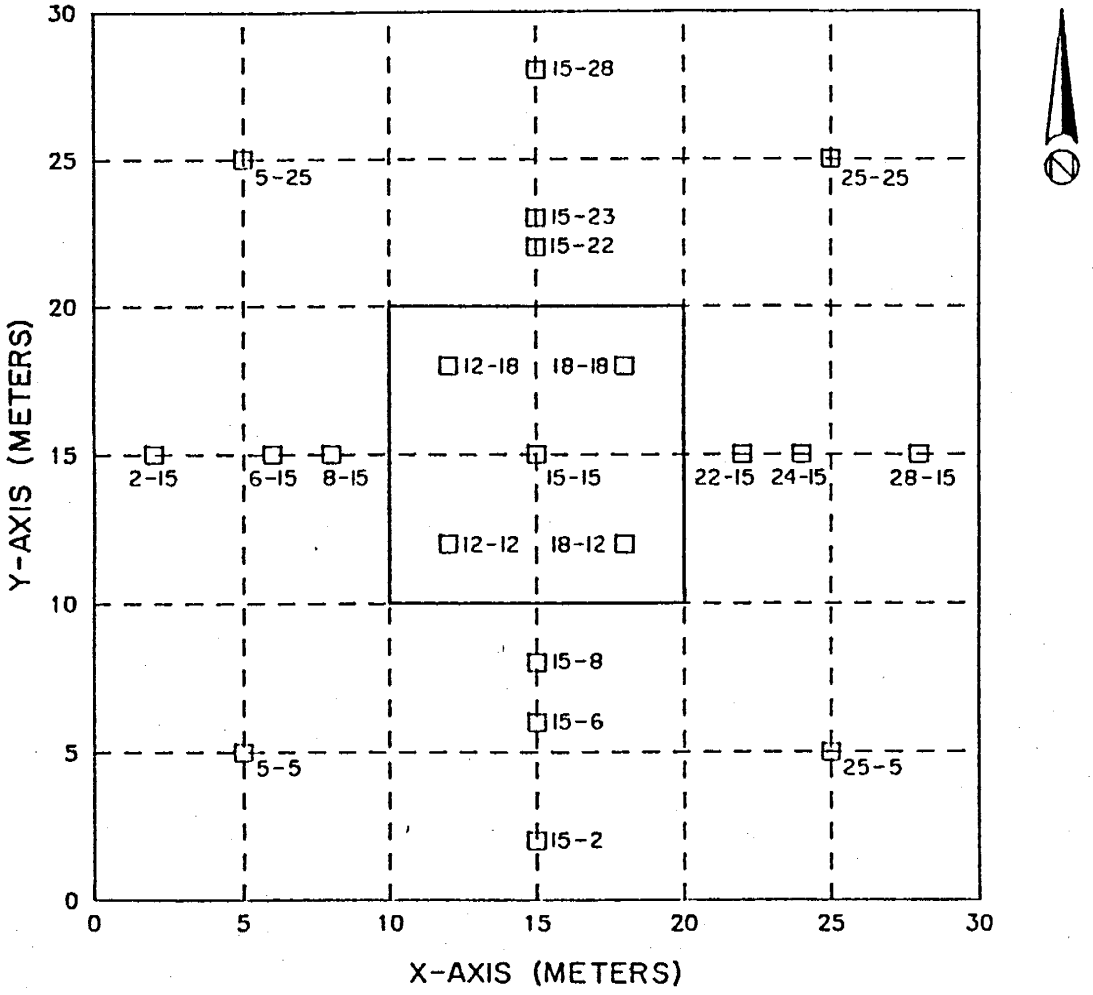

Figure 15. Monitoring station location numbers based on an X-Y grid with the ordinate in the southwest corner of the site. Heavy line in interior outlines the wetted area.

4.1.1. Split Spoon Samples

Two hundred and forty-seven (247) split spoon samples were collected at regular intervals to 10 meters depth, providing nearly continuous geologic logs of each of the 21 monitoring stations. To take a sample, auger flights were advanced with a star bit attached to the cable hammer at the bottom of the borehole to prevent soil from moving up the hollow stem. At each sampling location, the star bit was raised, and the 5.08 cm (2") outer diameter split spoon was lowered down the borehole. The drill hammer pounded the sampler into the ground for a 0.3 to 0.6 meter (1-2 ft) interval, yielding a core sample from that depth. Baskets inside the tip of the split spoon sampler prevented the soil from falling out during sample recovery.

An advantage of the split spoon sampling technique is the ability to observe textural contacts within the recovered core, thereby giving a good approximation of the contact location depth. However, soil cores obtained by split spoon sampling have been disturbed and compacted within the sampler, thus limiting their usefulness for further hydrologic laboratory analysis. Visual geologic descriptions of each split spoon soil sample were recorded in the field and later modified with more detail in the laboratory. The samples were analyzed for gravimetric moisture content and particle size distribution.

4.1.2. Soil Core Samples

Soil core samples (100 cc) allow more extensive hydrologic characterization in the laboratory. Due to many pebble and

cobble layers, cores are very difficult to obtain at the field site. Four different methods were employed to obtain 76 soil cores (Table 2).

The first method utilized hand augering techniques to obtain core samples from 5.08 cm (2") boreholes at shallow depths. This is a common sampling method, likely to provide a relatively undisturbed soil sample. However, we were unable to hand auger through cobble layers. Therefore, a second method was used which involved core sampling through the hollow stem 20.3 cm (8") diameter Mobil B-52 auger flights. Samples collected through the hollow stem auger were obtained after cleaning cuttings from the borehole by auger rotation, and it is uncertain whether all loose cuttings were removed prior to sampling. A third method was attempted at station 16-23, where cores were taken from a 5.08 cm (2") diameter borehole drilled with a hand power auger. In this case, samples were hand augered where possible, using the power auger to break through compacted dry soil or pebble zones. The power auger technique was tried at other locations without much success in drilling through cobble layers. The last core sampling method involved hand augering where possible using 5.08 cm (2") auger and using the New Mexico Tech Mobil B-30 auger rig to drill through cobble zones. This method was limited to about 4 meters depth by the total length of hand augering connections.

A suite of soil cores to a depth of six meters below datum along the north-south and east-west transects (Figure 16) were gathered using all four sample collection methods. Very few

Table 2. Core Sample Collection Methods

Method	Stations
1) 0.8 cm (2") hand augering, sometimes in conjunction with Mobil B-52 rig and 0.8 cm auger to break through cobbles.	8-16, 11-15, 14-15, 15-11, 15-19, 16-6, 16-16, 19-15
2) Taken through 20.3 cm (8") boreholes, minor hand augering.	2-28, 6-15,15-6, 15-23, 24-15
3) Hand auger when possible through 20.3 cm (8") auger.	15-7.5
4) 0.8 cm (2") hand augering and hand power auger to break through cobbles.	16-23

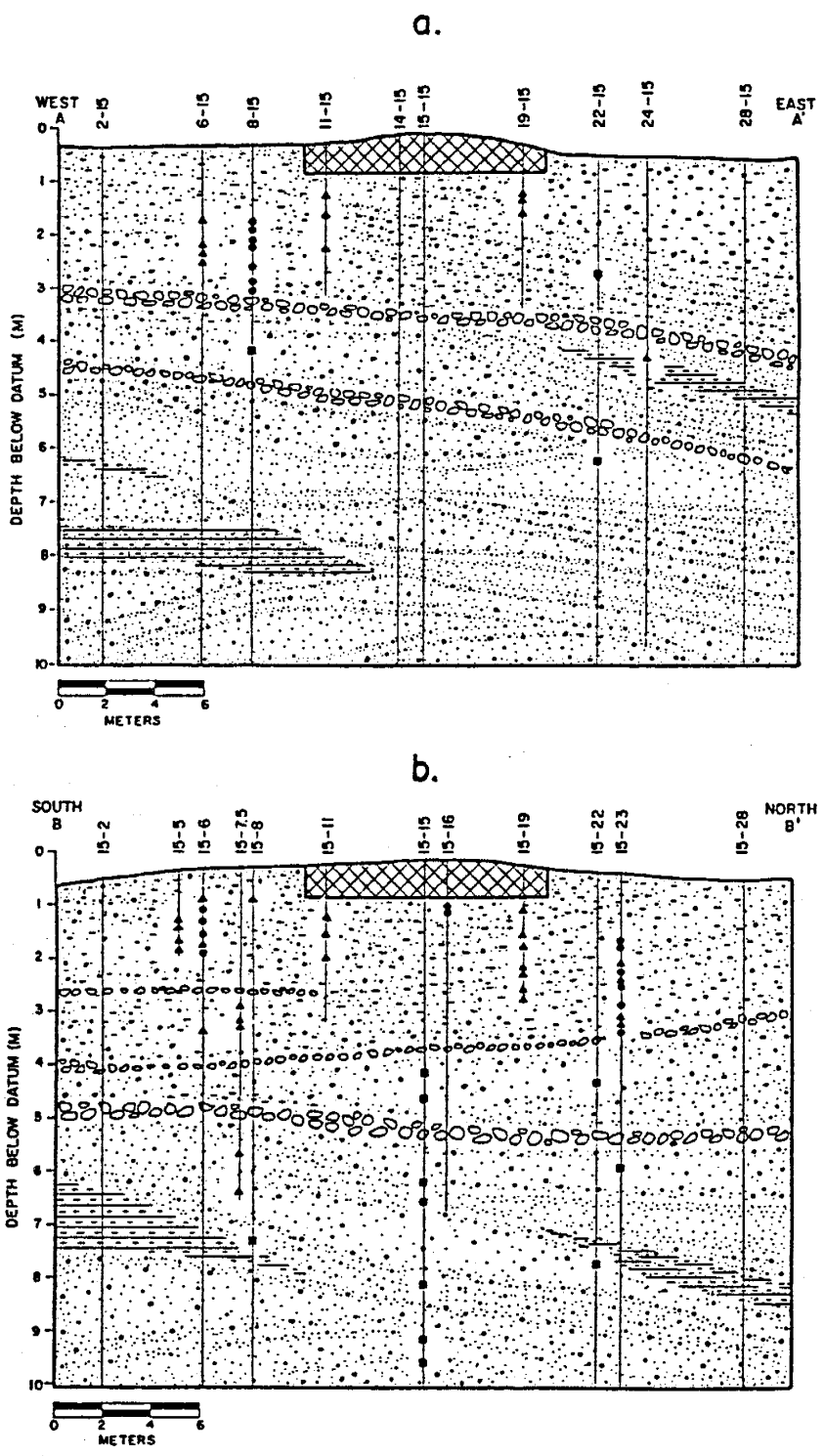

Figure 16. Location of soil core samples (100 cc) on the a) east-west and b) north-south transect. Circles are located directly on transect, triangles located up to a meter perpendicular to transect, and squares are repacked split spoon samples.

cores were obtained from depths below four meters. Consequently 15 of the split spoon samples collected from 4 to 9.5 meters below datum were repacked into rings at the in situ bulk density to determine hydraulic properties of the deeper fluvial sand facies (Figure 16).

Properly collected soil core samples provide a relatively undisturbed sample, but the core represents a point source. Since continuous soil cores are not available, it is not known whether the sample represents a major soil layer or a finer bed within that layer. Small scale variations in particle size and texture have a large effect on infiltration through the soil profile. Unfortunately, these variations cannot be detected by soil core sampling methods due to large spaces between samples or by split spoon sampling techniques due to soil disturbance during collection.

4.1.3. Cobble Zones

Cobble zones present a problem for both split spoon and soil core sampling techniques. Neither method was capable of sampling cobbles and coarse pebbles, and no samples were recovered from cobble zones or of the matrix material between cobbles. Cobble zone locations were noted as difficult areas to drill through in the field. The upper location of cobbles is determined more precisely than the bottom depth because the auger could drag cobbles down with the flights.

4.2 GEOLOGIC CROSS-SECTIONS

Borehole logs for each station show sample locations and geologic descriptions (Appendix B). Sample depths below land surface are adjusted to a datum reference elevation for ease in correlation between boreholes. Cross-sections of the east-west and north-south transects are determined by correlating visual characteristics of soil samples and cobble zone locations between sampling sites.

Figures 17 and 18 show the soil profiles exaggerated two-fold vertically to show different layers in more detail. The profile is stratified, consisting of an upper piedmont slope facies overlying ancient Rio Grande fluvial sands. Clay lenses up to a meter thick of undetermined lateral extent are present at all depths, but mainly in the fluvial facies. There are two major cobble zones, each about one half a meter thick found beneath the entire field site. The large rocks in the cobble zones range in size from pebbles to boulders (10-30 cm diameter)(Modified Wentworth scale) based on the rocks coming to the surface while drilling and noting that a 20.4 cm (8") auger could not drill around some of the rocks at depth.

The piedmont slope facies is present in the soil profile to depths of 3 to 4 meters below datum through the first major cobble zone. The second cobble zone ranges in depth from 4.5 - 5.0 meters below datum. There appears to be a transition zone from the piedmont slope to fluvial facies between the two major

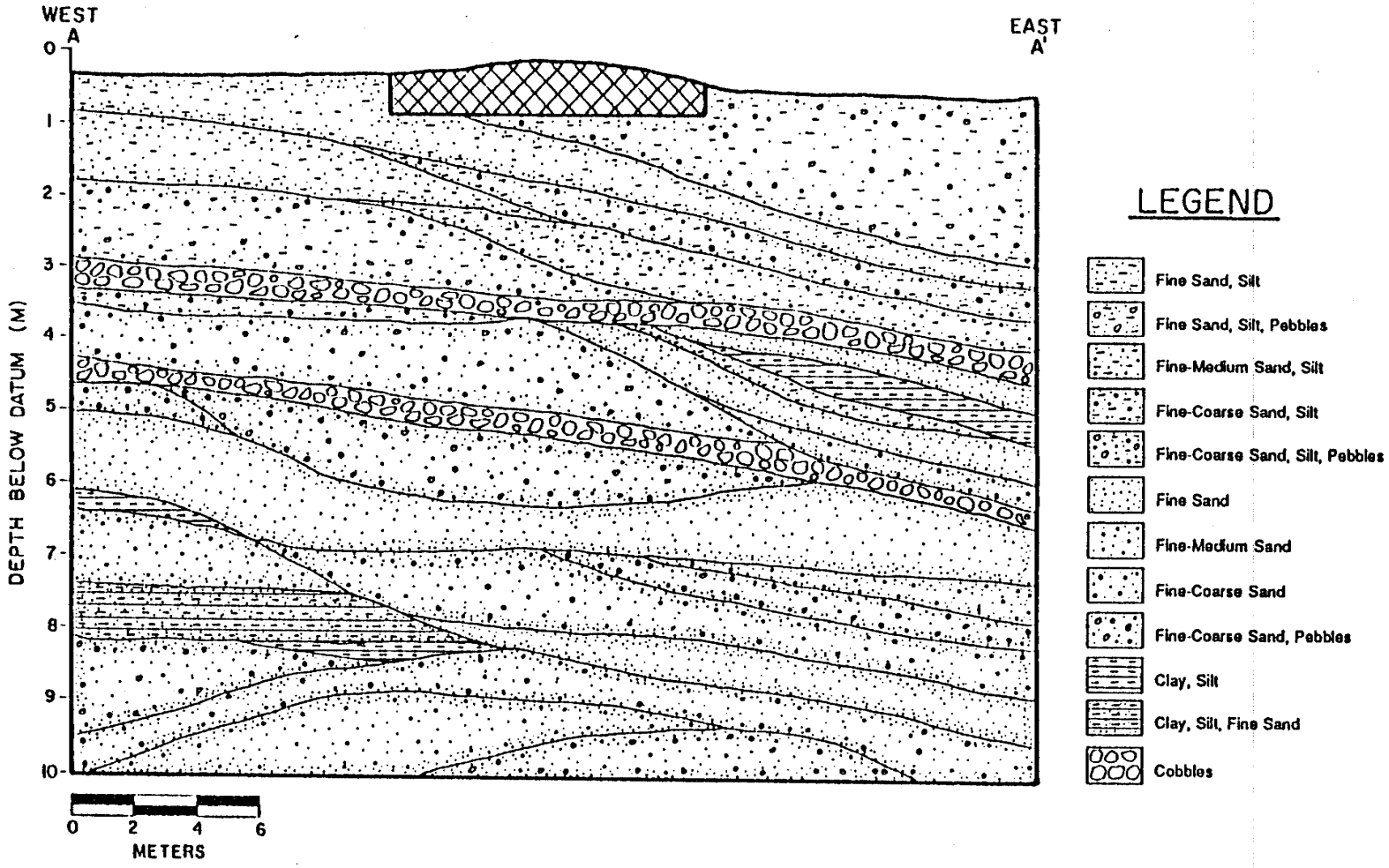

Figure 17. Geologic cross-section of the east-west transect.

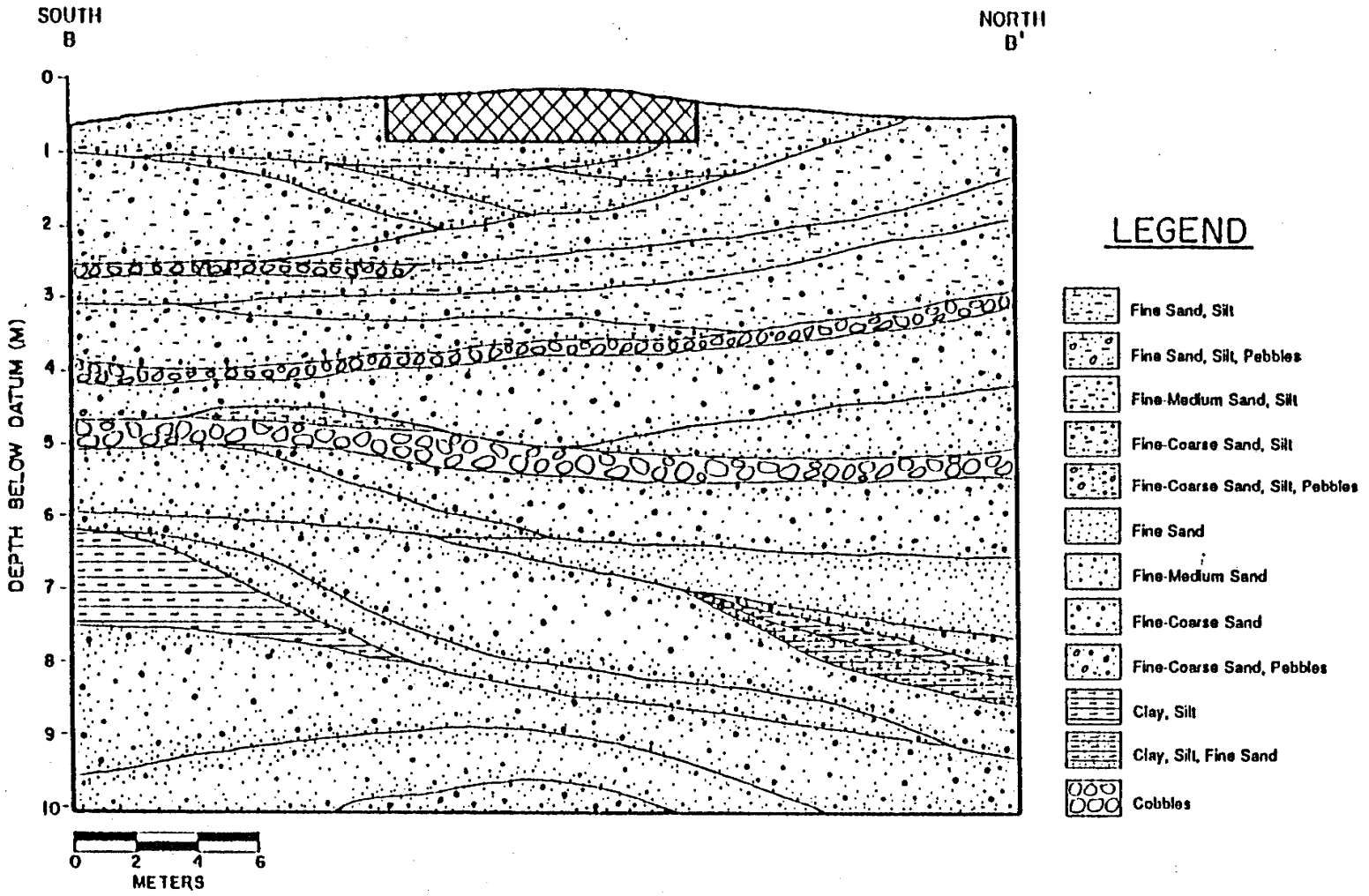

Figure 18. Geologic cross-section of the north-south transect.

cobble zones (see Section 3.3). Fluvial sand facies are found below the deeper cobble zone to 24 meters below datum. The exact thickness of the fluvial sand facies in this location is unknown, but the sands may be up to 250 meters thick in the area east of Socorro Peak (Chamberlain, 1980).

Piedmont slope stratification on the east-west profile (Figure 17) exhibits a slight inclination to the east. The apparent eastward inclination is presumed to reflect bedding structures from piedmont slope materials being derived from highlands directly to the west. A similar pattern does not appear to be present in the underlying fluvial sand facies, which probably were deposited in the north-south trending ancestral Rio Grande River system (Figure 18). Instead, the fluvial sands show sequences of meandering channels, consisting of well-sorted, fine sands alternating with fine to coarse sands and pebbles and overbank deposits of silts and clays.

4.3 LABORATORY ANALYSIS

Hydraulic properties of the split spoon and soil core samples were determined in the laboratory. The core samples were analyzed to determine: field moisture content (cc/cc), bulk density (g/cc), porosity (cc/cc), saturated hydraulic conductivity using a constant head permeameter, soil moisture characteristic curve measured in hanging columns, 15-bar moisture content determined in a pressure plate, and particle size distribution

from sieve and hydrometer tests. Unsaturated hydraulic conductivity relationships were calculated for each soil core sample using van Genuchten's closed form analytical solution (1980). The unsaturated hydraulic conductivities were also determined for eleven samples using the one-step outflow test (Kool, Parker, and van Genuchten, 1985).

Split spoon samples were analyzed for gravimetric field moisture content (g/g), and particle size distribution from sieve and hydrometer tests. Fifteen (15) split spoon samples from the fluvial sand facies were repacked in 100 cc rings at the in situ bulk density and analysed for hydraulic properties measured on soil cores.

All laboratory analysis results are tabulated by sample location in Appendix C. Appendix D presents core samples divided by facies type. The soil samples are identified by three numbers; the first two describe the sample location on the plan view X-Y coordinate system (Figure 15), and the third is the soil core ring number or split spoon sample number. The fifteen repacked split spoon samples are denoted by an "R" at the end of the sample number. Raw data collected during each experiment can be found in the '9I-KB' laboratory notebooks (Parsons, 1988).

4.3.1. Porosity

Two different methods are used to calculate porosity of the core samples. The first method involves measuring the saturated moisture content on a percent volume basis by weighing the soil core after removal from the constant head permeameter and

subtracting the sample's oven dry weight. The saturated moisture content is an approximation of porosity, assuming all entrapped air was eliminated during the permeameter run and that the density of water is 1.0 g/cc. The second method calculates porosity by the following equation (Hillel, 1980a):

$$n = 1 - \rho_b/\rho_s \qquad (9)$$

where n is the calculated porosity (%), ρ_b is dry bulk density (g/cc), and ρ_s is the particle density (g/cc) assumed to be 2.65 g/cc.

According to the first method, the porosity ranges from 30% to 57% in the piedmont slope facies, and from 27% to 46% in the fluvial sands (Appendix D). The arithmetic mean porosity of the finer piedmont slope material is 43% compared to 36% for fluvial sands (Table 3).

Saturated moisture content is a direct measure on each individual sample, whereas calculated porosity assumes a constant particle density which may vary according to soil type. Accordingly, the saturated moisture content should provide the most reliable porosity value. The saturated moisture contents will be subsequently used for porosity values necessary in analytic modeling analysis.

4.3.2. Moisture Content

Split spoon samples were analyzed for in situ gravimetric moisture content, and soil core samples provided volumetric moisture content information. The two different moisture content types are related by the following relationship (Hillel, 1980a):

TABLE 3. HYDROLOGIC PROPERTIES

PIEDMONT SLOPE FACIES	BULK DENSITY (g/cc)	Nc (%)	THETA sat. (%vol)	THETA 15b (%vol)	Ks (cm/sec)	ALPHA (1/cm)	Nv (--)
ARITHMETIC MEAN	1.50	43.4	42.3	12.0	2.7E-02	0.123	1.728
95% CONFIDENCE INTERVAL *	+/- 0.04	+/- 1.5	+/- 1.90	+/- 1.3	+/- 1.7E-02	+/- 0.08	+/- 0.16
VARIANCE	0.03	38.9	62.8	16.0	5.2E-03	0.101	0.414
COEFFICIENT OF VARIATION (%)	11.3	14.4	18.7	33.3	270.0	258.1	37.2
NUMBER OF SAMPLES (--)	68	68	67	35	66	62	62
FLUVIAL SAND FACIES							
ARITHMETIC MEAN	1.70	36.0	37.1	5.2	3.0E-02	0.087	2.704
95% CONFIDENCE INTERVAL **	+/- 0.05	+/- 2.1	+/- 3.45	+/- 1.7	+/- 3.2E-02	+/- 0.05	+/- 0.76
VARIANCE	0.01	20.6	54.4	4.9	3.3E-03	0.008	1.906
COEFFICIENT OF VARIATION (%)	7.1	12.6	19.9	42.6	190.0	105.0	51.0
NUMBER OF SAMPLES (--)	21	21	20	9	15	15	15
CLAY							
ARITHMETIC MEAN	1.38	47.9	52.8	28	2.9E-05	0.085	1.118
VARIANCE	---	---	---	---	---	---	---
COEFFICIENT OF VARIATION (%)	---	---	---	---	---	---	---
NUMBER OF SAMPLES (--)	1	1	1	1	1	1	1

Nc = calculated porosity
THETA sat = saturated hydraulic conductivity
THETA 15b = 15 bar moisture content
ALPHA, Nv = van Genuchten fitting parameters
* calculated for a normal distribution, applying the Central Limit Theorem
** calculated assuming t-distributions apply

$$\theta = w*\rho_b/\rho_w \quad (10)$$

where θ is the volumetric moisture content (cc/cc), w is the gravimetric moisture content (g/g), ρ_b is the dry bulk density (g/cc), and ρ_w is the density of water, assumed equal to 1.0 g/cc.

Gravimetric moisture contents are easily calculated for core samples, since θ and ρ_b are already measured. However, volumetric moisture content is a more commonly used parameter and can be directly compared to our neutron logging moisture content data. To convert gravimetric moisture content of disturbed samples to a volumetric basis, the average dry bulk density was used for each major soil type: 1.50 g/cc for piedmont slope material, 1.38 g/cc for clay (Table 3), and 1.64 g/cc for fluvial sand. The representative fluvial sand facies bulk density was calculated from the eight undisturbed fluvial sand core samples, eliminating repacked soil core samples (Appendix D2).

All split spoon samples were collected during spring 1986 during neutron access tube installation, and in fall 1986 when tensiometers were installed. Note that most soil core samples were collected after infiltration began (Appendix C). The core samples do not provide background moisture content data unless the wetting front had not reached the sample location prior to sampling.

Field moisture content profiles prior to the start of the experiment start are shown in Figures 19 and 20 (Appendix E). More data were available from March, 1986, when the neutron tubes were installed and continuous split spoon samples were collected

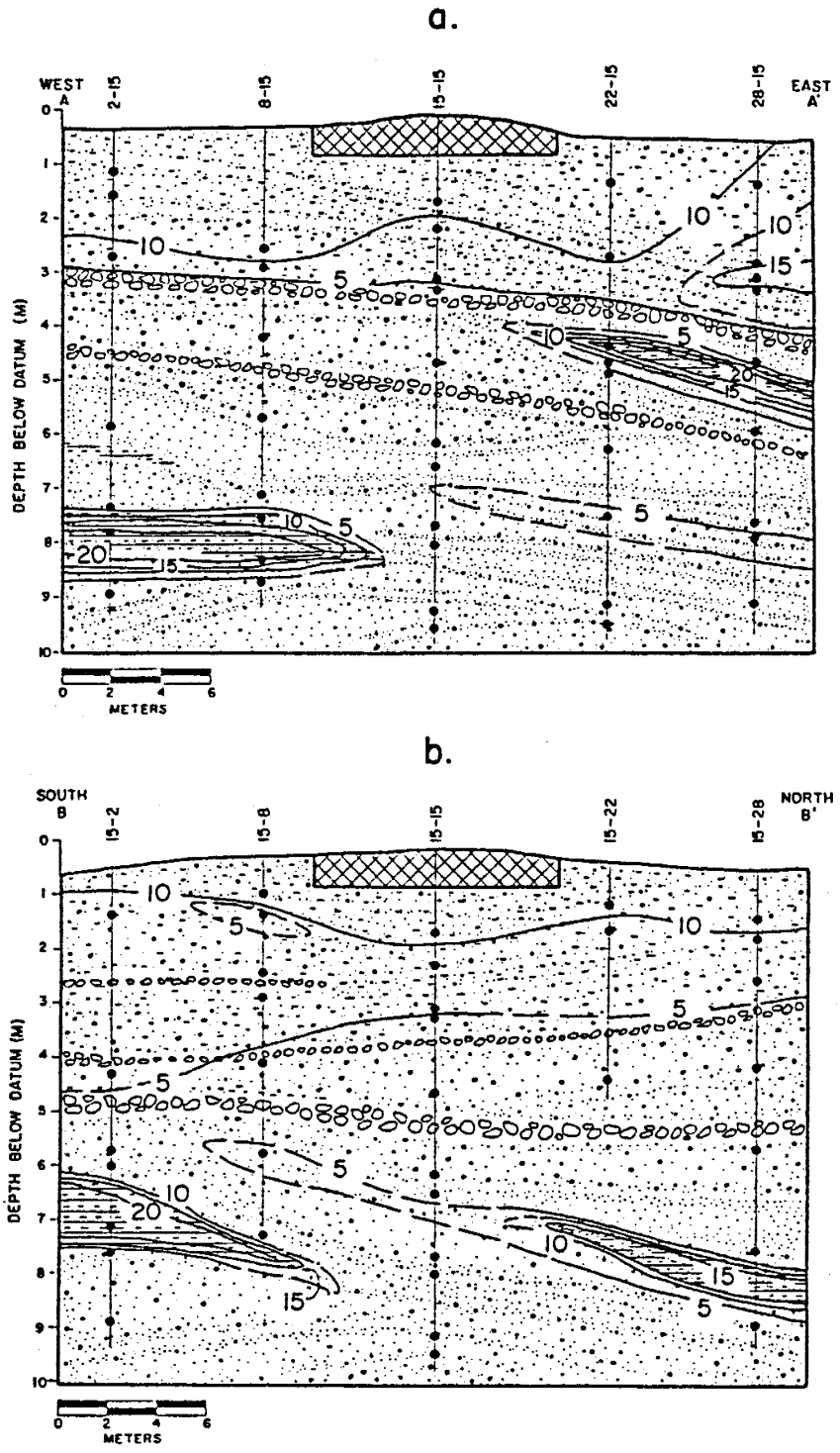

Figure 19. Volumetric field moisture content during February 1986 as estimated by converting split spoon sample gravimetric moisture content along the a) east-west and the b) north-south transect. Dots show sample locations.

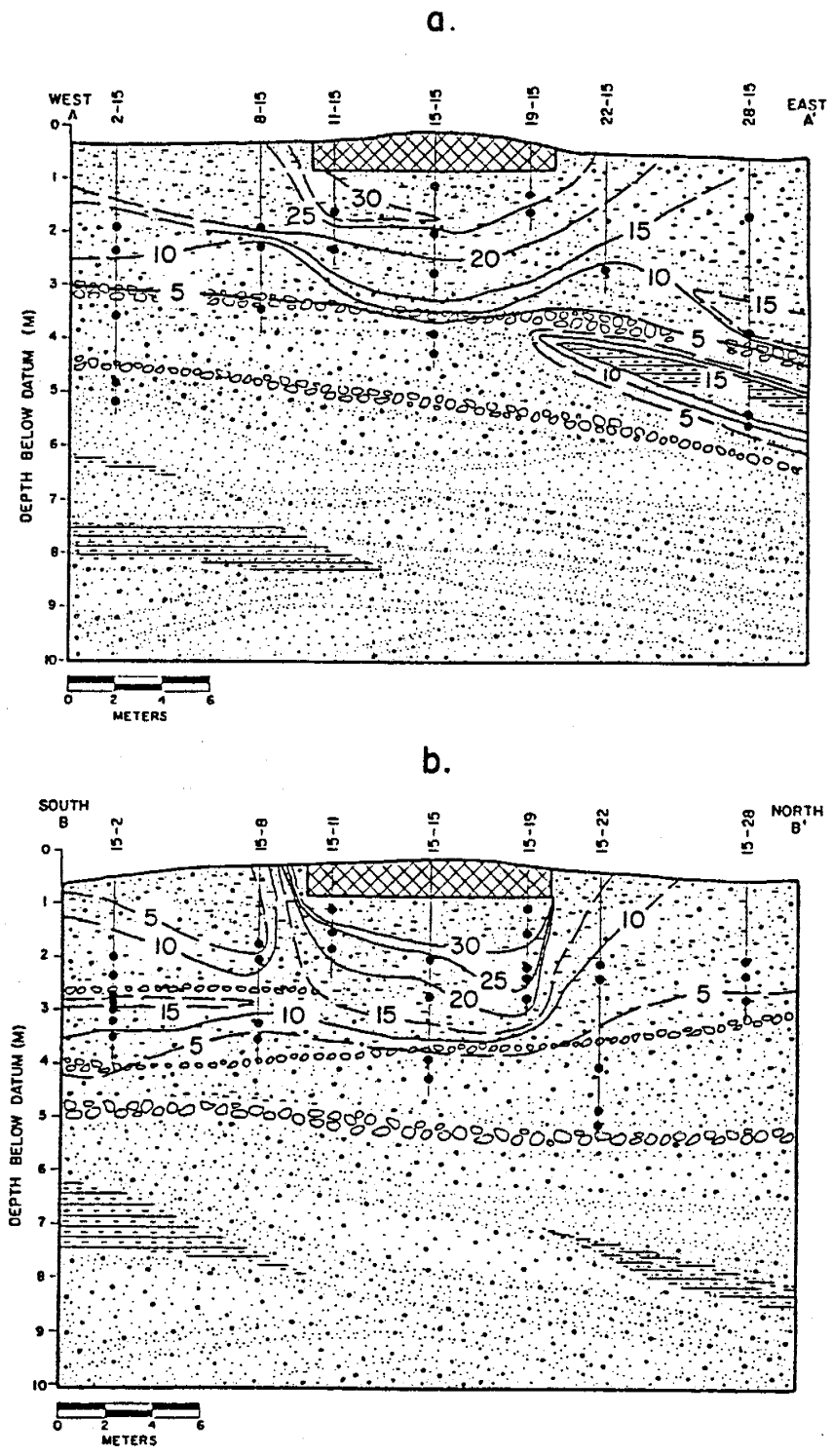

Figure 20. Volumetric field moisture content during August through September 1986 as estimated by converting split spoon sample gravimetric moisture content along the a) east-west and the b) north-south transect. Dots show sample locations.

to about 9 meters below datum. During the fall of 1986, tensiometers were emplaced, only to depths of five meters below datum. Limited numbers of split spoon samples were obtained during the fall at depths necessary to complete a continuous geologic log for each monitoring station location. Due to different sample collection depths in the spring and fall, direct comparisons of the moisture content present at each time period is difficult.

Initially the soil profile was very dry in the spring and fall of 1986. The upper piedmont slope facies remained consistently wetter than the underlying fluvial sands in the spring and fall. In the upper piedmont slope facies, the north and east ends of the vertical transects show more water present to about 3 meters below datum than at other locations at the same depths. The observed higher moisture contents are probably due to the slight land surface slope toward the northeast corner of the site. During large rain storm events, ponding was observed in the northeast corner of the field area on more than one occasion. Below the first major cobble zone, the fluvial sands are almost always uniformly less than 5% moisture while finer clay and silt lenses contain from 20 to 36% moisture (Figure 19).

Increases in moisture content which occurred at the center of the site from the spring to the fall are due to infiltration of water ponded in a pit excavated in the center of the field site during this time period. During the fall of 1986, rainfall infiltrated below the center portion of the field site (Figure

20). About 5 cm of rain fell during August and September, 1986 (Appendix F). Thus a large increase in moisture content beneath the excavated pit was observed from spring to fall 1986 (Figures 19,20), particularly in the north and east corner of the pit where ponding tended to occur. Partially due to these circumstances, the soil profile was not uniformly dry when infiltration began in January, 1987 (see Section 6.1).

4.3.3. Particle Size Distribution

The particle size distribution is the most extensively characterized parameter of the soil profile because both split spoon and soil core samples were analysed for this information. Standard sieve and hydrometer analyses were performed (ASTM, 1987). The particle size parameters measured include d_{10}, d_{30}, d_{50}, d_{60}, and d_{90}. These parameters indicate the percent of material by weight which is finer than the diameter given. Particle size distribution parameters calculated include the coefficient of uniformity (d60/d10) and the coefficient of curvature ($d30^2/(d10*d60)$) (Appendix C).

The standard method of analysis is to sieve the sample first, and save the remaining clay portion for hydrometer analysis if necessary to determine the percentage of silt and clay particles. For some of the finer clay and silt samples, the hydrometer analysis was conducted first due to the large percentage of particles smaller than the 200 mesh. Seventeen percent of the total number of soil samples were analyzed first by the hydrometer method and then by the sieve method. The very finest textured

samples of the piedmont slope facies were hydrometered first. The samples analysed by the hydrometer method first were disaggregated with liquid dispersing agent. The samples sieved first were disaggregated by a manual grinding technique which possibly left some clay size particles clinging to sand particles. Therefore, the sample analysis inconsistency may have some effect on apparent variations in particle size in the piedmont slope facies which contains more clay and silt size particles than the fluvial sand facies.

According to grain size results, two major sediment types are present in the field site soil profile. Underlying fluvial sands are coarser and more uniform than the upper piedmont slope facies (Figure 21). The median grain size is 2 times larger, and the coefficient of uniformity is eight times smaller in the fluvial sand facies than in piedmont slope facies material (Table 4).

The average 10% passing diameter (d_{10}) is 2.5 times finer in the piedmont slope facies than in the fluvial sands (Table 4). Similar trends are apparent comparing the borehole logs of the five center monitoring stations (Figure 22). d_{10} is very fine from 2 to 4 meters below datum, then becomes coarser. Station 18-12 is the exception, with a coarser layer at 2 meters below datum, becoming very fine from 2.5 to 8 meters below datum; however there are no soil samples from 4 to 7 meters below datum due to a cobble and gravel zone (Appendix B).

The fact that soil texture can strongly affect soil moisture properties is well known (Hendrickx and others, 1986). Vachaud

a.

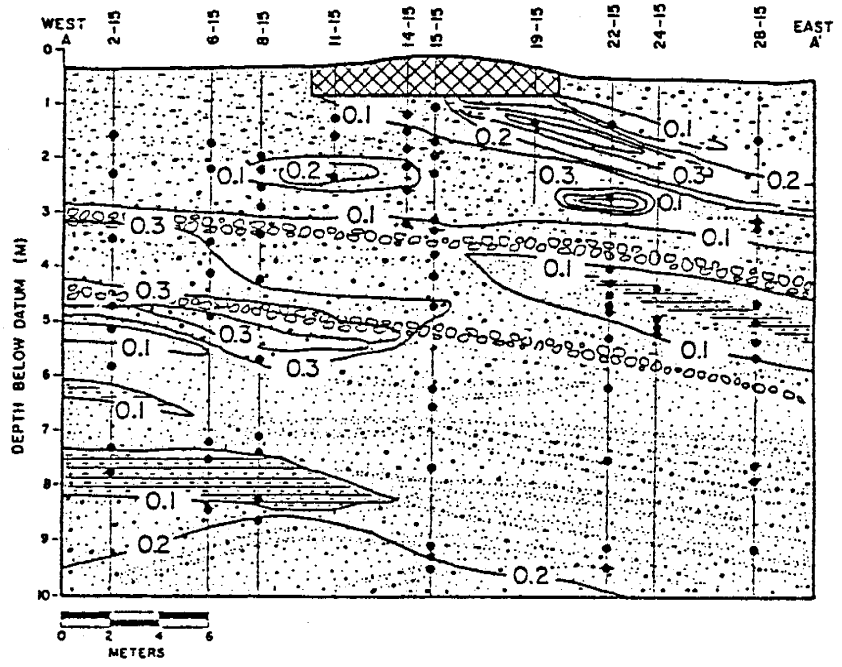

b.

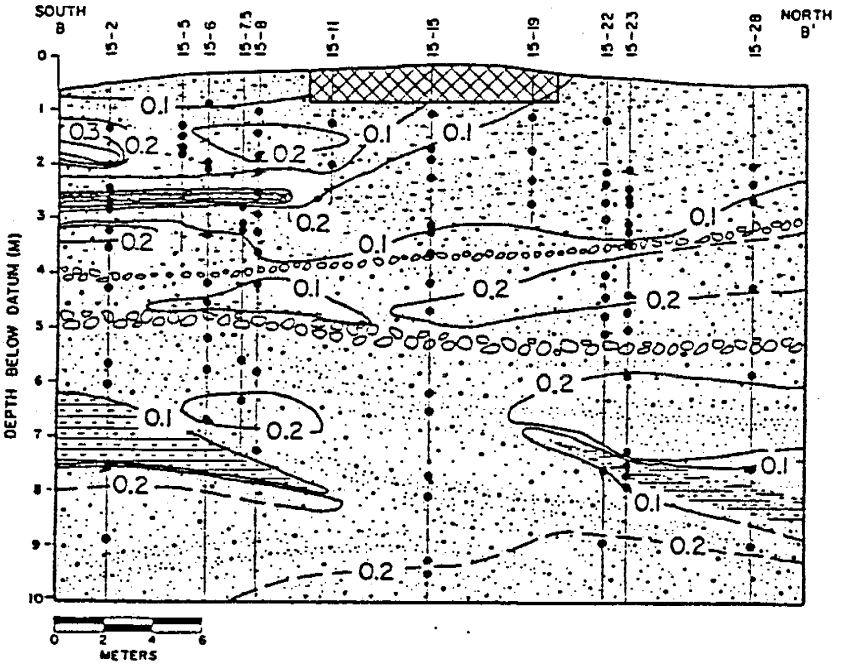

Figure 21. Particle size parameter d_{10} (mm) along the a) east-west and b) north-south transect. Dots show sample locations.

TABLE 4. PARTICLE SIZE PARAMETERS

PIEDMONT SLOPE FACIES	d10 (mm)	d30 (mm)	d50 (mm)	d60 (mm)	d90 (mm)	Cu (--)	Cc (--)
ARITHMETIC MEAN	0.067	0.197	0.390	0.566	3.851	59.256	3.115
VARIANCE	0.008	0.098	0.353	0.710	15.342	14161.430	18.253
COEFFICIENT OF VARIATION (%)	134.2	158.7	152.5	149.0	101.7	200.8	137.2
NUMBER OF SAMPLES (--)	59	59	59	59	59	59	59
FLUVIAL SAND FACIES							
ARITHMETIC MEAN	0.163	0.359	0.803	1.223	4.549	7.071	0.888
VARIANCE	0.002	0.066	0.994	2.709	25.112	102.87	0.053
COEFFICIENT OF VARIATION (%)	25.0	71.3	124.1	134.6	110.2	143.4	25.9
NUMBER OF SAMPLES (--)	21	21	21	21	21	21	21
CLAY							
ARITHMETIC MEAN	4.27E-04	1.34E-03	6.31E-03	2.62E-02	1.98E-01	145.143	4.572
VARIANCE	2.24E-04	1.16E-06	7.24E-05	1.43E-03	6.60E-02	110743.934	189.799
COEFFICIENT OF VARIATION (%)	110.9	80.5	134.9	145.2	130.3	229.3	301.4
NUMBER OF SAMPLES (--)	11	11	11	11	11	11	11

d10 - d90 = particle size % finer by weight than size indicated
Cu = coefficient of uniformity (d60/d10)
Cc = coefficient of curvature ((d30*d30)/(d10*d60))

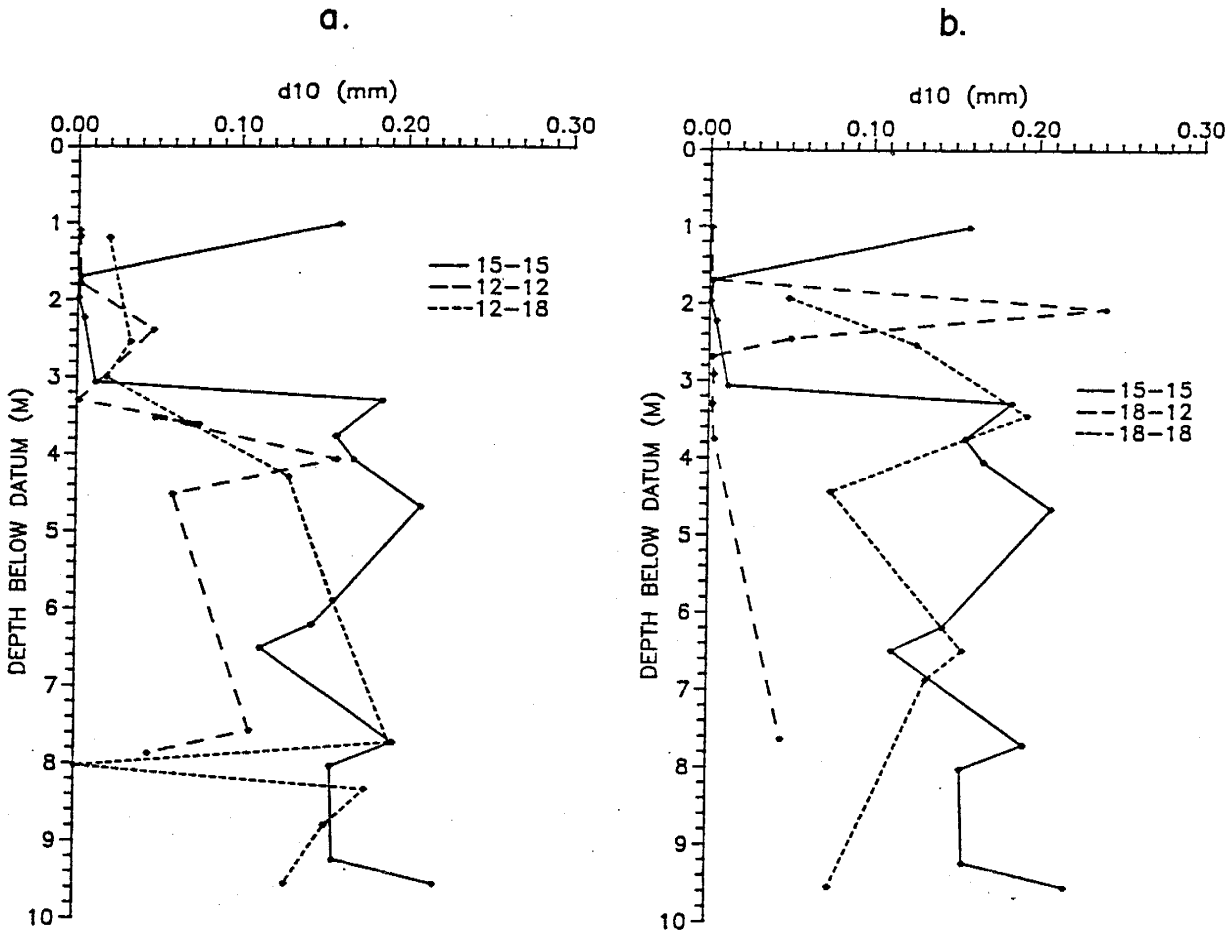

Figure 22. Particle size parameter d_{10} (mm) located at the five monitoring stations within the central irrigation plot.

and others (1985) found that a strong correlation exists between soil water content and the silt and clay content of a soil profile. Soil with high silt and clay content tended to exhibit higher stable moisture content through time compared to soils with less silt and clay fractions. At our field site, the soil zones with the smallest d_{10} particle size also contain the largest amount of moisture. The piedmont slope facies were initially about twice as moist volumetrically as the fluvial sand facies (Figures 19,20). Correspondingly, the piedmont slope facies average d10 parameter is approximately two times smaller than the fluvial sand facies (Table 4).

4.3.4. Moisture Retention Relationships

The soil moisture retention relationship (θ-ψ curve) for each soil core is measured by the hanging column apparatus and a 15-bar pressure plate. Hanging columns determine the drainage and imbibition cycles to negative pressures of about 200 cm (Vomocil, 1965). An equilibrium period of 24 hours was allowed between moisture content determinations at varying pressure values, which may not have been entirely adequate for the finer samples. Next, a pressure plate assembly (15 Bar Ceramic Plate Extractor Cat. # 1500, Soil Moisture Equipment Co.,Santa Barbara,CA) is used to apply a positive pressure to displace water from the sample at an equilibrium pressure of 15 bars. All clays and most silty samples were placed in the pressure plate. Selected typical θ-ψ curves are shown from the piedmont slope facies, the

fluvial sand facies, and clay material from the fluvial sand facies (Figure 23).

4.3.5. Saturated Hydraulic Conductivity

Saturated hydraulic conductivity (K_S), or the maximum conductivity of the soil, is found by placing soil core samples in a constant head permeameter for several days until equilibrium flow is reached. At that time it is assumed the sample is entirely saturated and all entrapped air is eliminated. Some problems with channeling were encountered, especially in repacked soil core samples and those cores taken from 20.8 cm diameter (8") boreholes.

Saturated hydraulic conductivities measured in the soil profile range from $2x10^{-1}$ cm/sec in coarse sand and pebbles to $8x10^{-6}$ cm/sec in clays. The average saturated hydraulic conductivity of the piedmont slope facies is $2.7x10^{-2}$ cm/sec, and the fluvial sands are slightly more conductive, with an average of $3.0x10^{-2}$ cm/sec (Table 3).

The stratified, heterogeneous nature of the soil profile becomes very apparent as saturated hydraulic conductivities may vary by several orders of magnitude within a meter change in depth (Figure 24). Based on K_S it is difficult to know whether the soil core sample represents a major stratigraphic layer or a minor variation within the layer.

4.3.6. Unsaturated Hydraulic Conductivity

The unsaturated hydraulic conductivity varies with pressure and moisture content. Two methods to establish the conductivity

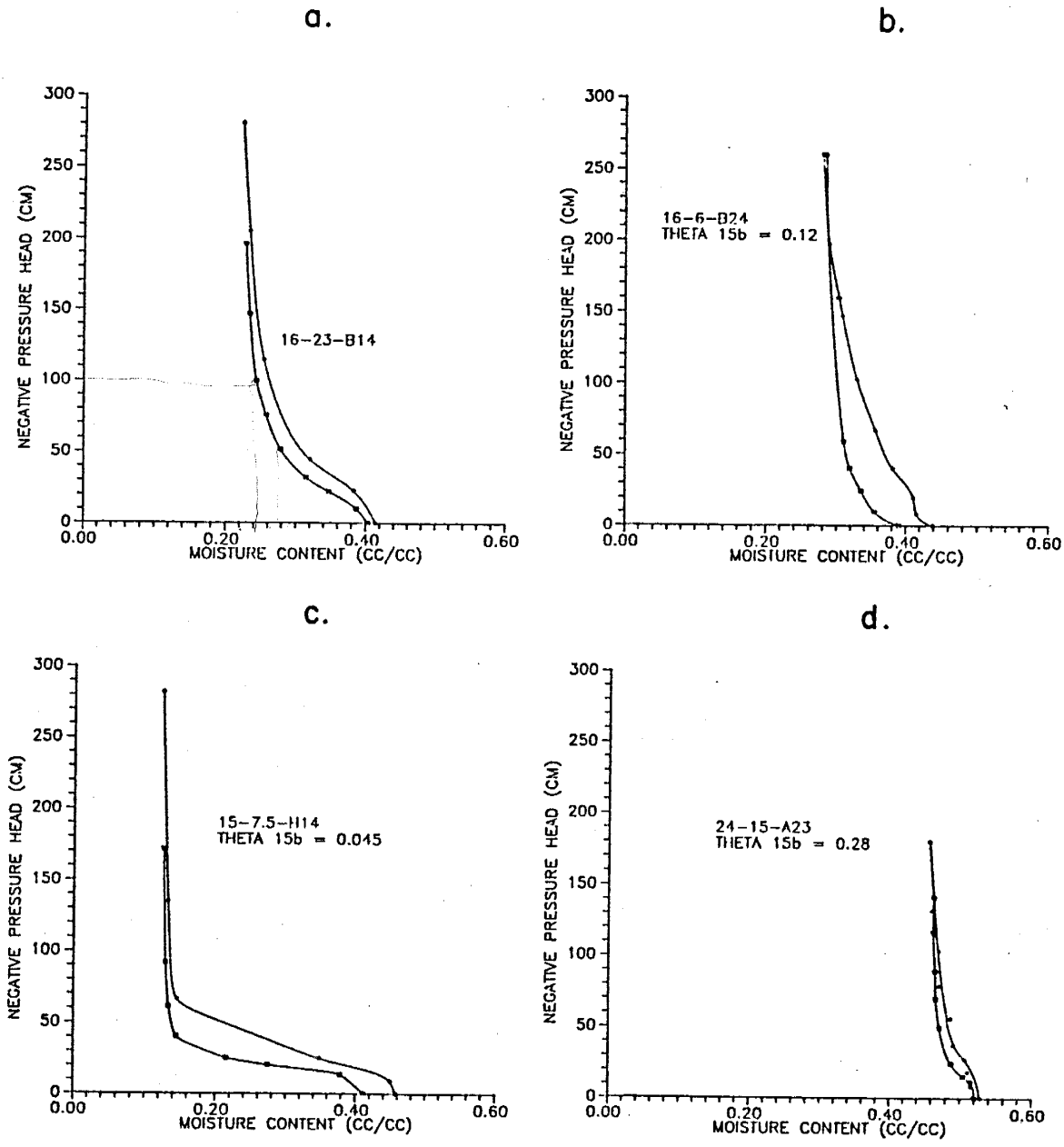

Figure 23. Typical moisture retention relationships from a,b) the piedmont slope facies, c) the fluvial sand facies, and d) a clay layer.

a.

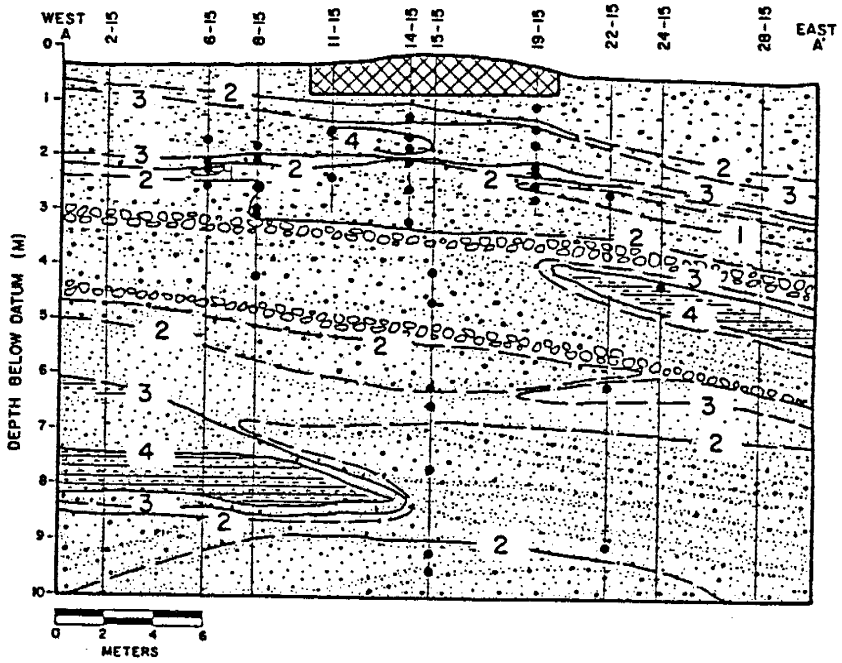

b.

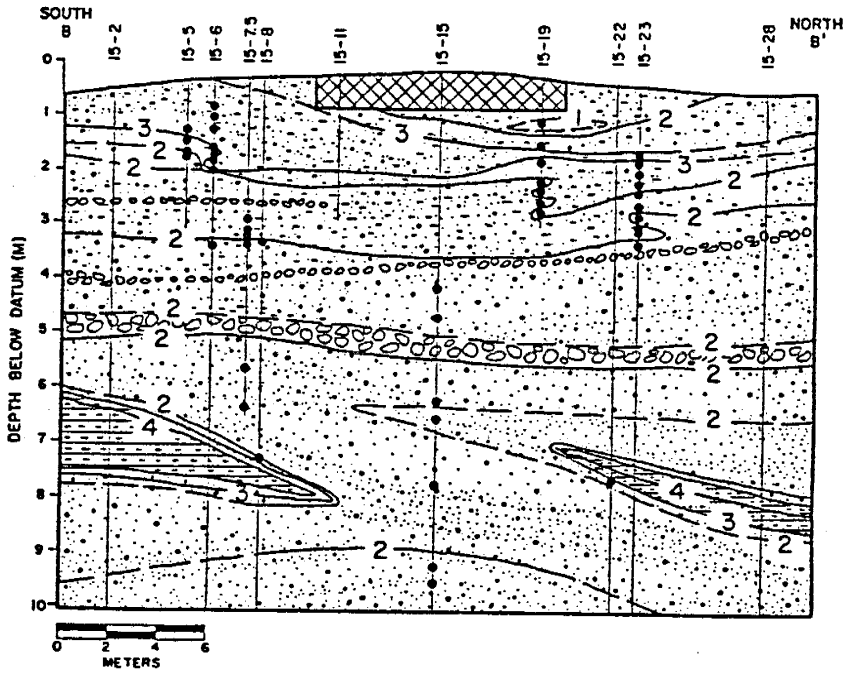

Figure 24. Logarithm of saturated hydraulic conductivity (cm/sec) along the a) east-west and b) north-south transects. Dots show sample locations.

versus pressure (K-ψ) and conductivity versus moisture content (K-θ) curves are applied in our study. The unsaturated hydraulic conductivity relationship is calculated by a closed form analytic solution for all the soil core samples (van Genuchten, 1980), and it is also determined for eleven soil cores using the one-step outflow method (Kool, Parker, and van Genuchten, 1985).

4.3.6.1. Closed Form Approximation

van Genuchten developed a closed form analytical solution (1980) to calculate the relative hydraulic conductivity (K_r) from the θ-ψ relationship based on Mualem's pore structure model (1976). Water content is expressed in a dimensionless form:

$$S_e = (\theta - \theta_r)/(\theta_s - \theta_r) \qquad (11)$$

where S_e is the effective moisture content (dimensionless), θ is the moisture content (cc/cc), and subscripts r and s refer to residual and saturated volumetric moisture contents, respectively. van Genuchten used the following relationship to represent the θ-ψ curve:

$$S_e = [1/(1 + \alpha\psi)^{n_v}]^m \qquad (12)$$

where α, n_v, and m are parameters depending on the shape of the curve. Mualem's model (1976) for relative hydraulic conductivity is based on the moisture retention relationship:

$$K_r(S_e) = S_e^{1/2} \left[\int_0^{S_e} \{1/\psi(x)\}dx \,/ \int_0^1 \{1/\psi(x)\}dx\right]^2 \qquad (13)$$

where x is a dummy variable, and ψ is the pressure head. van Genuchten's closed form solution combines Mualem's theory (equation 13) with equation 12 leading to:

$$K_r(S_e) = S_e^{1/2} [1 - (1 - S_e^{1/m})^m]^2 \qquad (14)$$

or:

$$K_r(\psi) = \{1 - (\alpha\psi)^{n-1} [1 + (\alpha\psi)^n]^{-m}\}^2 / [1 + (\alpha\psi)^n]^{m/2} \quad (15)$$
$$(m = 1-1/n)$$

van Genuchten's model estimates α and n_v by a non-linear least squares regression procedure, and calculates K_r by equation 13. Input data includes laboratory parameters previously measured: the θ-ψ relationship, θ_s, θ_r, and saturated hydraulic conductivity. Residual moisture content is assumed to be the 15 bar moisture content, the maximum operating pressure of the pressure plate apparatus. When the two-parameter model is run, only α and n_v are calculated, leaving θ_r fixed. If residual moisture content is unknown, the three-parameter model will calculate α, n, and θ_r.

van Genuchten's method has been found by numerous researchers to produce good agreement between observed and predicted unsaturated hydraulic conductivity in the field and laboratory (van Genuchten, 1980; Dane, 1980; Ward, 1983; Stephens and Rehfeldt, 1985). van Genuchten (1980) found good agreement between observed and predicted K_r-ψ curves for several loam materials, but not for clay where the model predicted a residual moisture content of zero, thereby underestimating conductivity in the wet range, and overestimating conductivities in the dry range. He suggested that an independent means be used to determine residual moisture.

Stephens and Rehfeldt (1985) conducted a sensitivity analysis comparing the two- and three-parameter models to measured unsaturated conductivities for dune sand. They found that both models did an equally good job of predicting θ-ψ relation-

ships, but that a good visual fit to a given θ-ψ curve does not guarantee an accurate K_r-ψ prediction. The two-parameter model does a good job in predicting K_r-ψ compared to their field data. Again, the three-parameter model tends to overestimate hydraulic conductivity at high negative pressure heads due indirectly to a low estimate of θ_r. Stephens and Rehfeldt note that improved results may be obtained by estimating θ_r from physical characteristics and holding it constant by running the two-parameter model.

We have no actual field K-ψ data, but the upper piedmont slope facies at the field site exhibits similar saturated hydraulic conductivity, θ_s, and θ_r values to the Silt Loam G.E.3. (van Genuchten, 1980). The underlying fluvial sands are similar to dune sand described by Stephens and Rehfeldt (1985) (Table 3).

All soil core samples are evaluated by van Genuchten's method. Moisture retention data from the imbibition cycle is input to the model, to more closely approximate field infiltration conditions. Thus the input maximum water content is assumed to be 90% of the measured θ_s, unless the θ-ψ curve indicates a significantly different saturation value. Based on results of previous studies by van Genuchten (1980) and Stephens and Rehfeldt (1985), the two-parameter model is run for all cases where residual moisture content data (15 bar moisture content) are available. When θ_r is not measured, the three-parameter model is run.

A limited number of soil cores (34 samples) with measured residual moisture content values are analyzed by both of the approaches. First, the two-parameter model was run with the 15 bar moisture content fixed. Second, the three-parameter model was run setting the 15 bar moisture content as the first approximation of θ_r, but not using the 15 bar moisture content as a data point. A third approach involved running the three-parameter model, using the 15 bar moisture content only as a data point. The latter method was unsuccessful because the model did not converge without some intermediate data points such as the 5 bar moisture content, which are not available. The maximum moisture content obtained by the hanging column corresponds to a negative pressure head of about 0.25 bars, and the next lowest moisture content measurement is at a negative pressure of 15 bars.

The residual moisture content predicted from the three-parameter model exceeds by a factor of two the measured 15 bar moisture content for 96% of the samples analyzed by the first and second methods (Appendix G). The 15 bar moisture content is not always equal to θ_r, but the equality has been assumed in this exercise. A regression between measured and predicted θ_r shows very weak correlation (Figure 25). Due to the low correlation coefficient, r^2, between the two parameters, θ_r predicted by the three-parameter model can not be corrected to the measured 15 bar moisture content value by a linear equation.

Preliminary results indicate that although the fitted parameters α and n_v calculated by the two- and three-parameter

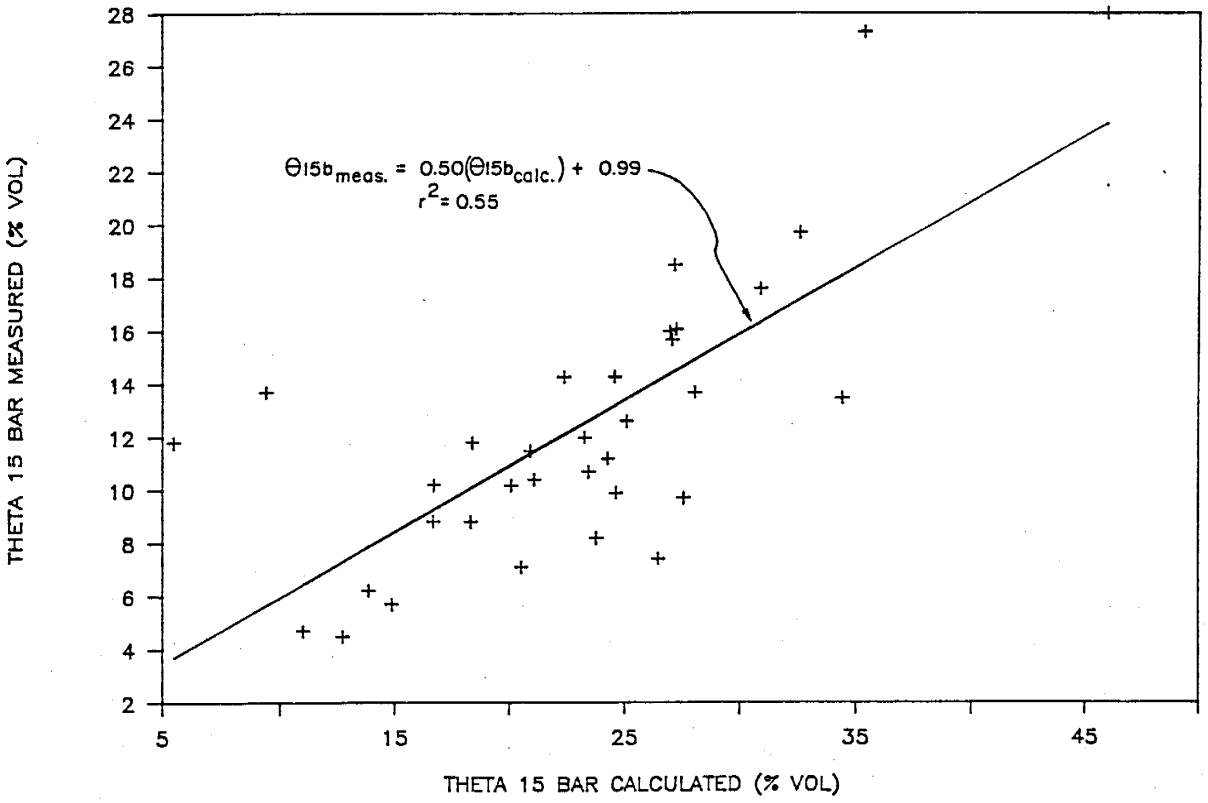

Figure 25. Linear regression between residual moisture content calculated by van Genuchten's three-parameter model (1980) and measured in the pressure plate.

models differ by up to 216% (Appendix G), the two- and three-parameter K-ψ curves calculated for selected samples agree within an order of magnitude in the pressure range of interest for infiltration (ψ > -1000 cm) (Figure 26). A program was written, KREL.FOR (Appendix M1), to compute K(θ) using the two sets of α, n_v, and θ_r data according to Mualem (1976). K-ψ curves are computed for only four of 36 samples; these were selected to represent the range of expected values. For three of the four samples graphed, the two-parameter and three-parameter K-ψ curves compare within an order of magnitude to at least 2000 cm negative pressure head (Figure 26). The K-ψ curves for sample 8-16-H15 differed by over four orders of magnitude at 2000 cm negative pressure head, but the residual moisture content values from the two- and three- parameter models differed by 257% (Figure 26d). None of the other samples disagreed to such a large extent between θ_r values (Appendix G).

In summary, θ_r values calculated by van Genuchten's code are greater than measured (15 bar moisture content) values in almost all cases. Residual moisture content values calculated by the three-parameter model are not used for analytic modeling. However, for this soil type, K-ψ curves appear to be relatively insensitive to α and n_v parameter values for both the two- and three-parameter models in the wet region of the curve. Accordingly, parameters α and n_v from van Genuchten's two- and three-parameter model are both used for analytic analysis.

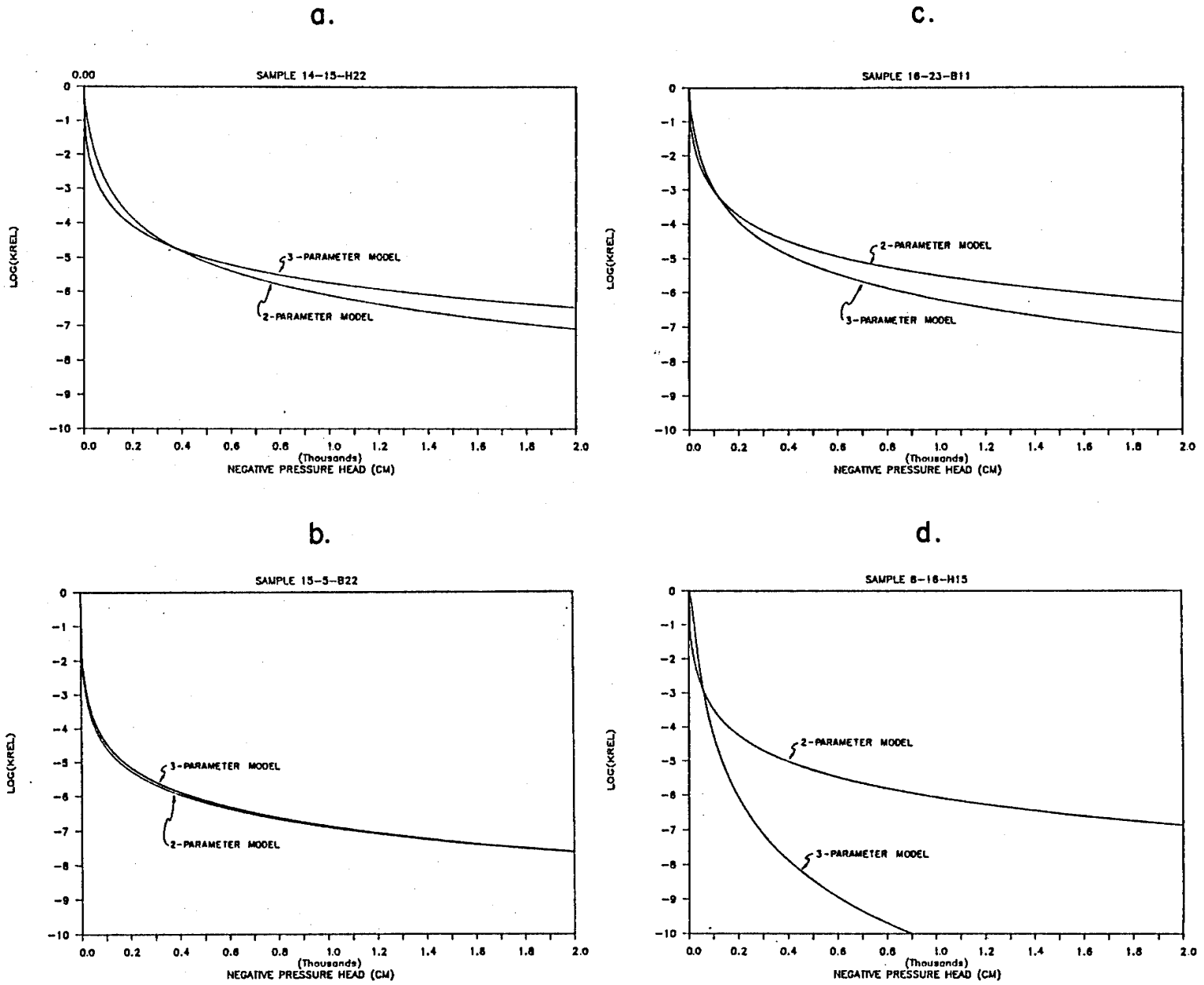

Figure 26. Selected unsaturated hydraulic conductivity curves calculated by van Genuchten's two- and three- parameter models (1980).

4.3.6.2. One-Step Outflow Experiment

Unsaturated hydraulic conductivities were determined for eleven ring samples, using the one-step outflow method (Kool, Parker, and van Genuchten, 1985). The one-step computer program will estimate up to five unknown parameters in the van Genuchten soil hydraulic property model (1980) from measurements of cumulative outflow with time after an instantaneous decrease in pressure during one-step flow experiments. The one-step program combines a nonlinear optimization routine with a Galerkin finite element model for the one-dimensional flow equation.

The one-step laboratory experiment simulates field drainage conditions, while our field experiment involves the process of infiltration. The maximum hysteresis effect between drainage and imbibition soil moisture retention curves is about 5% to 7% volume near saturation (Figure 23). For our application, hysteresis effects are considered negligible and the one-step outflow test is assumed to apply to the field experiment conditions.

4.3.6.3. Comparison Between Unsaturated Hydraulic Conductivities Determined by Closed Form Analytic Solution and One-Step Outflow Test

van Genuchten's closed form analytic solution (1980) to calculate unsaturated hydraulic conductivity is an approximation using the moisture retention curve. Conversely, the one-step test (Kool, Parker, and van Genuchten, 1985) uses actual drainage versus time data to determine the unsaturated hydraulic conductivity, and may be expected to provide more realistic unsaturated hydraulic conductivity curves.

Although the one-step test may be more reliable, the one-step test requires an extra laboratory experiment of several days duration, and the one-step computer code requires an hour for execution on an IBM-XT. Conversely, van Genuchten's analytic solution utilizes laboratory data already available and takes seconds to run on an IBM-XT. As a result of this convenience, all soil core samples are analysed by van Genuchten's analytic solution, but only 11 cores are analysed for unsaturated hydraulic conductivity by the one-step outflow test.

Eleven (11) core samples are evaluated for unsaturated hydraulic conductivity using both methods. Seven (7) of these samples are analyzed using both drainage and imbibition θ-ψ data in van Genuchten's code. Soil types range from fine silty sand and clay to coarse sand and pebbles. Saturated hydraulic conductivities range from 8.2×10^{-6} cm/sec to 1.1×10^{-2} cm/sec (Table 5).

Only half of the soil core samples exhibit K-ψ curves from van Genuchten's code (imbibition θ-ψ data) and the one-step test which compare within an order of magnitude to each other within the 0 to 2000 cm negative pressure head range (Table 5) (Figure 27a). K-ψ curves from the other samples disagree by as much as five orders of magnitude (Figure 27b), particularly in the dry range.

The K-ψ curves estimated by van Genuchten's code appear to be insensitive to hysteresis. Drainage curve θ-ψ data is expected to approximate the one-step outflow drainage experiment most

TABLE 5. VAN GENUCHTEN AND ONE-STEP OUTFLOW TEST RESULTS IN THE PIEDMONT SLOPE FACIES AND FLUVIAL SAND FACIES

SAMPLE	ALPHAos (1/cm)	ALPHAvgw (1/cm)	ALPHAvgd (1/cm)	Nos (--)	Nvgw (--)	Nvgd (--)	DESCRIPTION	Ks (cm/sec)	K vs. PSI CURVES AGREE? IMBIBITION	DRAINAGE
14-15-11C	0.2058	0.2839	0.0867	1.1927	1.5858	1.9768	crs sand,silt,pbls	6.1E-03	N	N
14-15-H17	0.0571	0.0217		1.2999	1.4444		fine sand, silt	5.7E-04	Y	
14-15-H22	0.0107	0.0476	0.0668	1.5312	1.1697	1.5387	f.sand,silt,clay	8.2E-06	Y	Y
14-15-H23	0.2419	0.5780		1.1725	1.1883		coarse sand	3.0E-02	Y	
14-15-15C	0.2000	0.0231	0.0116	1.1000	1.1566	1.2793	fine sand, silt	1.1E-02	N	N
15-15-A20	0.3557	0.2242		1.1944	1.2596		coarse sand	3.5E-02	Y	
15-7.5-3C	0.2079	0.0367	0.0270	1.1698	1.5236	1.6364	fine sand, silt	7.4E-03	N	N
15-7.5-H10	0.1260	0.1103		1.2490	1.3313		f-crs sand, silt	1.1E-02	Y	
15-7.5-A13	0.0661	0.0527	0.0333	1.4064	2.1855	2.3551	fine-medium sand	3.0E-02	N	N
15-7.5-H14	0.1801	0.0695	0.0411	1.2812	1.8438	1.9939	fine-medium sand	2.8E-02	Y	Y
16-6-B24	0.0217	0.3347	0.0320	1.2753	1.1077	1.3201	fine sand, silt	3.5E-04	N	Y
AVERAGE	0.1521	0.1620	0.0426	1.2611	1.4360	1.7286		1.4E-02		
VARIANCE	0.0113	0.0313	0.0007	0.0148	0.1118	0.1563		1.8E-04		
C.V.	69.80	109.11	60.13	9.63	23.29	22.87		93.41		

ALPHA, N = fitting parameters
os = one step test
vgw = van Genuchten estimation, imbibition curve
vgd = van Genuchten estimation, drying curve
Ks = saturated hydraulic conductivity determined in a constant head permeameter.
K vs. PSI CURVES AGREE? = van Genuchten and one-step outflow unsaturated hydraulic conductivity curves within order of magnitude for pressure heads greater than -2000 cm.

a.

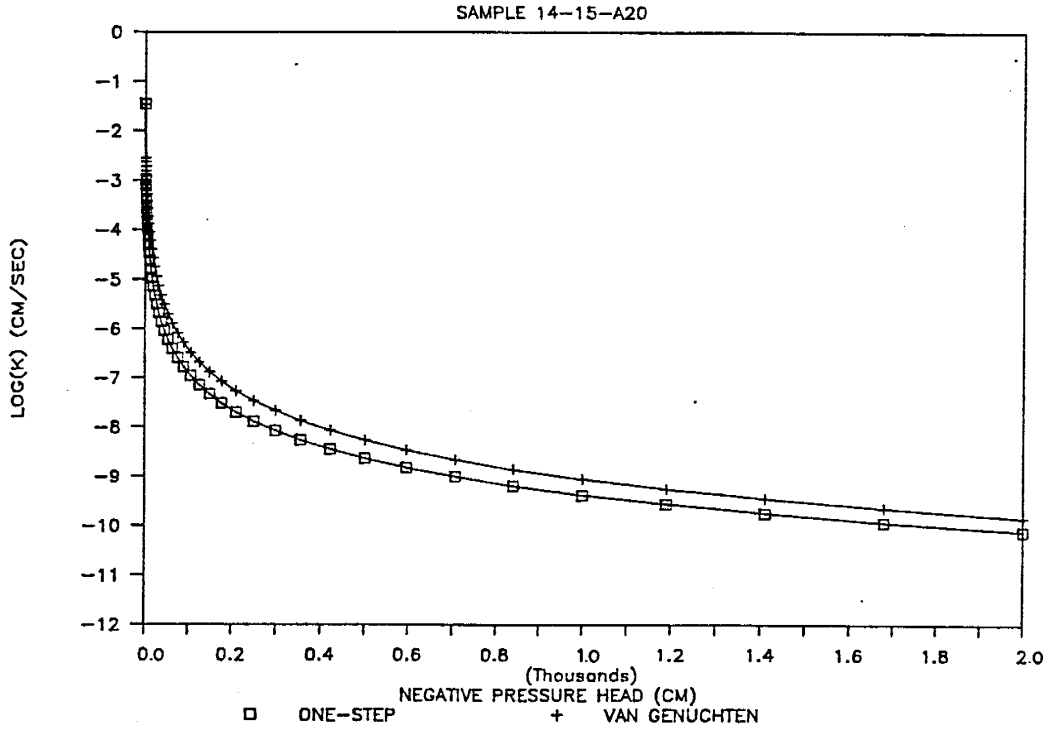

b.

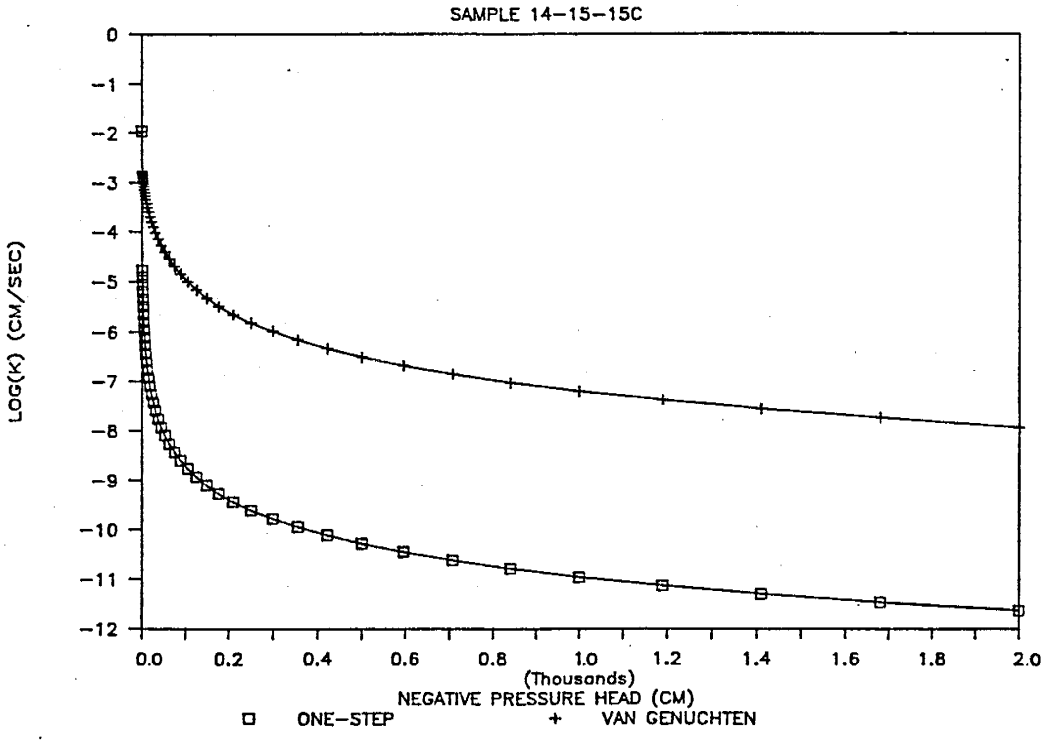

Figure 27. Comparison of unsaturated hydraulic conductivity curves calculated by van Genuchten's two-parameter model (1980) and the one-step outflow test (Kool, Parker, and van Genuchten, 1985).

accurately. Five samples have K-ψ curves which do not agree within an order of magnitude when comparing van Genuchten's code (imbibition θ-ψ curve) and the one-step outflow test (Table 5). When these five samples are analyzed using drainage θ-ψ data, only one core sample (16-6-B24) improves to compare within an order of magnitude (Figure 28). In general, the K-ψ curve appears to change very little no matter whether the imbibition or drainage moisture retention curve is used in van Genuchten's code.

Preliminary results indicate that K-ψ curves estimated by the van Genuchten method may represent K-ψ curves similar to those a one-step outflow test measures. Our limited results show that 64% of the K-ψ curves generated by both methods compare within an order of magnitude within a negative pressure range of 0 to 2000 cm. Hysteresis effects seem to have little control on the K-ψ curve comparisons. However, a larger sample population is necessary to verify these results in a more quantitative manner applying statistical analyses.

4.3.6.4. Effective K-θ Curves

Within each facies there is variability in unsaturated hydraulic properties. Each individual soil core sample has a different moisture retention relationship, thus different K-ψ and K-θ relationships are estimated in van Genuchten's code. It is important to simplify the mathematical analysis of seepage by averaging the hydraulic properties within zones or layers. Average hydraulic properties for each designated layer give information on the expected moisture behavior in that layer.

a.

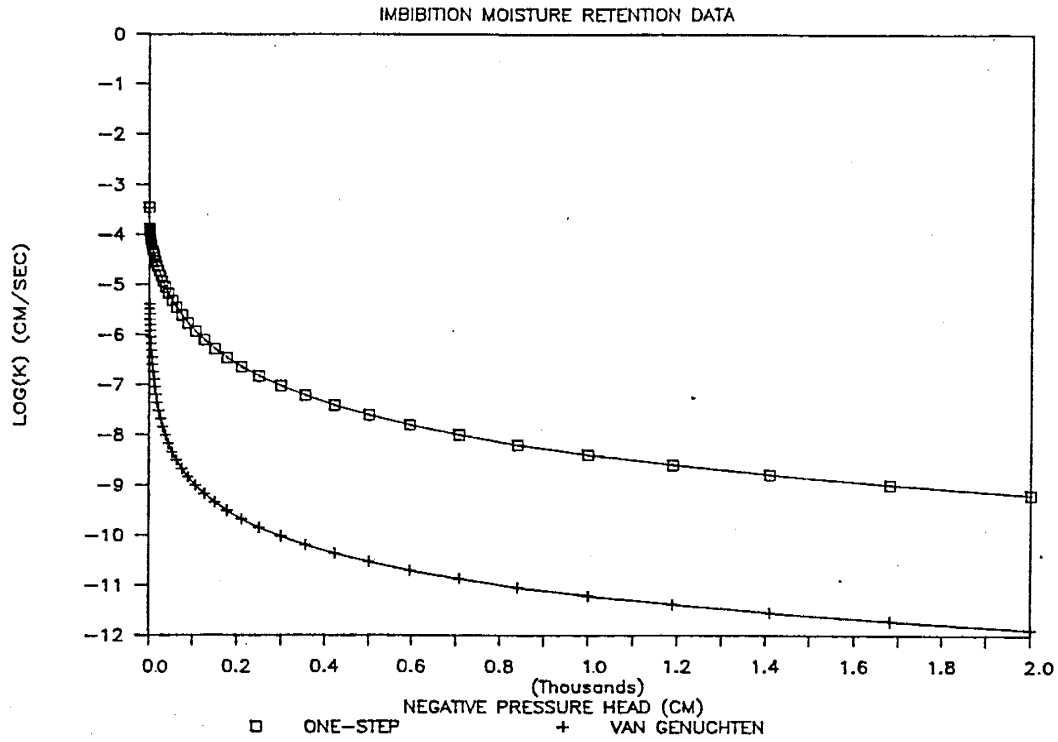

b.

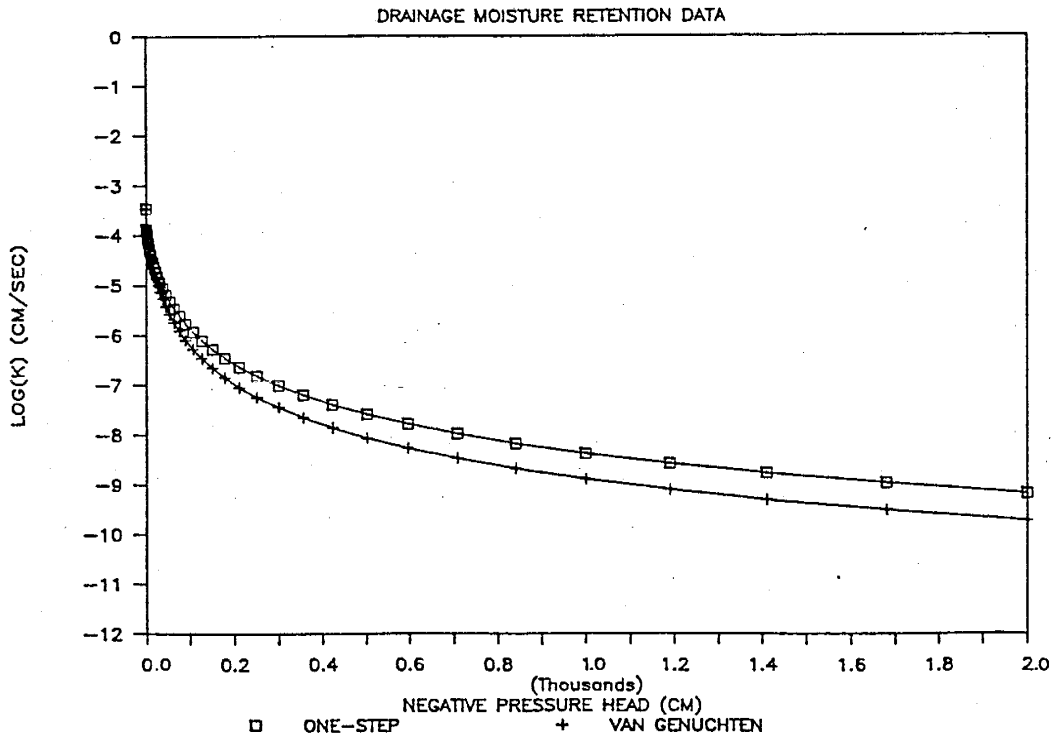

Figure 28. Comparison of unsaturated hydraulic conductivity curves for soil core sample 16-6-B24 calculated by van Genuchten's model (1980) using a) imbibition and b) drainage moisture retention relationships compared to one-step outflow test results (Kool, Parker, and van Genuchten, 1985).

One method to obtain an average or effective K-θ curve involves using all moisture retention data from a particular layer of interest as input to van Genuchten's code. A second approach is to tabulate each separate soil sample K-θ curve calculated by van Genuchten's code and take the average conductivity corresponding to a particular moisture content. The large amount of available moisture retention data make these approaches time consuming tasks; for example, there are sixty-nine (69) core samples from the piedmont slope facies (Appendix D).

An alternate method to find effective K-θ curves is applied in this research. The effective K-θ relationship is calculated by Mualem's theory (equation 13) using the computer program KREL.FOR (Appendix M1). Four different effective K-θ curves are calculated for the piedmont slope facies according to Mualem's theory (Program KREL.FOR). The four effective curves are compared with K-θ curves for selected samples from the piedmont slope facies calculated by van Genuchten's two-parameter model (1980) (Figure 29). The arithmetic mean θ_s, θ_r, and Ks are used for each effective curve. The arithmetic mean and mode α and n_v are used for two of the effective K-θ curves. According to Stephens and Rehfeldt (1985), the n_v parameter has the most effect on the K-ψ curve slope. The effect of n_v on the K-θ curve is not known. Therefore, the two extreme effective K-θ curve examples use the highest n_v and lowest n_v value found in the piedmont slope facies, with the corresponding α value for each sample (Table 6).

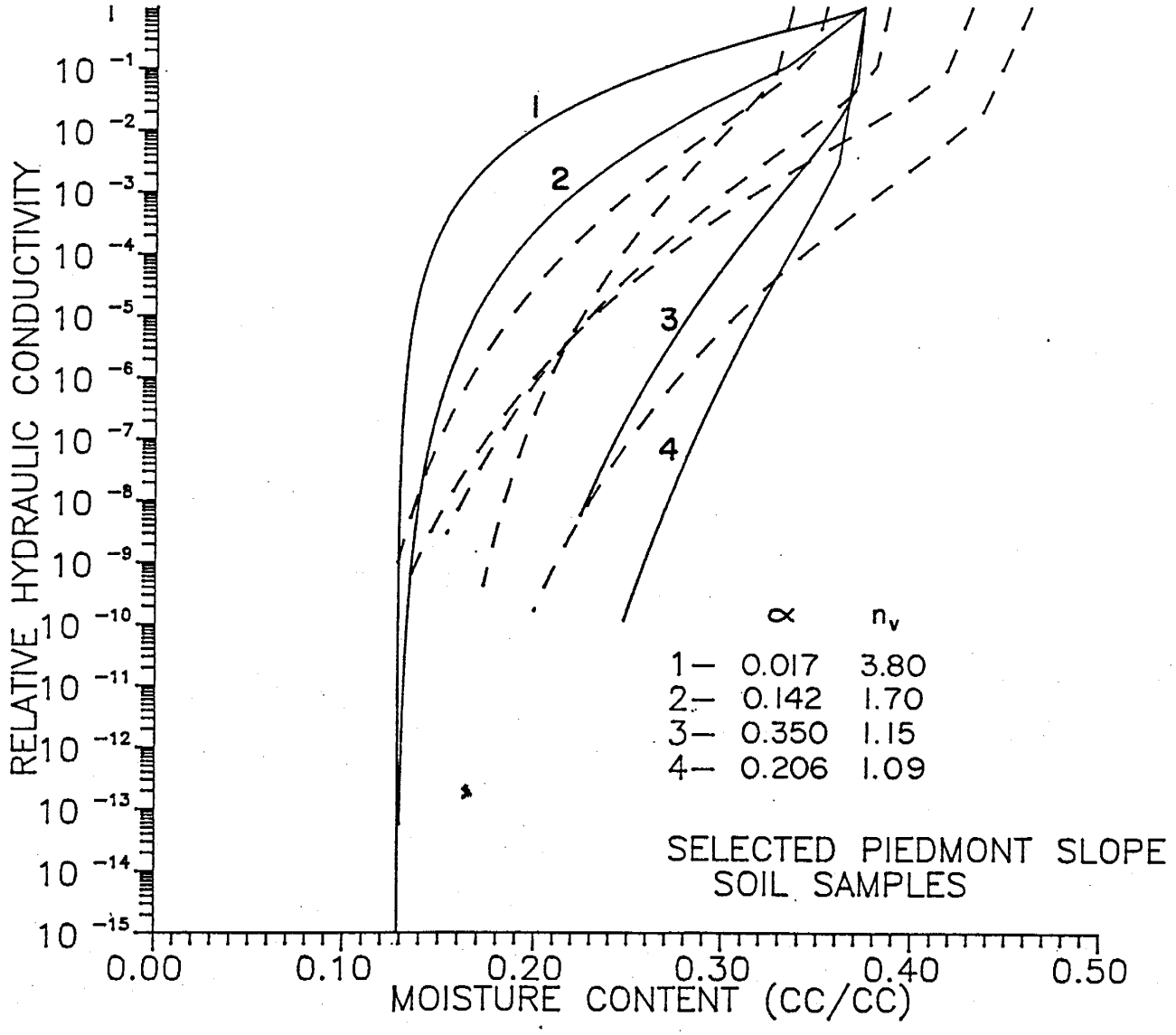

Figure 29. Effective unsaturated hydraulic conductivity curves for the piedmont slope facies calculated according to Mualem's theory (Program KREL.FOR) and unsaturated hydraulic conductivity curves for selected samples from the piedmont slope facies calculated by van Genuchten's two-parameter model (1980).

Table 6. Average fitted parameters used to calculate effective K-θ curves

CASE	α	n_v	θ_s*	θ_r
Piedmont slope:				
Arithmetic mean	0.142	1.70	0.374	0.128
Mode	0.350	1.15	0.374	0.128
High n_v	0.017	3.80	0.374	0.128
Low n_v	0.206	1.09	0.374	0.128
Number of samples	46	46	50	29
Fluvial sands:				
Arithmetic mean	0.087	2.70	0.334	0.052
Mode	0.050	1.45	0.334	0.052
Number of samples	15	15	20	9

α (1/cm), n_v (--) = van Genuchten parameters
θ_s = saturated moisture content (% vol)
θ_r = residual moisture content (15 bar moisture, % vol)
K_s = saturated hydraulic conductivity (m/day)

* saturated moisture content for imbibition considered as 90% of the actual measured mean value.

No study to determine the validity of such an approach is known (Stephens, pers. comm., 1988).

The van Genuchten α and n_v parameter values have an extreme effect on the shape of the calculated effective K-θ curve. The arithmetic mean and mode effective K-θ curves bracket some arbitrarily selected piedmont slope sample K-θ curves determined by van Genuchten's model except near saturation (Figure 29). The arithmetic mean curve exhibits higher conductivity values for any corresponding moisture content. The effective K-θ curve calculated with the largest n_v parameter results in the highest conductivity values for any moisture content while the effective curve calculated with the smallest n_v parameter has the lowest conductivities.

The finer textured piedmont slope facies are more conductive than the fluvial sands at any negative pressure greater than 40 cm (Figure 30b). There is over an order of magnitude difference between the two conductivity curves at 200 cm negative pressure. Due to the different moisture retention characteristics in the two materials, for any moisture content the fluvial sands are more conductive than the piedmont slope facies (Figure 30c).

4.4. STATISTICAL ANALYSIS

Saturated and residual moisture contents, saturated hydraulic conductivity, and van Genuchten parameters α and n_v are used to calculate unsaturated hydraulic conductivity relationships. A

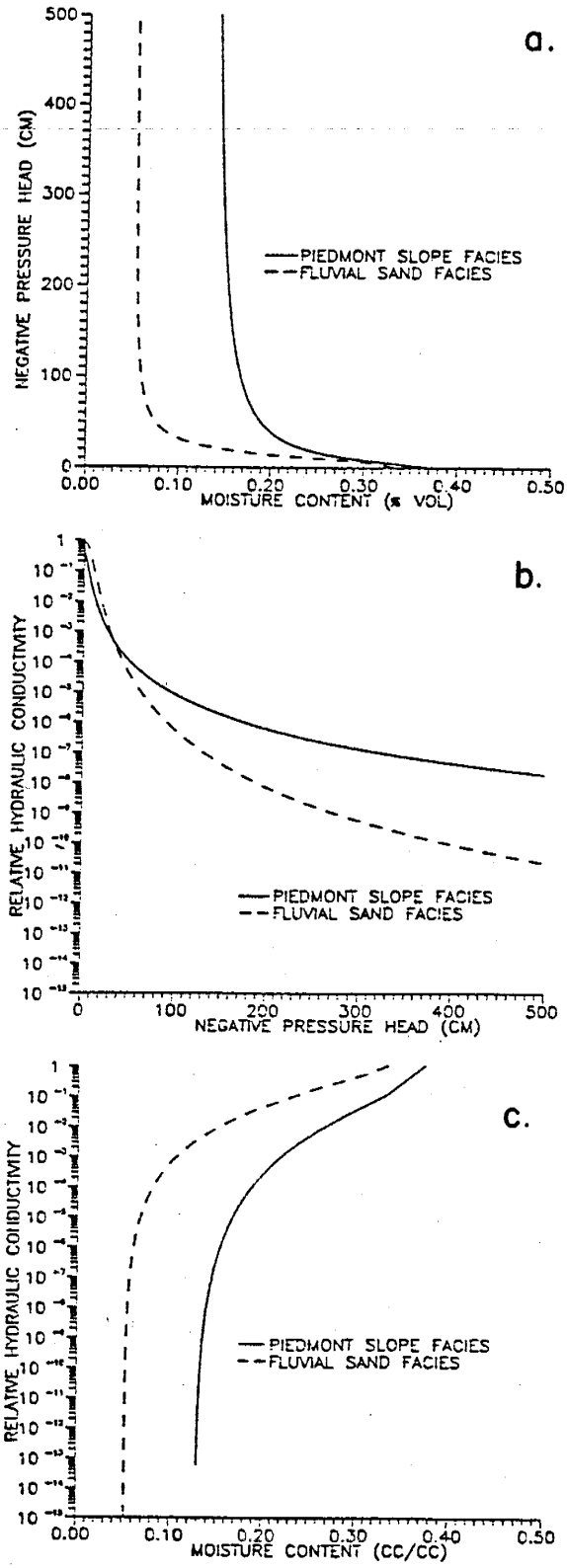

Figure 30. Piedmont slope facies and fluvial sand facies effective a) moisture retention and b,c)unsaturated hydraulic conductivity curves calculated using arithmetic mean hydrologic properties.

brief discussion of some statistical properties of these parameters follows. The stratified soil profile is divided into two layers for statistical analysis; the piedmont slope facies and fluvial sand facies. The upper piedmont slope facies is studied most intensively due to a larger sample population.

4.4.1. Frequency Distributions

The fractile diagram is a common method to determine if a distribution is normal or log-normally distributed. The value of parameters and their logarithm are arranged in separate columns by order of increasing magnitude. The cumulative probability for each observed value (v_o) is approximated by the relationship (i-0.5)/N where i is the observation number, and N the number of observations. Fractile diagrams are obtained by plotting cumulative probability versus the observed value. If the values or log of the values plot along a straight line, the distribution is either normal or log-normally distributed (Warrick and Nielsen, 1980).

Sixty-eight (68) soil core samples from the piedmont slope facies are utilized to determine the distributions of select hydrologic properties. Saturated moisture content (θ_s), 15 bar moisture content (θ_{15b}), saturated hydraulic conductivity (K_s), and the van Genuchten parameters α and n_v are all plotted on fractile diagrams. Calculations for constructing the diagrams are found in Appendix H.

K_s and θ_{15b} for the piedmont slope facies are log-normally distributed based on fractile diagram results (Figure 31). K_s is

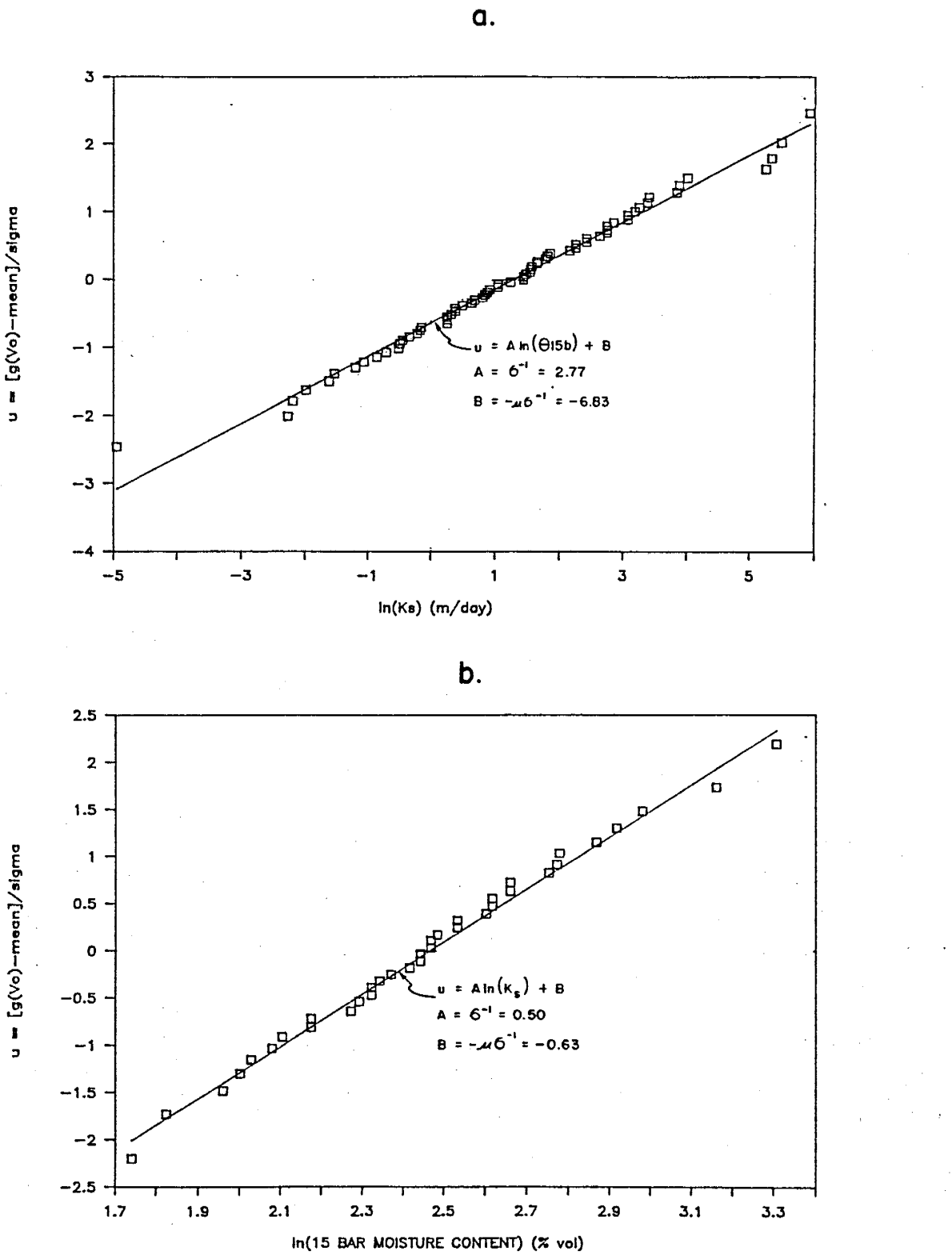

Figure 31. Fractile diagrams of log normally distributed saturated hydraulic conductivity and 15 bar moisture content in the piedmont slope facies.

generally accepted to be log-normally distributed (Kempthorne and Allamaras, 1986). Soil moisture content is often assumed to be normally distributed (Kempthorne and Allamaras, 1986), but Wang and Narasimhan (1988) found no conclusive frequency distribution for residual moisture content (θ_{15b}).

Saturated moisture content and fitting parameters α and n_v are neither normal or log-normally distributed (Figures 32, 33, 34). Frequency distributions for α and n_v are highly skewed (Figure 35), but there does not appear to be a linear correlation between the α and n_v values (Figure 36). Previous work suggests that the inverse of α is log-normal (Wang and Narasimhan, 1988). Perhaps these distributions reflect a mixture of more than one population, or they fit a different type of distribution (Gutjahr, pers.comm., 1988).

4.4.2. 95% Confidence Intervals

Confidence intervals are established for each hydrologic parameter (Table 3) by the following relationship:

$$\bar{x} +/- Z_\gamma(\sigma/N^{1/2}) \qquad (16)$$

where $\bar{x}$ is the mean, $Z\gamma$ the value for Z such that the area under a normal curve between $+Z\gamma$ and $-Z\gamma$ is γ, σ the standard deviation, and N the number of samples. If the number of samples is greater than 30, it is assumed the central limit theorem applies. Even if a population is skewed the mean distribution is approximately normal for a large population. If the sample population is less than 30, it is assumed the distribution is

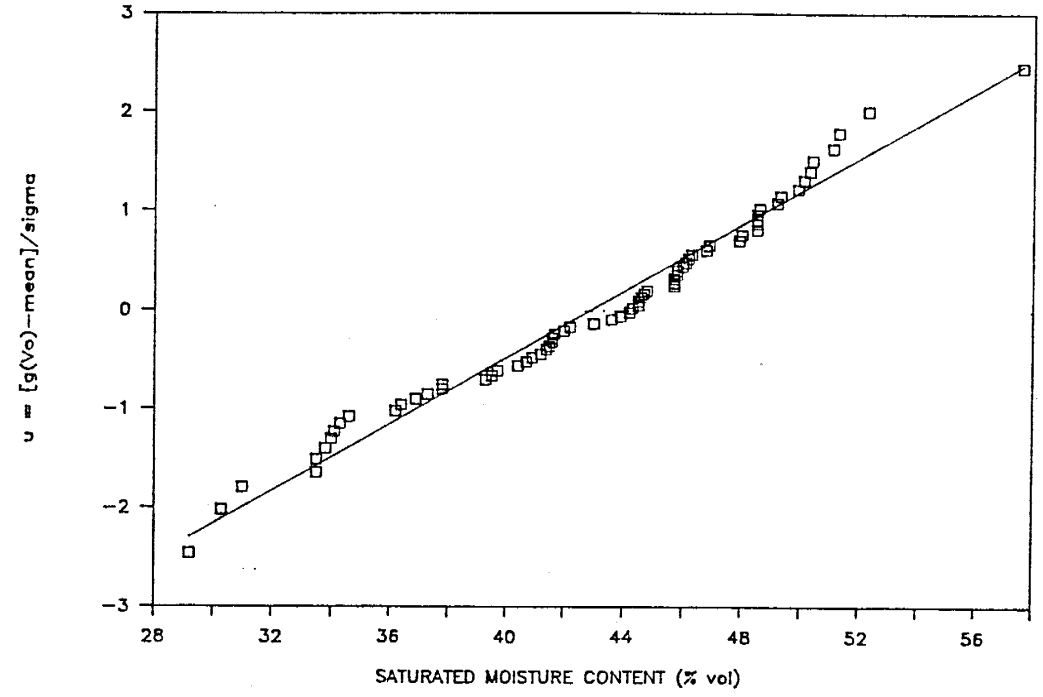

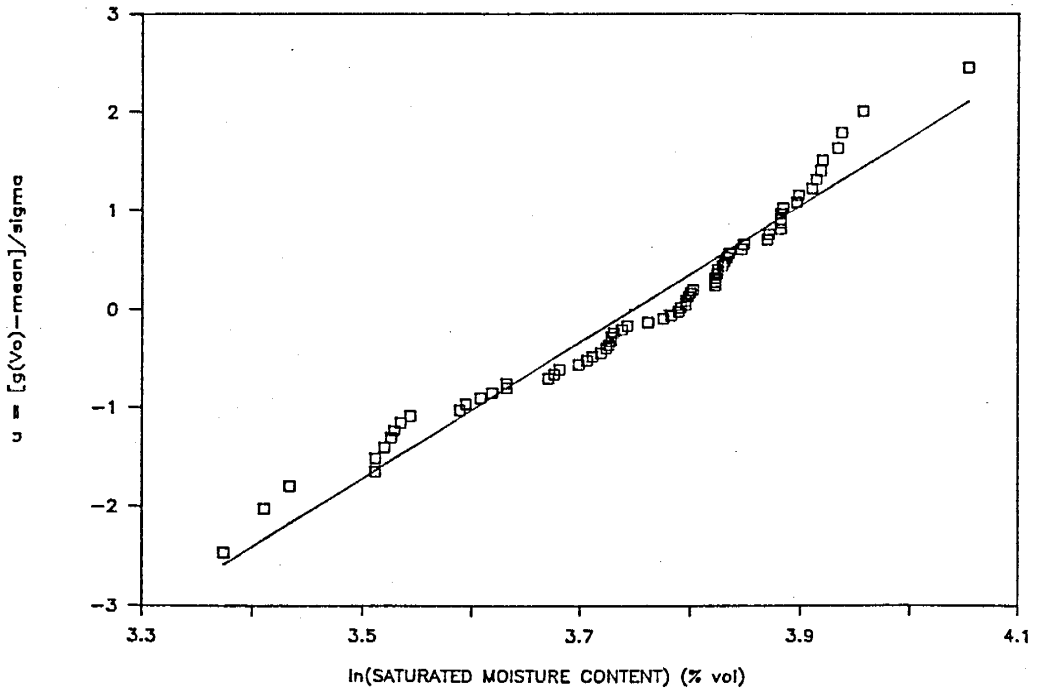

Figure 32. Fractile diagrams for saturated volumetric moisture content in the piedmont slope facies.

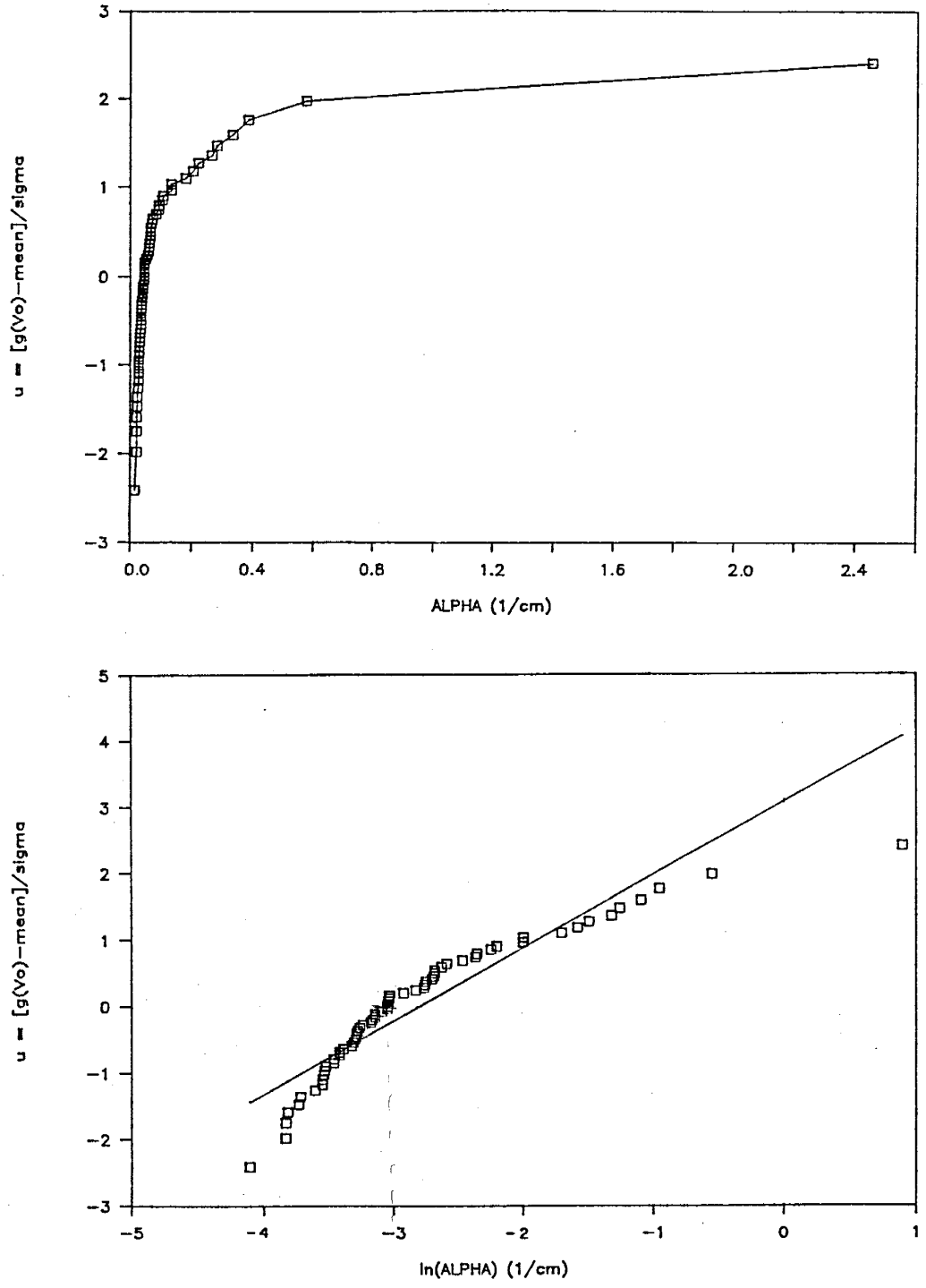

Figure 33. Fractile diagrams for parameter α in the piedmont slope facies.

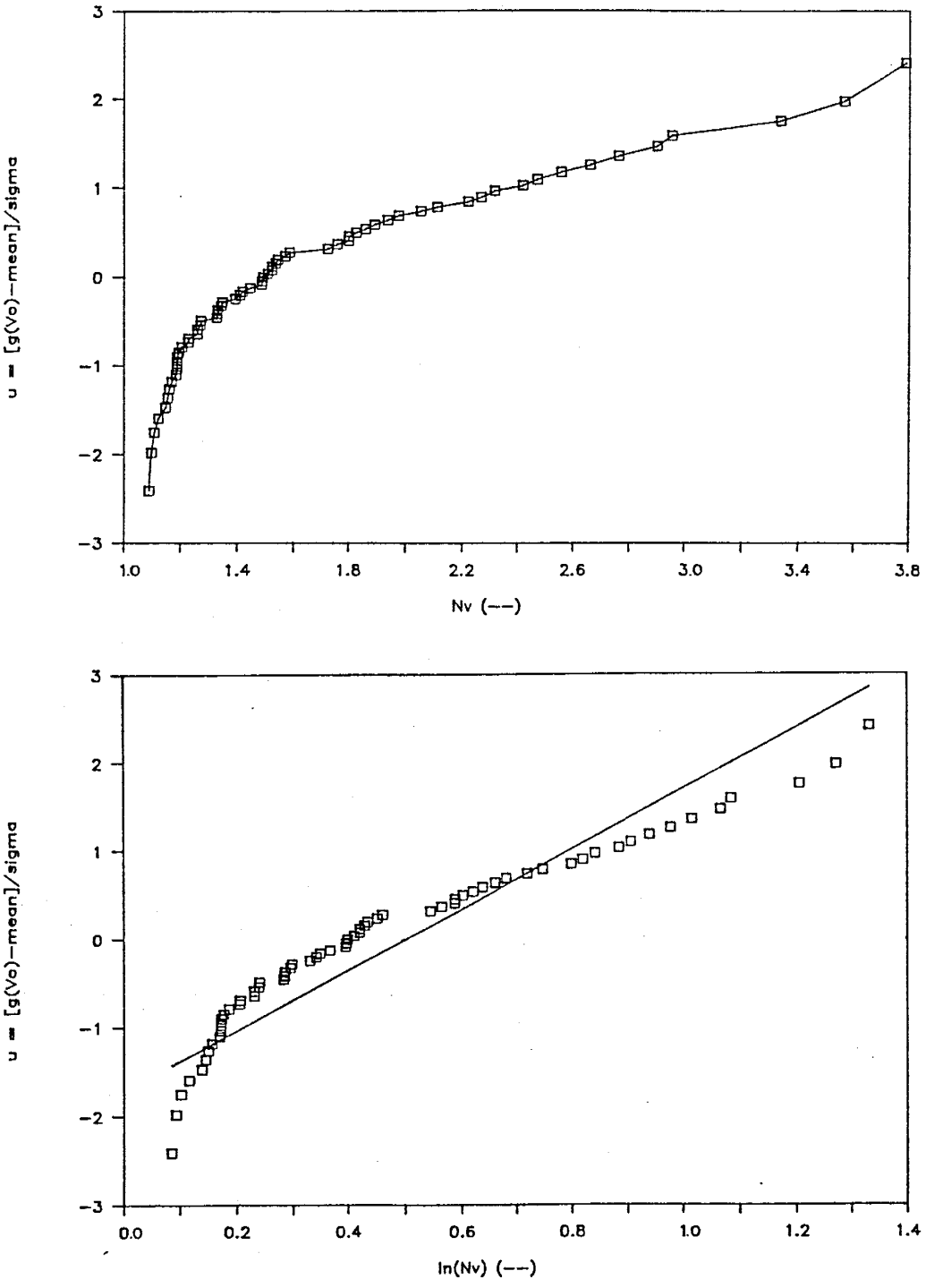

Figure 34. Fractile diagrams for parameter n_V in the piedmont slope facies.

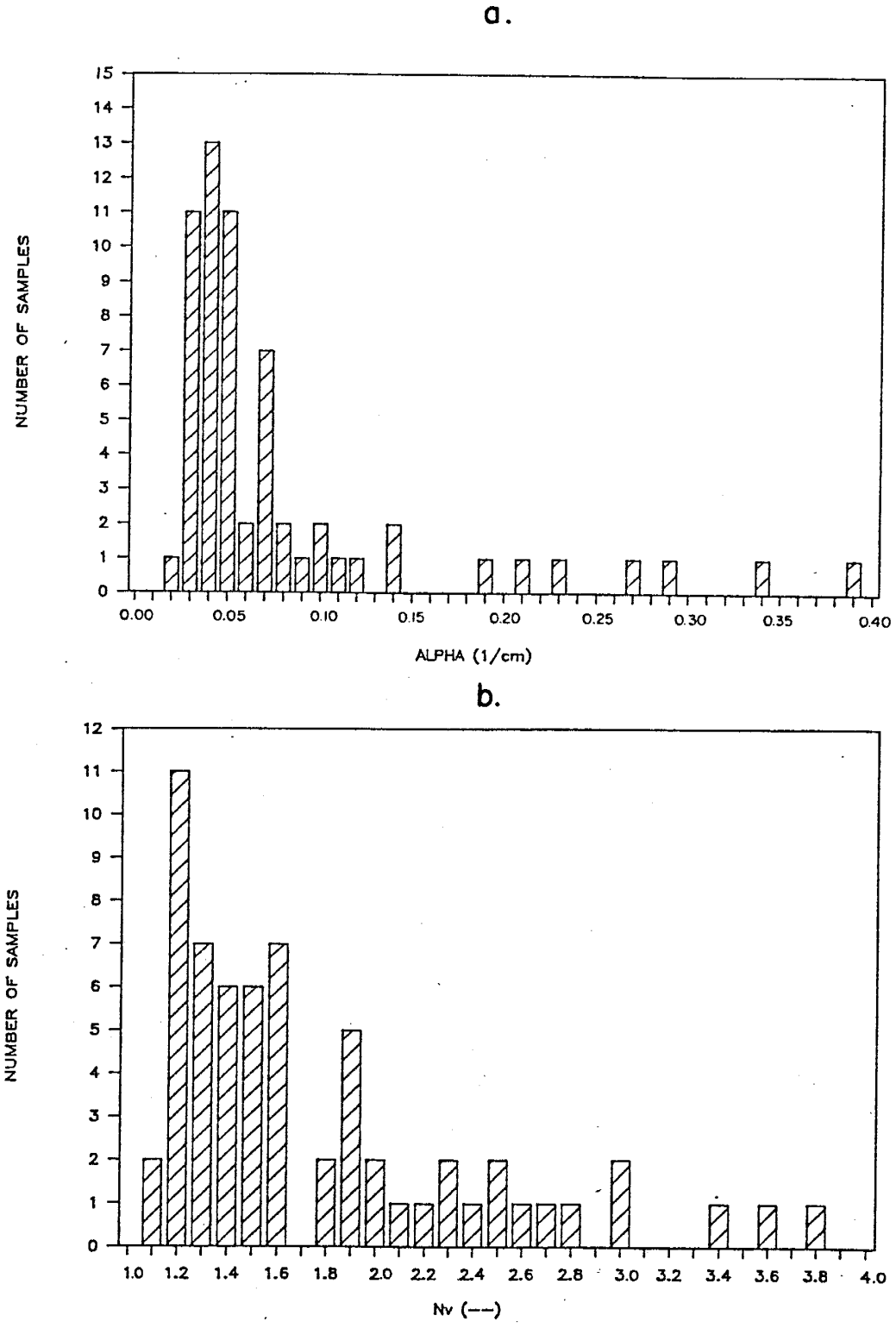

Figure 35. Frequency distributions for parameters a) α and b) n_v in the piedmont slope facies.

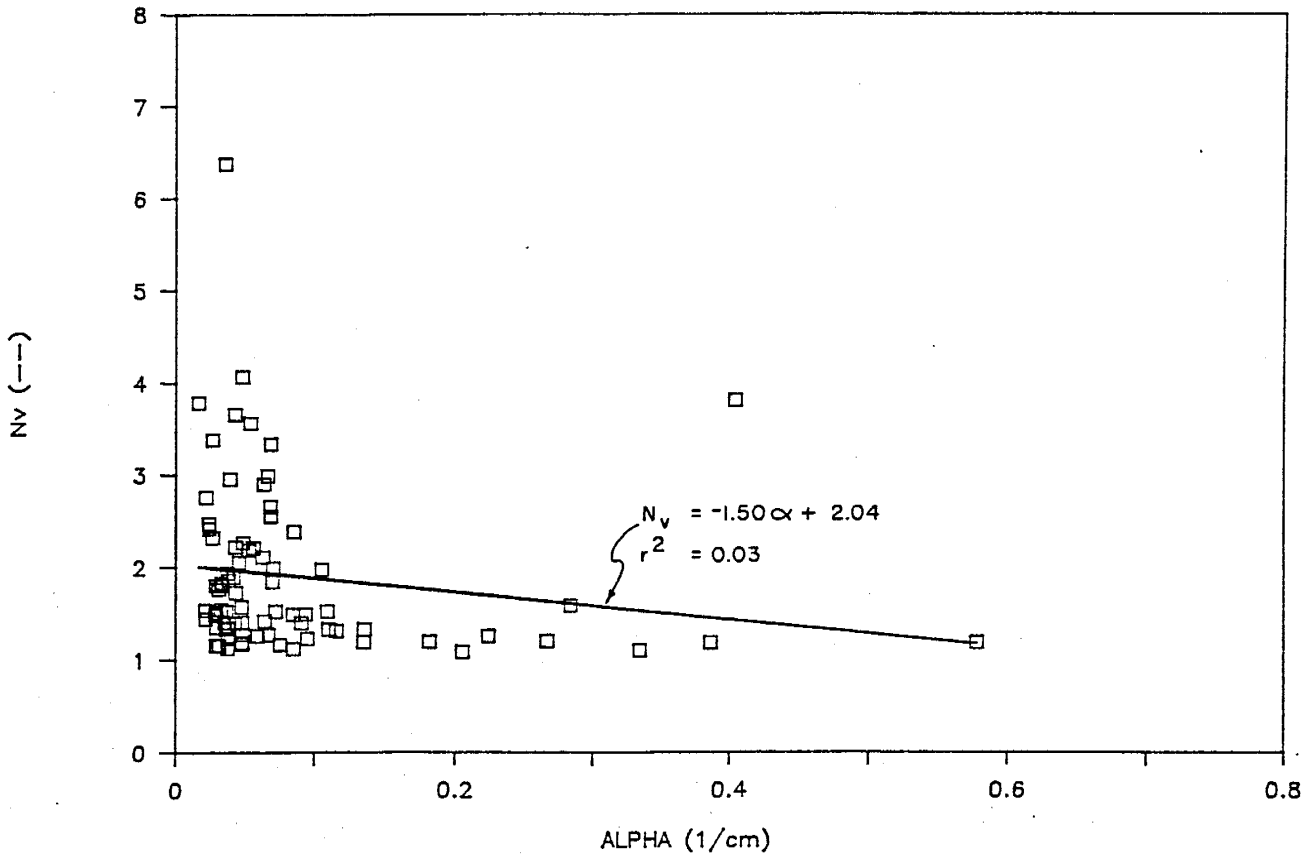

Figure 36. Linear regression between parameters α and n_v using 78 soil core samples from the piedmont slope facies and fluvial sand facies.

normal and t_γ from standard t-distribution tables replaces $Z\gamma$ in equation 16.

4.4.3. Sampling Requirements

The number of samples statistically required for 95% confidence that the true mean will lie within the estimated mean value plus or minus a specified value, D, is similar to equation 16, applying the same assumptions:

$$N = Z\gamma^2\sigma^2/D^2 \qquad (17)$$

where variables are previously defined.

K_S is by far the most uncertain measured hydraulic property studied. It would require almost 200 samples to designate the mean piedmont slope facies K_S within plus or minus 1x10-2 cm/sec, or within about 37% of the presently estimated K_S mean (Table 7). Eight hundred (800) samples from the piedmont slope facies are necessary to be 95% certain the mean is within about 20% of the estimated K_S mean.

An adequate number of samples are available in the piedmont slope facies for characterizing the selected hydrologic properties listed in Table 7 with the exception of K_S. The fluvial sands show similar results, but more fluvial sand samples are required to determine van Genuchten's n_V parameter within plus or minus 0.5.

4.4.4. Student's t-Test

Many differences are noted between the piedmont slope facies and the fluvial sand facies such as color, texture, in situ moisture content, variability as determined by the coefficient of variation,

TABLE 7. NUMBER OF SAMPLES REQUIRED FOR 95% CONFIDENCE

PROPERTY	PIEDMONT SLOPE FACIES			FLUVIAL SAND FACIES		
	D	N	# OF DATA POINTS	D	N	# OF DATA POINTS
THETAsat (%vol)	5 (%vol)	10	67	5 (%vol)	10	20
THETA15b (%vol)	2 (%vol)	16	35	2 (%vol)	5	9
Ks (cm/sec)	5.0E-03 (cm/sec)	800	66	5.0E-03 (cm/sec)	508	15
Ks (cm/sec)	1.0E-02 (cm/sec)	200	66	1.0E-02 (cm/sec)	127	15
ALPHA (1/cm)	0.1 (1/cm)	39	62	0.1 (1/cm)	4	15
Nv (--)	0.5 (--)	6	62	0.5 (--)	35	15

D = SPECIFIED RANGE
N = NUMBER OF SAMPLES STATISTICALLY REQUIRED FOR 95% CONFIDENCE THE TRUE MEAN WILL LIE WITHIN THE ESTIMATED MEAN PLUS OR MINUS THE SPECIFIED RANGE.
THETAsat = SATURATED MOISTURE CONTENT
THETA15b = 15 BAR MOISTURE CONTENT
Ks = SATURATED HYDRAULIC CONDUCTIVITY
ALPHA, Nv = VAN GENUCHTEN FITTING PARAMETERS
DATA POINTS = NUMBER OF DATA POINTS AVAILABLE

grain size, and uniformity coefficient (Tables 3,4). Statistically, the difference between the two soil types is quantified.

A Student's t-test assumes the parameters, or their logarithms, are normally distributed. The logarithms of K_s and θ_{15b} are the only properties studied which satisfy the requirement. Therefore, until more detailed distribution studies are conducted, the logarithm of K_s and the logarithm of θ_{15b} are the only properties which are appropriate to use in t-test analysis.

Statistical evidence supports the inference that significant hydrologic differences exist between the piedmont slope facies and fluvial sands. Comparing mean values, the fluvial sands are more conductive than the piedmont slope facies at the 0.05 level of significance according to t-test results. Similarly, the mean piedmont slope θ_r is greater than the mean fluvial sand θ_r at the 0.01 level of significance.

4.5. CONCEPTUAL FRAMEWORK FOR MODELING

The soil stratification is represented by three different conceptual models, for simplification in analytical modeling. First, the system is represented as a single layer which is a composite of piedmont slope facies and fluvial sand facies. Second, based on different geologic characteristics, the profile is divided into two layers, the upper piedmont slope facies and lower fluvial sand facies. Third, and most applicable to the

hydrologist, the profile is divided into five layers according to distinct changes in hydraulic characteristics.

4.5.1. One-Layer Model

A homogeneous layer of the stratified profile is obtained by combining all the layers into one layer. Mean hydrologic properties are calculated from all soil core samples from the center of the field site (Appendix I1). The data set consists of eight core samples from the piedmont slope facies and seven core samples from the fluvial sand facies. All soil core samples from the center of the field site are used. Lateral variations in hydrologic properties present in the field site are eliminated by only using samples from the center of the site at locations 15-15, 16-16, and 14-15.

4.5.2. Two-Layer Model

The most obvious conceptual model involves dividing the profile into two layers based on the two major geologic facies present. The distinct color change between the two facies determines which layer a sample belongs to; red brown silty piedmont slope material or tan fluvial sand. The approximate interface between the upper and lower facies ranges from 3.6 to 5.5 meters below datum, but it is a subjective division based on a color and texture change.

Mean hydrologic properties are calculated for each soil facies type. Analytic modeling efforts are focused on the center of the field site. Therefore, selected piedmont slope facies soil core samples from locations within the center 12m x 12m area

of the field site are used for the piedmont slope facies characterization to minimize lateral variations in hydrologic properties. All fluvial sand facies soil core samples and repacked core samples are used to characterize the fluvial sands due to a smaller sample population (Appendix I2).

4.5.3. Five-Layer Model

The third conceptual model divides the soil profile into layers based on hydrologic property variation. Regardless of color, the profile is split into five layers where hydrologic properties markedly change with depth.

Some diagnostic hydrologic properties from boreholes 15-15, 14-15, and 16-16 located in the center of the wetted area are shown in Figure 37. Locations of distinct hydrologic layers can be approximated based on changes with depth observed in saturated moisture content, log of saturated hydraulic conductivity, and particle size (10 and 50% passing). Fine particle size generally corresponds to a larger saturated moisture content and smaller $\ln(K_s)$. The most distinct hydrologic interfaces inferred by this data are located at 2.0, 3.2, 4.7, and 6.4 meters below datum. These interfaces roughly correspond to visually distinct layers shown in the geologic log (Figure 37). There is more variability that can be observed through visual geologic descriptions of the samples compared to variability in measured hydraulic properties. However, more of the visual geologic information is available.

Means of all hydraulic properties for the five distinct hydrologic layers are calculated, using selected soil samples

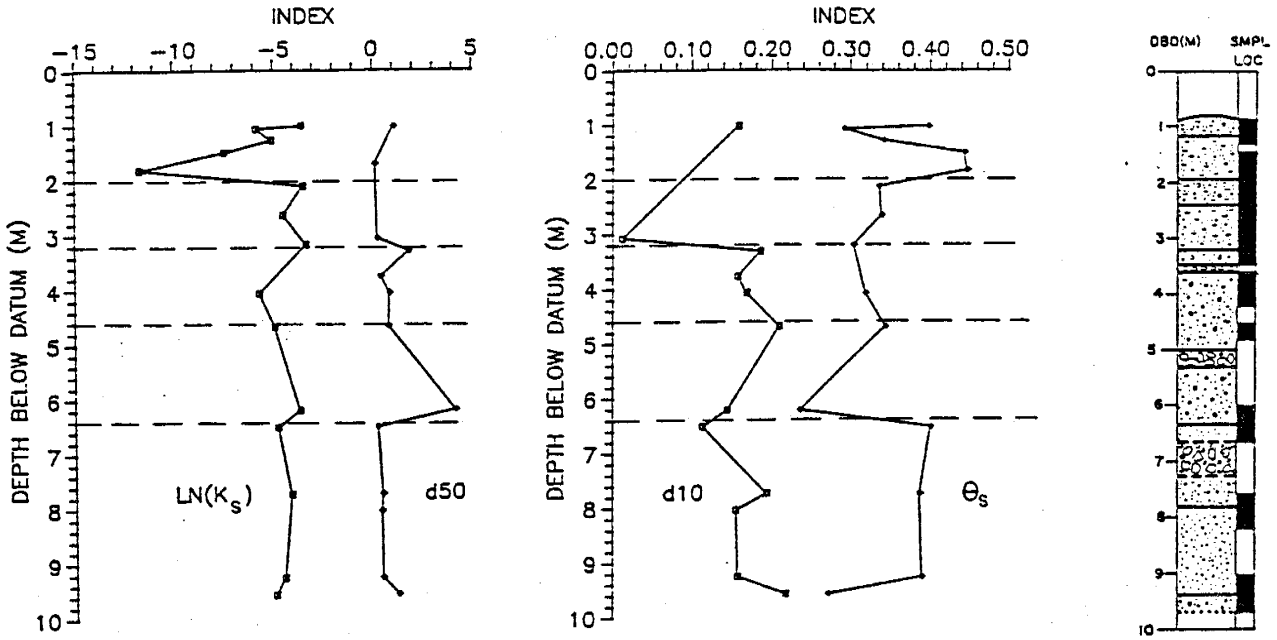

Figure 37. Compiled hydrologic data from locations 15-15, 14-15, and 16-16, in the center of the field site. $Ln(K_S)$ (cm/sec), saturated moisture content (cc/cc), and particle size parameters d_{10} and d_{50} (mm) are shown compared to the geologic log of station 15-15. Dashed lines represent boundaries between each layer determined by changes in hydrologic properties.

collected from each layer (Appendix I3). Table 8 summarizes the mean properties for each conceptual model. Averaging all the soil samples within a particular layer together removes the fine scale stratification. The result is a heterogeneous five layer system.

Table 8. Mean Hydrologic Properties used in Conceptual Models

Model	Layer Depth (mbd)	K_s (m/day)	θ_s (cc/cc)	θ_r (cc/cc)	α (1/cm)	n_v (-)
One-Layer	0.9-10.0	44	0.314	0.108	0.117	1.90
Two-Layer	0.9-4.6	36	0.374	0.128	0.142	1.70
	4.6-10.0	26	0.334	0.052	0.087	2.70
Five-Layer	0.9-2.0	235	0.363	0.198	0.061	2.08
	2.0-3.2	34	0.355	0.108	0.147	1.78
	3.2-4.7	74	0.291	0.055	0.087	2.05
	4.7-6.4	23	0.323	0.044	0.046	2.20
	6.4-10.0	17	0.337	0.033	0.067	2.71

mbd = meters below datum

5. FIELD EXPERIMENT DESIGN

The field site selection, preparation, system design, monitoring instrumentation, and monitoring strategies are briefly described in this section. Mattson (1988) explains these topics in more detail.

5.1. SITE SELECTION

Several criteria were used in defining an ideal location for the experimental field site. Favorable characteristics include depth to the water table exceeding a few tens of meters to eliminate capillary fringe effects; relatively high soil permeability to insure sufficient infiltration data within several years; a stratified soil profile with no unusual geologic features; close proximity to a water supply and electricity; convenient access for vehicles; fairly level topography with good drainage; favorable drilling characteristics; security from vandalism; and, sufficient distance from potable water supplies.

Three locations west of New Mexico Tech campus appeared to satisfy the above criteria. West of the three sites, a surficial boulder zone thickens, and to the east toward the Rio Grande River depth to the water table diminishes rapidly (Betson, 1984). Therefore, these sites were chosen for further investigation.

Several test boreholes were drilled in each locality to determine boulder zone thickness and ease in drilling.

The selected experimental field site is located next to the New Mexico Tech golf course in the extreme northeast corner of the Physical Plant boneyard. The surficial boulder zone is absent, although drilling is difficult through some cobbles and boulders found at depth. The site is fairly level; sufficient runoff from Socorro Peak is diverted by a large flood control dike to the east finished in 1963; the site has never been previously irrigated; and depth to water is about 24 meters.

5.2. SITE PREPARATION

The experimental field site was cleared of debris, and bermed on the eastern and southern edges to deter runoff. A five meter interval grid system was surveyed into position (Figure 15). A trailer was placed adjacent to the site for use as a field office.

Water was applied over a 10.5m x 10.5m area in the center of the field site, approximately 60 cm below the land surface. The area for the water application system was excavated using a backhoe, and final leveling was accomplished by hand. A thin layer (2 cm thick) of uniform sand was spread over the area, and twenty-one drip irrigation lines were placed on the flat surface, creating a grid of emitters spaced at 50 cm intervals. To prevent evaporation, plastic was placed over the drip lines.

Next, the drip system was covered with hay for insulation, then earthen fill to slightly above land surface. A second layer of plastic covered the fill to prevent infiltration of precipitation. The second plastic layer was covered by about 2 cm of soil (Figure 38).

5.3. SYSTEM DESIGN

City water used for the infiltration experiment is piped to a water tank at the field office (Figure 39). The tap water has a pH of 7.8 and hardness equal to 273 ppm $CaCO_3$ based on a major cation-anion laboratory analysis (Appendix J). pH of the water should be maintained at 6.5 to prevent carbonate precipitation in the drip line and pipe system (Bucks and Nakayama, 1985). This is accomplished by injecting muriatic acid (31.41% HCl) to the water tank prior to each pump run. Bacteria and algae should not create emitter clogging. Algae will not appear unless water is exposed to light, and the city water is previously treated with chlorine to control bacteria (Kieft, pers. comm., 1986).

Water flow to the emitters is controlled by a positive displacement pump which delivers a prescribed volume of water to the drip lines from the water supply tank. The pump is turned on for approximately one minute each hour by an electric timer. It is turned off when the water level in the water tank reaches the bottom float switch. After the pump is off, the storage tank is refilled to an upper float switch (Figure 39). This system

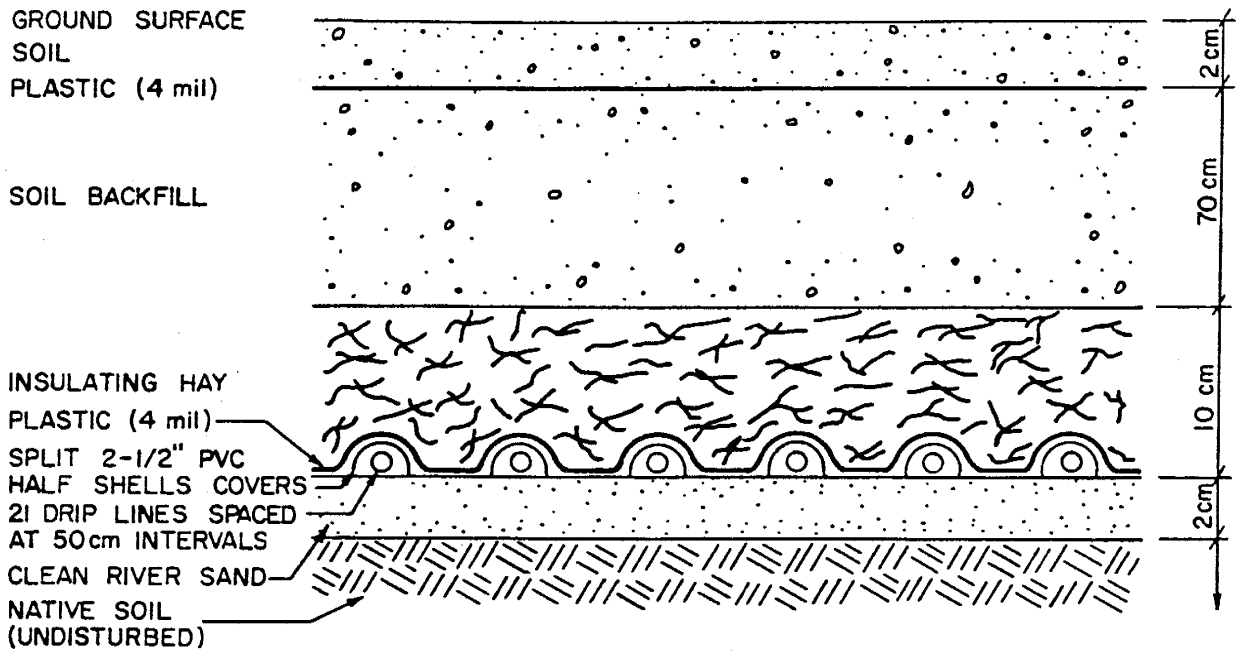

Figure 38. Cross-section through the irrigation plot.

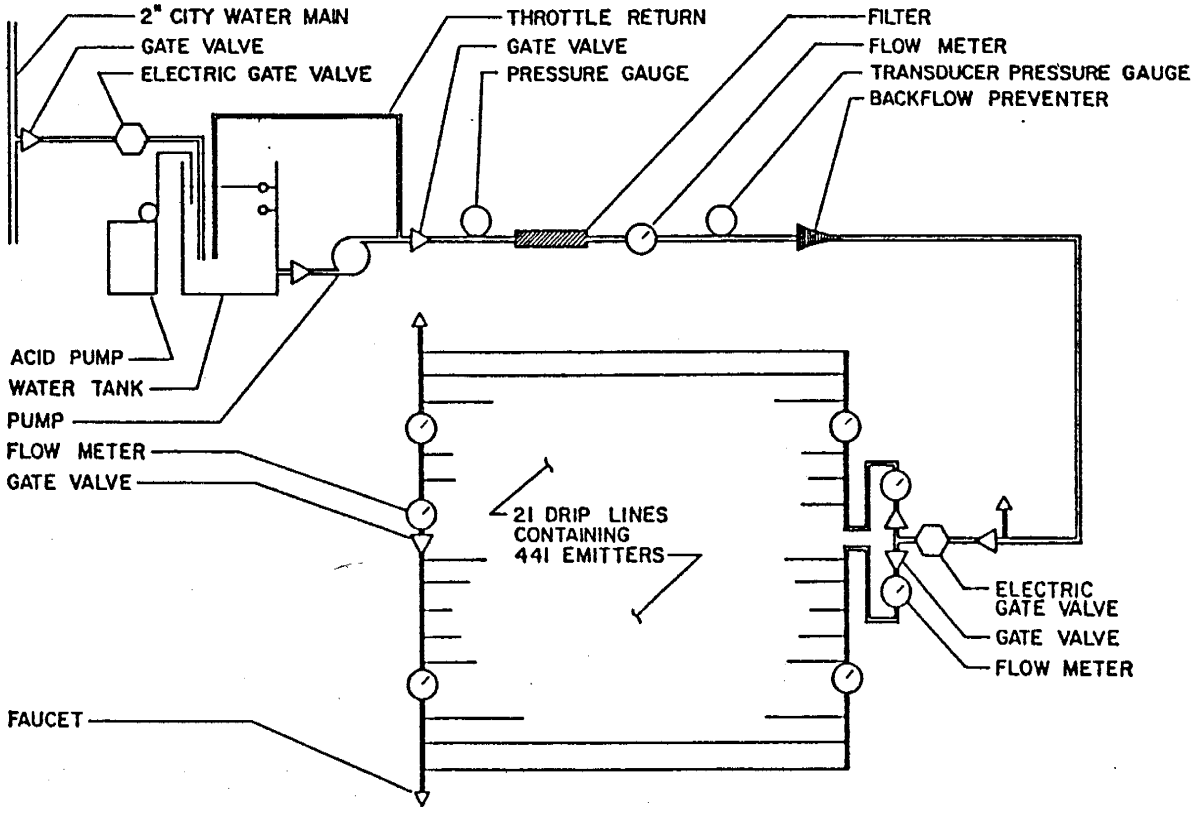

Figure 39. Schematic of water application system.

insures that a constant volume of water is pumped each cycle. Water flow through the drip lines is monitored by eight totalizing flow meters, used to check for uniform flow to the drip lines. Total volume of water pumped per run can be adjusted such that different magnitudes of the flux can be applied through the drip line grid. A data logger (CR7, Campbell Scientific, Logan, Utah) in the field office records pump run time and inline water pressure.

During each pumping cycle, about 36.0 liters (9.5 gal) of water are delivered to the plot, generating a constant flux rate of about $1x10^{-5}$ cm/sec. The flux was chosen based on preliminary laboratory results for saturated hydraulic conductivity. The lowest K_s found in the soil profile is roughly 100-fold more than the flux rate with the exception of minor clay lenses.

5.4. INSTRUMENTATION

Twenty-one soil-water monitoring stations are located in the field site (Figure 40). Each station is numerically identified, based on an X-Y grid system with the origin in the southwest corner. The exact location of each station was determined by surveying techniques (Table 9). Every monitoring station contains a neutron access tube and tensiometers installed in duplicate nests at approximately 50 cm intervals to 4 meters depth below land surface. Due to the stoney nature of the soil profile, instrumentation is installed in 20.3 cm diameter (8")

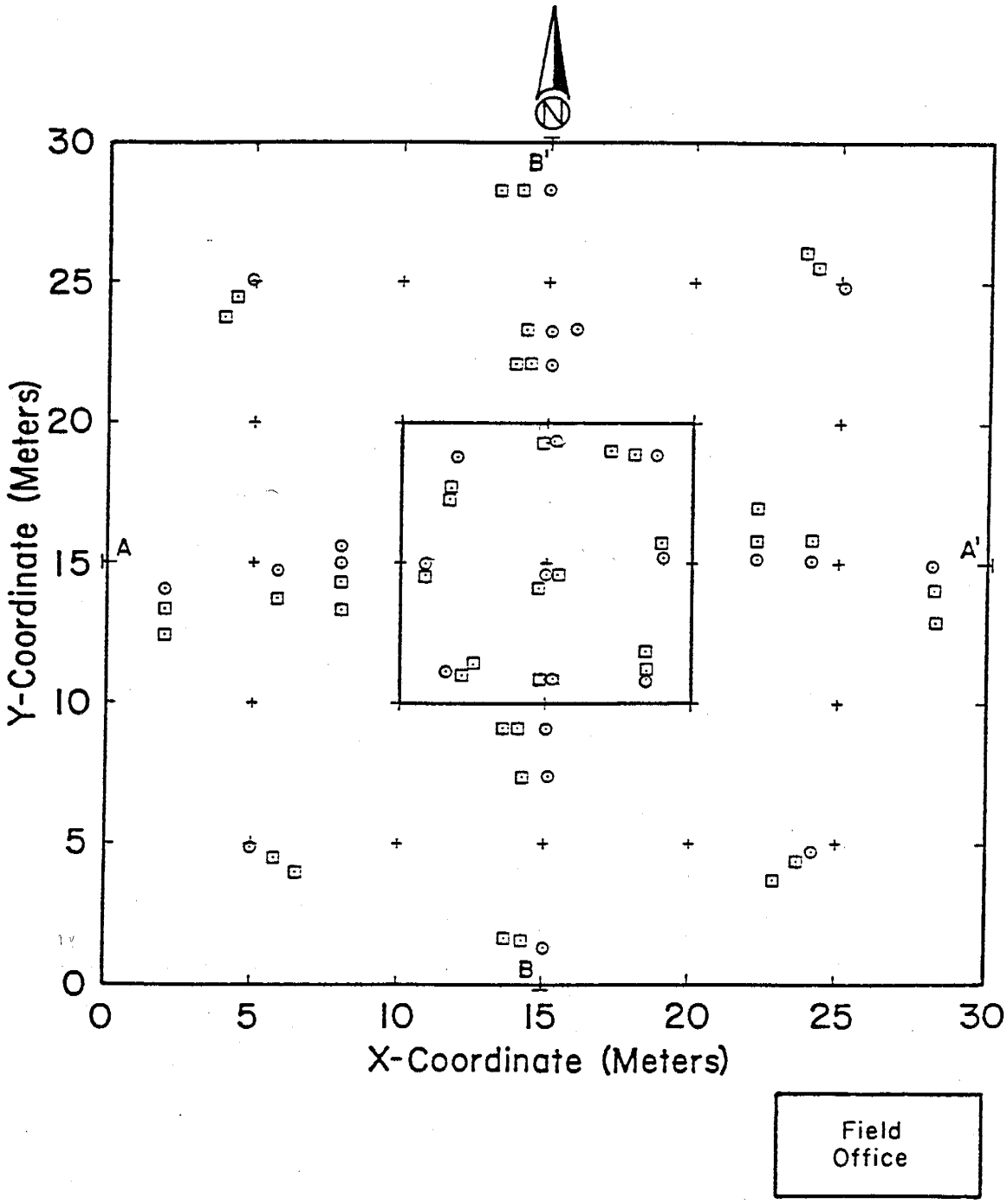

Figure 40. Plan view of field site. Circles represent neutron access tubes, squares show tensiometer nests, and crosses are five meter grid locations.

TABLE 9. PLAN VIEW STATION LOCATIONS

STATION		X-LOC (m)	Y-LOC (m)	STATION		X-LOC (m)	Y-LOC (m)
2-15	NT	2.00	14.05	15-19	NT	15.29	19.40
	A	2.00	13.30		A	15.00	14.35
	B	2.00	12.40		SWS	15.60	19.25
5-5	NT	5.00	4.95	15-22	NT	15.13	22.05
	A	5.70	4.50		A	14.45	22.10
	B	6.50	4.00		B	13.90	22.10
5-25	NT	4.95	25.05	15-23	NT	15.14	23.25
	A	4.35	24.45		A	14.25	23.30
	B	3.90	23.70	15-28	NT	15.00	28.27
6-15	NT	5.93	14.77		A	14.10	28.30
	A	5.93	13.70		B	13.30	28.30
8-15	NT	8.01	15.00	16-23	NT	16.00	23.39
	A	8.00	14.30	18-12	NT	18.44	10.90
	B	8.00	13.30		A	18.44	11.20
8-16	NT	8.01	15.57		B	18.44	11.90
11-15	NT	10.85	15.00	18-18	NT	18.73	18.87
	A	10.85	14.55		A	18.00	18.90
	SWS	11.05	15.35		B	17.20	19.00
12-12	NT	11.63	11.20	19-15	NT	19.00	15.22
	A	12.10	11.00		A	18.95	15.75
	B	12.50	11.40		SWS	19.00	14.72
12-18	NT	11.90	18.75	22-15	NT	22.21	15.17
	A	11.90	17.60		A	22.21	15.80
	B	11.70	17.35		B	22.21	17.00
15-2	NT	15.00	1.35	24-15	NT	24.05	15.12
	A	14.20	1.60		A	24.05	15.85
	B	13.60	1.70	25-5	NT	24.30	4.75
15-6	NT	15.10	7.40		A	23.60	4.40
	A	14.15	7.40		B	22.80	3.75
15-8	NT	15.05	9.14	25-25	NT	25.16	24.86
	A	14.10	9.14		A	24.25	25.60
	B	13.60	9.14		B	23.70	26.10
15-11	NT	15.28	10.90	28-15	NT	28.20	14.94
	A	15.00	10.90		A	28.25	14.10
	SWS	15.50	10.90		B	28.25	12.90
15-15	NT	15.00	14.59				
	E	15.40	14.59				
	S	14.75	14.10				

STATION = station descriptive location
NT = neutron access tube
A = tensimeter nest nearest NT
B = tensiometer nest furthest from NT
SWS = soil water sampler
X- and Y-LOC = station location on X-Y grid system determined by surveying techniques.

boreholes. Native soil was compacted in the borehole annulus using the drill rig or by hand. Layers of bentonite were placed between tensiometer intervals and at the land surface to deter channeling of infiltrated water.

Tensiometers were constructed using 3/4" PVC pipe, one bar standard ceramic cups, and a septum rubber stopper. Pressure head is recorded by a Tensimeter (Soil Moisture Measurement Systems, Las Cruces, NM), a pressure transducer connected to a hypodermic needle inserted through the rubber stopper. The depth of each tensiometer cup is determined by pre-installation measured marks on the tensiometer PVC pipe. Actual field depths were later checked by lowering a wire down the tensiometer pipe to the neck of the porous cup throat. Tensimeters were calibrated to both water and mercury manometers to insure coverage over the entire range of pressures likely to be encountered in the field. Mattson (1988) describes the calibration procedure.

Neutron logging occurs through a vertical 5 cm diameter x 9.1 m (30 ft) long thin wall aluminum access tube. The neutron probe (Model 503DR, CPN Corp., Pacheco, CA) emits fast neutrons radially into the soil where they are scattered and slowed, or thermalized, by various atomic nuclei. The number of thermalized neutrons measured by the probe is linearly related to the concentration of soil moisture (Hillel, 1980a). Neutron probe calibration is difficult in a stratified soil such as found at our field site. Also, neutron access tube installation methods increased calibration difficulties, inasmuch as backfilled soil

around the neutron tube is a mixture of soil types and recompacted bulk densities which may not be a representation of in situ conditions. See Mattson (1988) for a complete description of neutron probe calibration techniques and results.

5.5. MONITORING

Prior to the experiment start on January 29, 1987, the instrumentation was monitored weekly to provide background information from September 1986 through January 1987. After water began infiltrating into the soil, data was collected daily, bi-weekly, and then weekly as the experiment progressed, generating a broad data base to characterize transient and steady state flow patterns.

The data logger is connected to a weather station which records precipitation; wind speed; barometric pressure; humidity; and temperature of the soil, air, and water in water tank each hour. A standard class A evaporation pan situated on the field site is measured weekly.

6. FIELD EXPERIMENT RESULTS

The infiltration phase of the field experiment began at 1500 hours, January 29, 1987. The region beneath the irrigation plot is most likely to exhibit vertical downward flow of moisture, allowing comparison with one-dimensional analytic solutions which predict depth to the wetting front at early time. The McWhorter and Nelson analytical model is used to predict the field moisture content and rate of wetting front advance. Accordingly, only observations based on neutron probe measurements are included in the following discussion. Emphasis will be placed on water movement directly beneath the irrigation plot observed at the center five monitoring stations: 15-15, 12-12, 12-18, 18-12, and 18-18 (Figure 15).

6.1. INITIAL MOISTURE CONTENT CONDITIONS

The background moisture content in the soil profile beneath the irrigation plot was not constant in the months prior to our controlled infiltration experiment. Based on destructive sample results, there is indication of increased initial moisture content below the center area which occurred between spring 1986 and fall 1986 (see Section 4.3.2.). Background neutron logging data indicates that moisture contents increased in the fall of

1986 after large precipitation events. In situ moisture content decreased after the drip lines were emplaced and the irrigation plot was covered with plastic.

Three periods of time are studied for background moisture content behavior in the center region: 7/15/86 to 10/3/86, 10/3/86 to 12/5/86, and 12/5/86 to 1/23/87. Moisture contents at the end of each time period are subtracted from moisture content at the beginning of that time period, to determine the change in moisture content for that period. A positive change in moisture content represents net wetting for that time period and negative changes show regions of drying (Figure 41). The excavated plot elevation is located at an approximate elevation of 0.86 meters below datum.

All stations show significant wetting occurred during late summer and fall 1986 (July through September) from 2 to 4 meters below datum (Figure 41). The center 10.5m x 10.5m irrigation plot was excavated during this time and several centimeters of rain fell throughout the late summer (Appendix F). Infiltration of this precipitation results in increases of volumetric moisture content near the surface of the excavated plot up to 8.5%. At greater depths, another region of wetting is located from about 6 to 8 meters below datum. Moisture content increases at these depths may be due to an earlier infiltration event.

Throughout the late fall (October through November), net drying took place at stations 12-18 and 18-12 (Figure 41). Downward movement of previously infiltrated water is apparent at

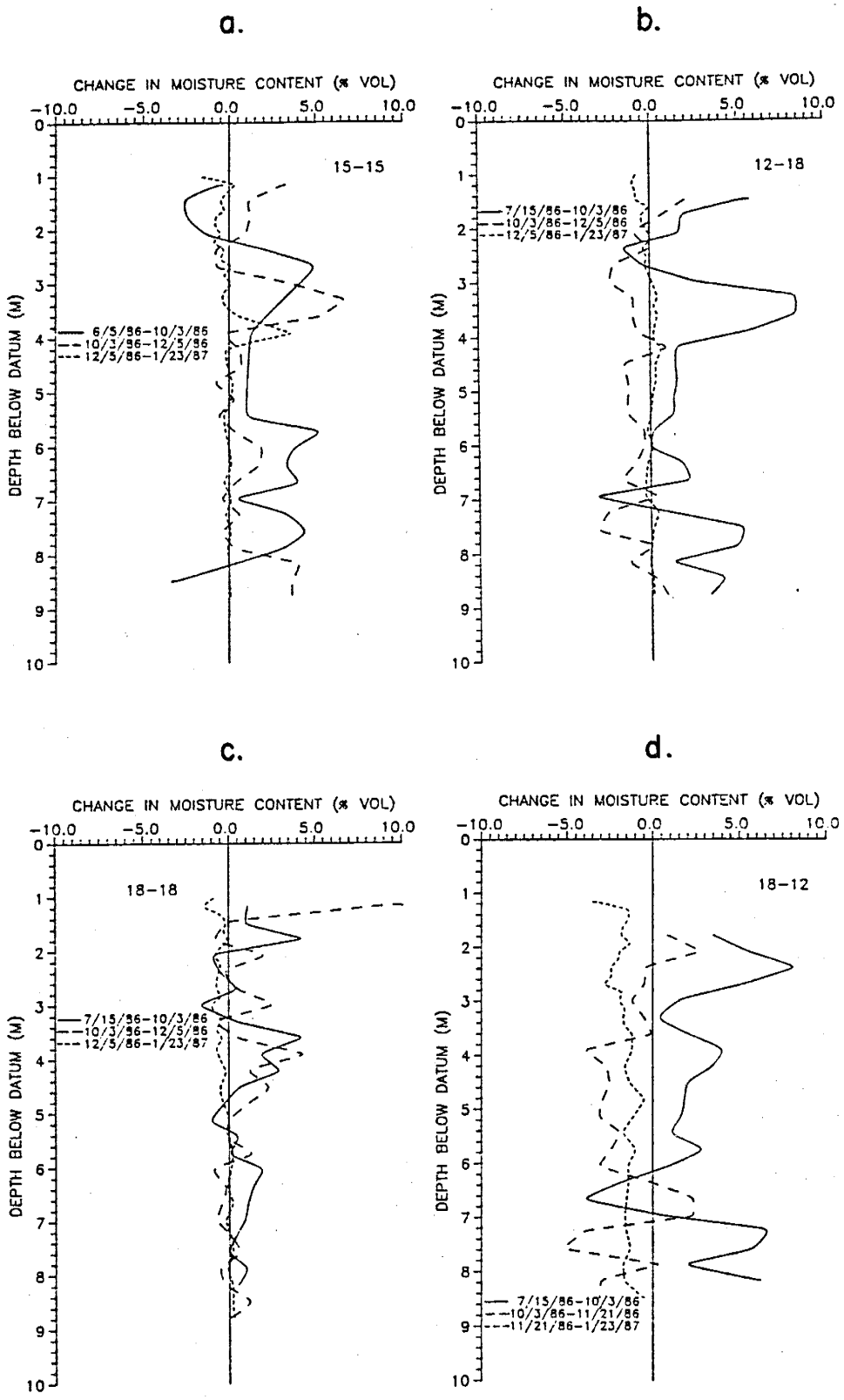

Figure 41. Change in volumetric moisture content before the experiment began at four of the center stations; a) 15-15, b) 12-18, c) 18-18, and d) 18-12.

stations 15-15 and 18-18 where moisture redistributes in the late summer redistributes, and wetting proceeds slightly deeper. A 10% increase in moisture content at one meter below datum at station 18-18 (Figure 41c) coincides with a large precipitation event which took place on 10/21/86 (Appendix F). Because station 18-18 is located at the lowest elevation before final leveling of the excavated plot, rainfall tended to pond in the northeast corner of the excavated pit. Infiltration of ponded water in the northeast corner of the plot during the fall may explain why wetting occurred at station 18-18 while drying took place at the other center monitoring stations.

The drip irrigation system was emplaced by 11/25/86, and the excavated plot filled in. Plastic covering the emitters minimizes evaporation, and plastic at the land surface prevents further infiltration of water. From December 1986 through January 1987, temporal variations in moisture content decreased significantly (Figure 41). Near zero changes in moisture content occurred during the winter, with some downward moisture movement evident at station 15-15 at 4 meters below datum. The two layers of plastic and the earthen fill account for smaller changes in moisture content during the winter months.

Immediately before the infiltration experiment began, the initial moisture content present in the first four meters below datum was higher than moisture content below 4 meters depth (Figure 42). Note that this region roughly coincides with the zone of piedmont slope facies which has finer particle size and a

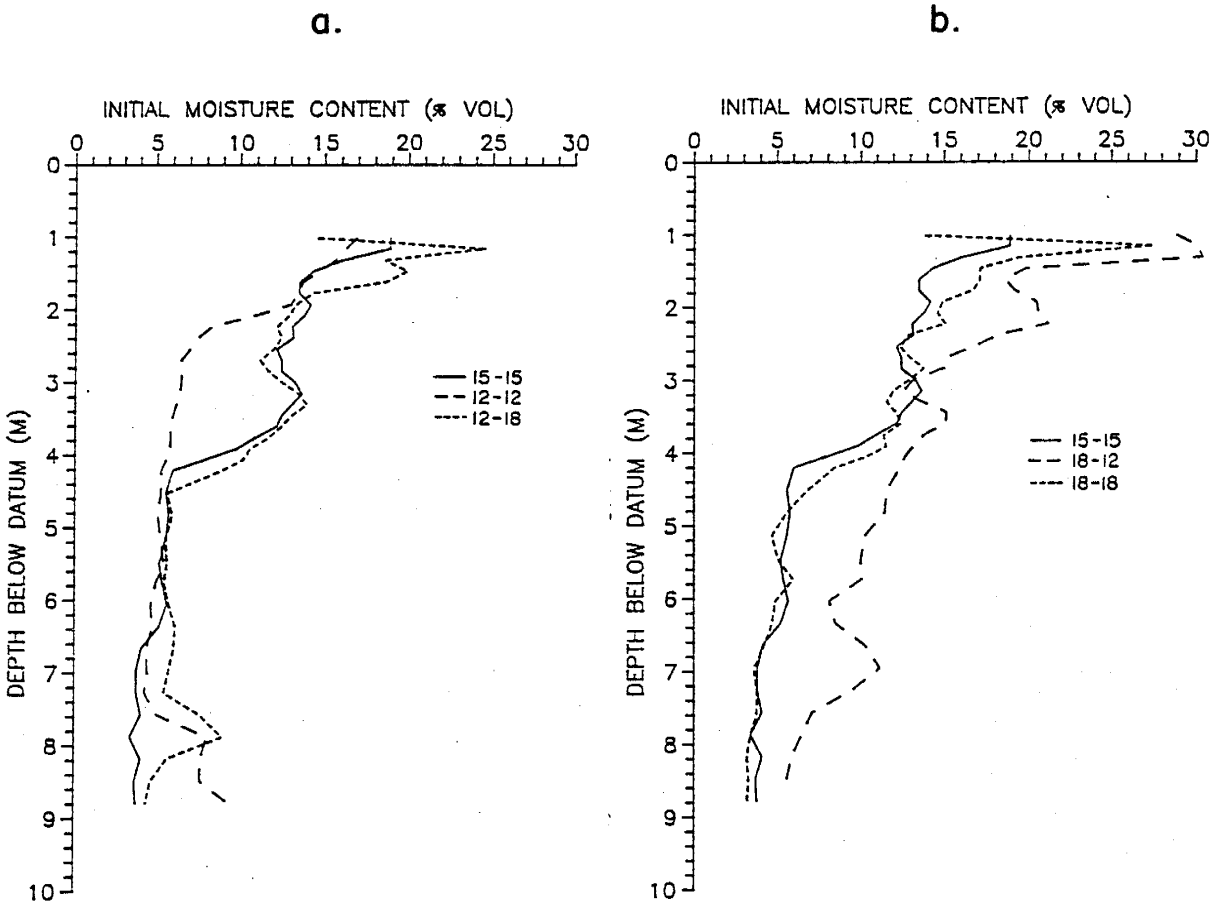

Figure 42. Initial volumetric moisture content five days prior to the experiment start.

higher average residual moisture content (Tables 3,4). The central stations have similar initial moisture content profiles with the exception of 12-12 and 18-12. Station 12-12 was the driest initially and station 18-12 was initially the wettest. According to particle size analyses and visual geologic descriptions, there is no significant textural difference between station 12-12 and station 18-12. In general, stations on the east half of the irrigated plot (18-18, 18-12) are initially wettest due to predominance of previously ponded conditions in that region.

6.2. WATER APPLICATION RATE

The flux of water applied to the soil profile during the first 60 days of infiltration is shown in Figure 43. The three mean flux rates which occurred for the first 60 days are indicated by solid lines (Figure 43). The three mean flux rates for 60 days are applied in analytic modeling.

An unfortunate leak occurred in one of the emitter line connections to the water supply manifolds located in the north-east corner of the irrigation plot from days 26 to 39 (Figure 43). Consequentially, we estimate the infiltration rate through the emitters was reduced by one third during this 14 day period (Mattson, 1988). For simplicity in calculations, Mattson assumes the flux remained uniform in the irrigation system during the period of leakage. More realistically, the plumbing leak

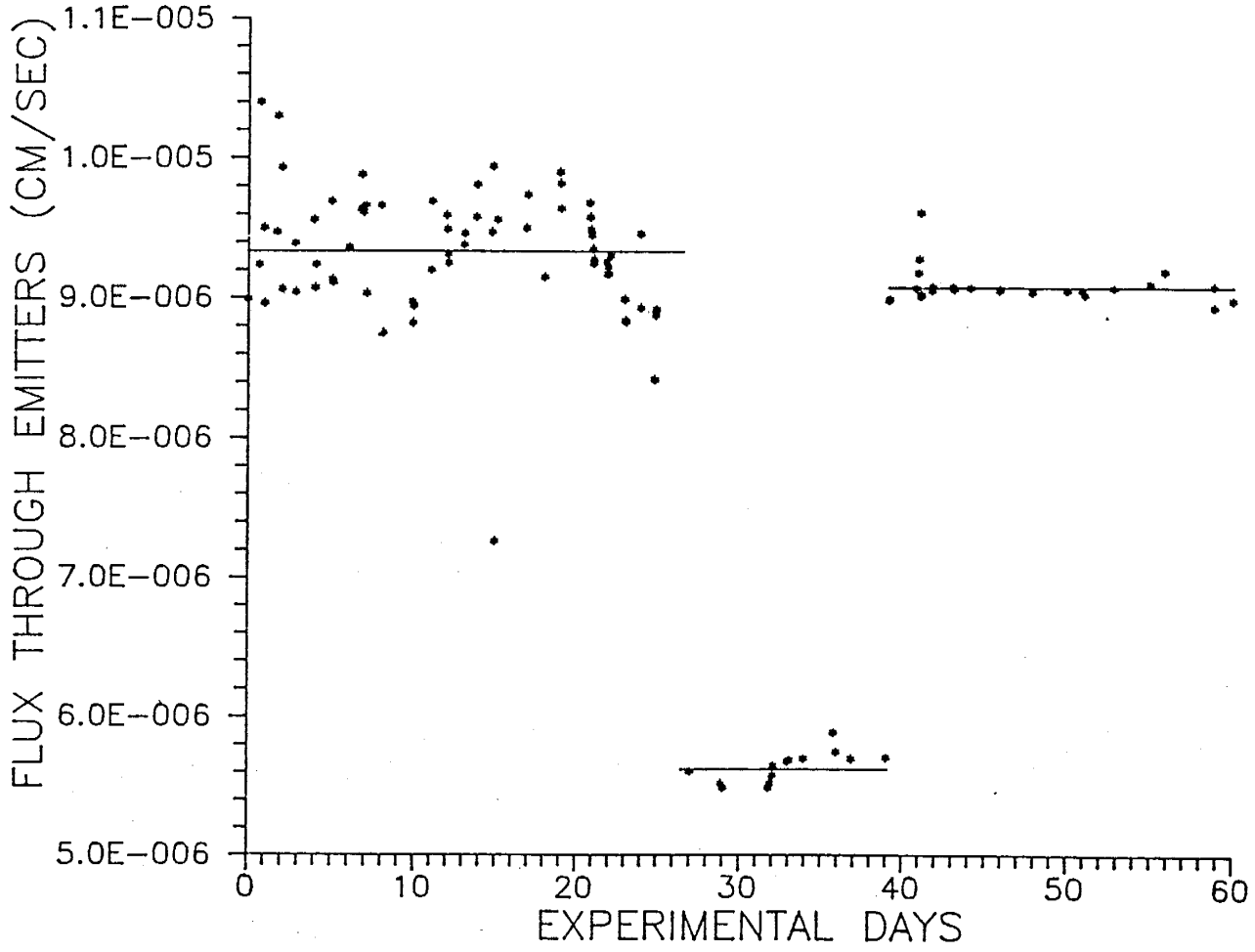

Figure 43. Flux through the emitters for the first 60 days of infiltration. Dots show actual flow and horizontal lines indicate three mean flux rates.

probably created non-uniform flow paths in the irrigation system, thus the pattern of flow during leakage is unknown.

6.3. MOISTURE MOVEMENT

Wetting front locations and rates of advance of the wetting front are determined by neutron logging moisture content data. Water content profiles from each monitoring session are used to determine the depth of greatest moisture content gradient, ie. the wetting front location. Several examples of wetting front locations determined by this method are shown in Figure 44. This visual, graphical method is arbitrary at times due to several possible depths where the moisture content versus depth curve is the steepest. The location of the wetting front is shown more clearly when each day of neutron logging data is graphed simultaneously. Next, the rate of wetting front advance is calculated from the change in wetting front location per change in time. All moisture movement observations from the center five monitoring stations are compiled in Appendix K.

For the first 10 to 25 days of infiltration, the wetting front location advanced at a fairly constant rate. The front initially advanced uniformly to depths of 2 to 7.5 meters below datum, depending on location (Figures 45a-49a). The average rate of downward movement for the first four meters was 0.17 m/day, and then the rate decreased to 0.07 m/day from 4 to 8 meters below datum (Table 10).

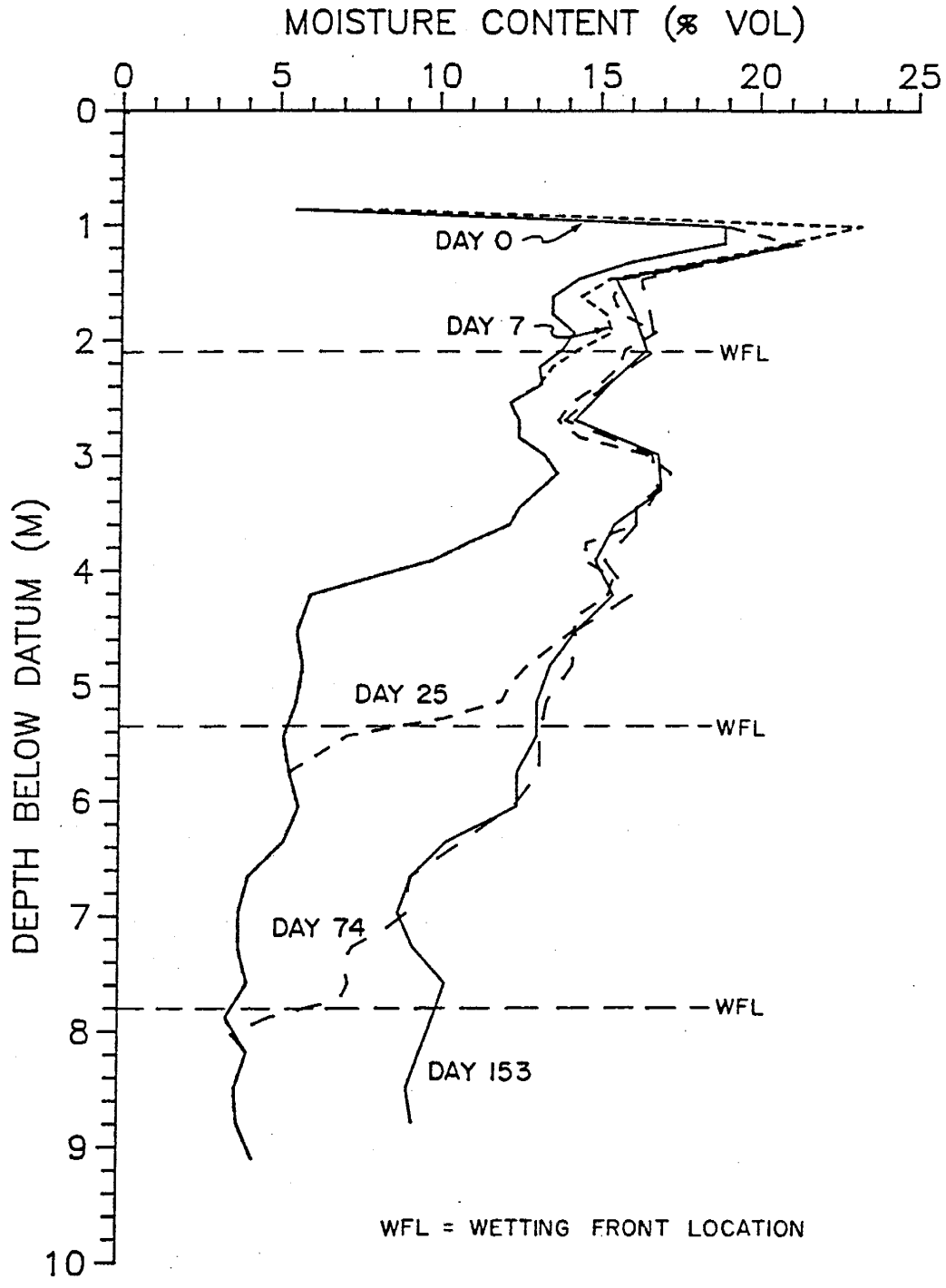

Figure 44. Moisture content profiles for selected days after infiltration began at station 15-15. Wetting front locations are determined from graphs such as this.

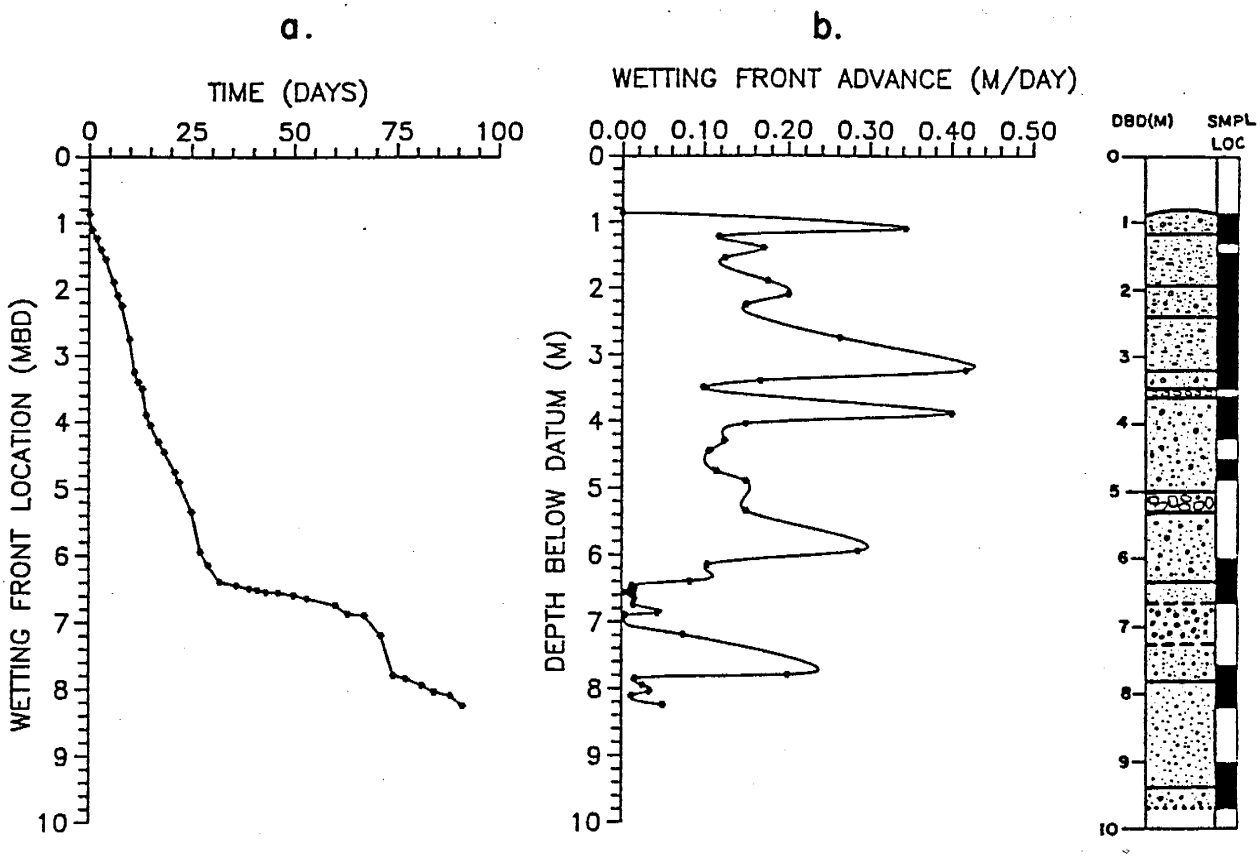

Figure 45. a) Wetting front location, b) rate of wetting front advance, and the geologic log for station 15-15.

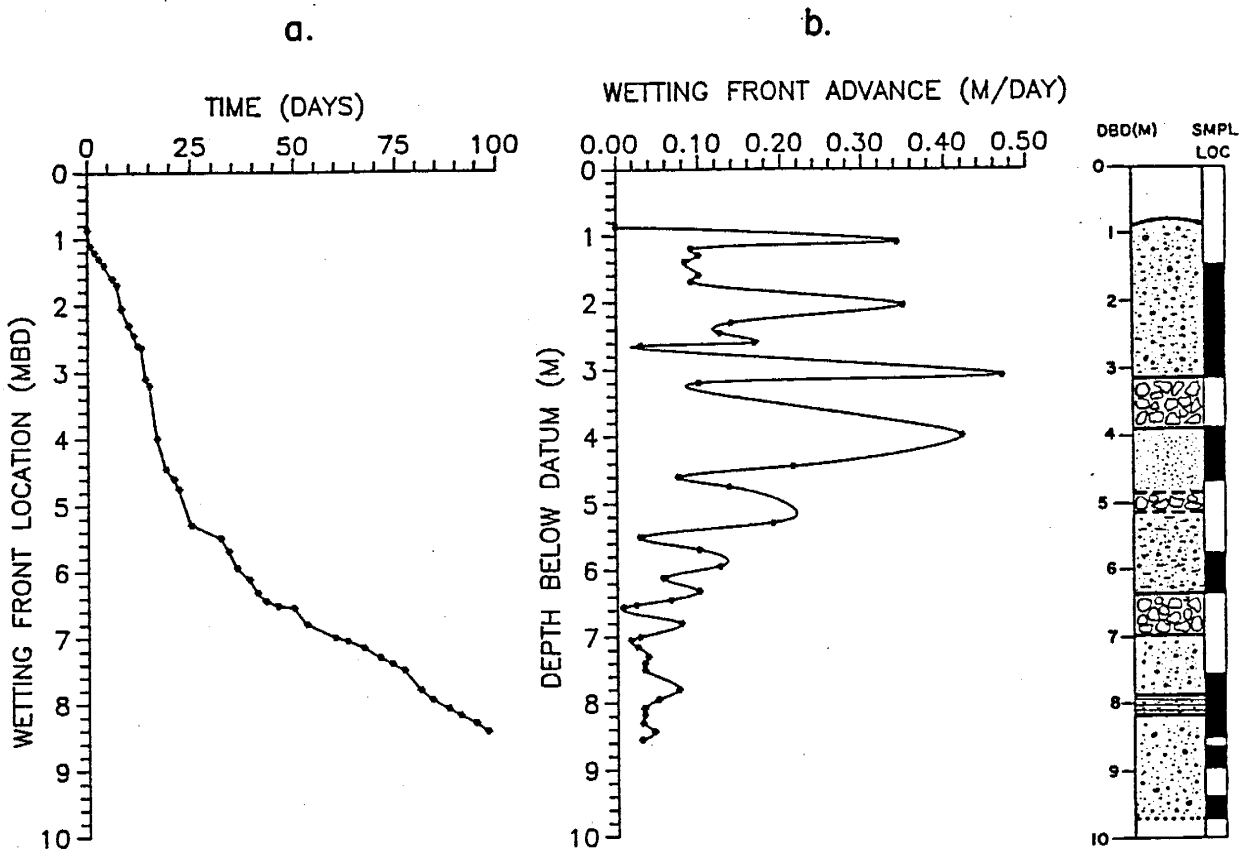

Figure 46. a) Wetting front location, b) rate of wetting front advance, and the geologic log for station 12-18.

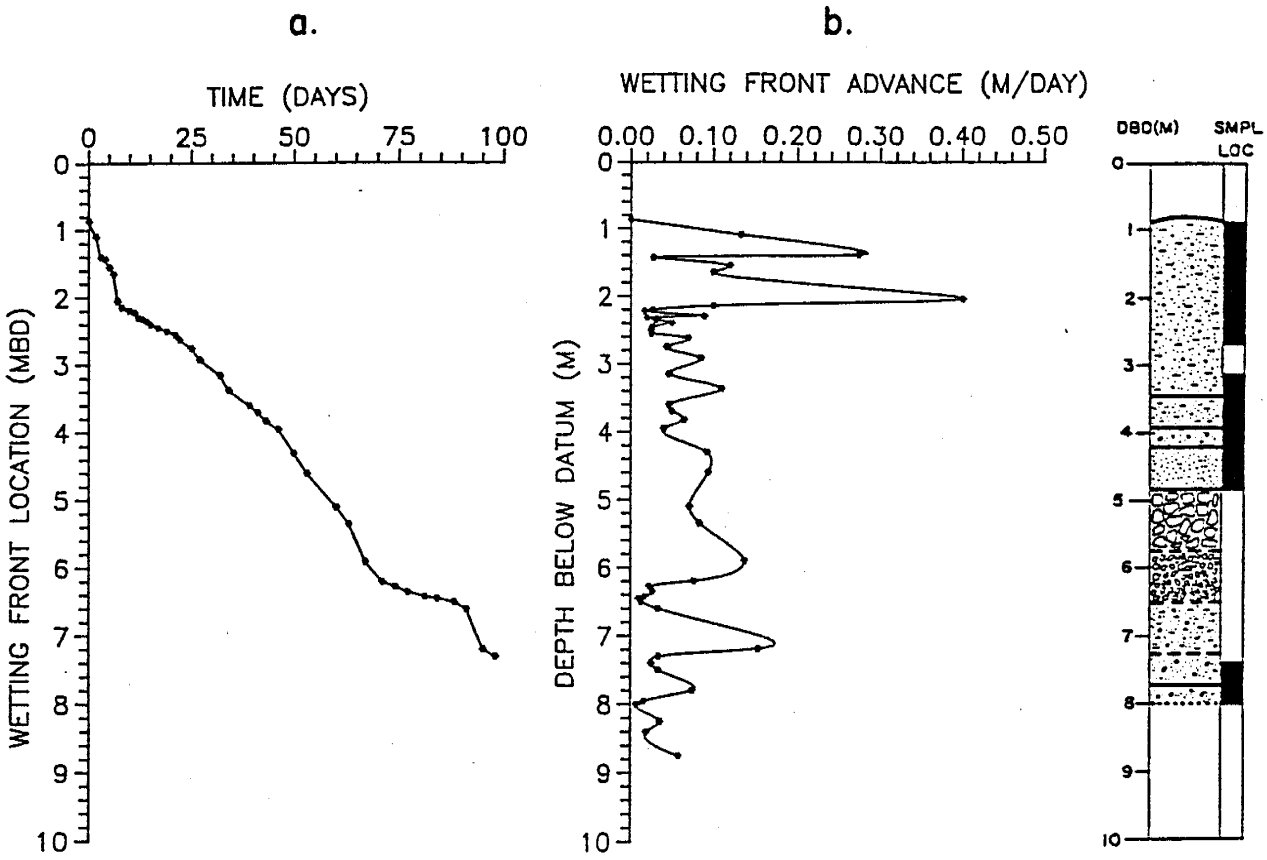

Figure 47. a) Wetting front location, b) rate of wetting front advance, and the geologic log for station 12-12.

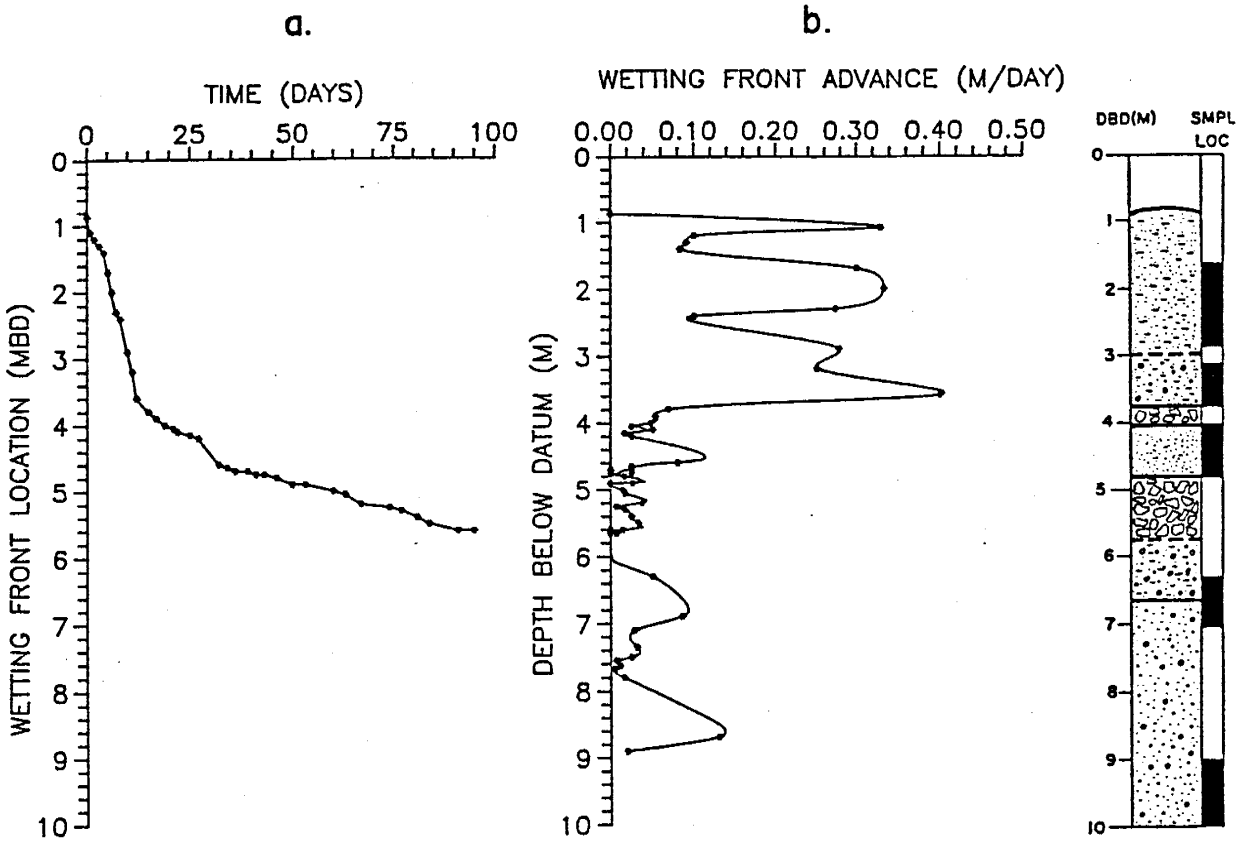

Figure 48. a) Wetting front location, b) rate of wetting front advance, and the geologic log for station 18-18.

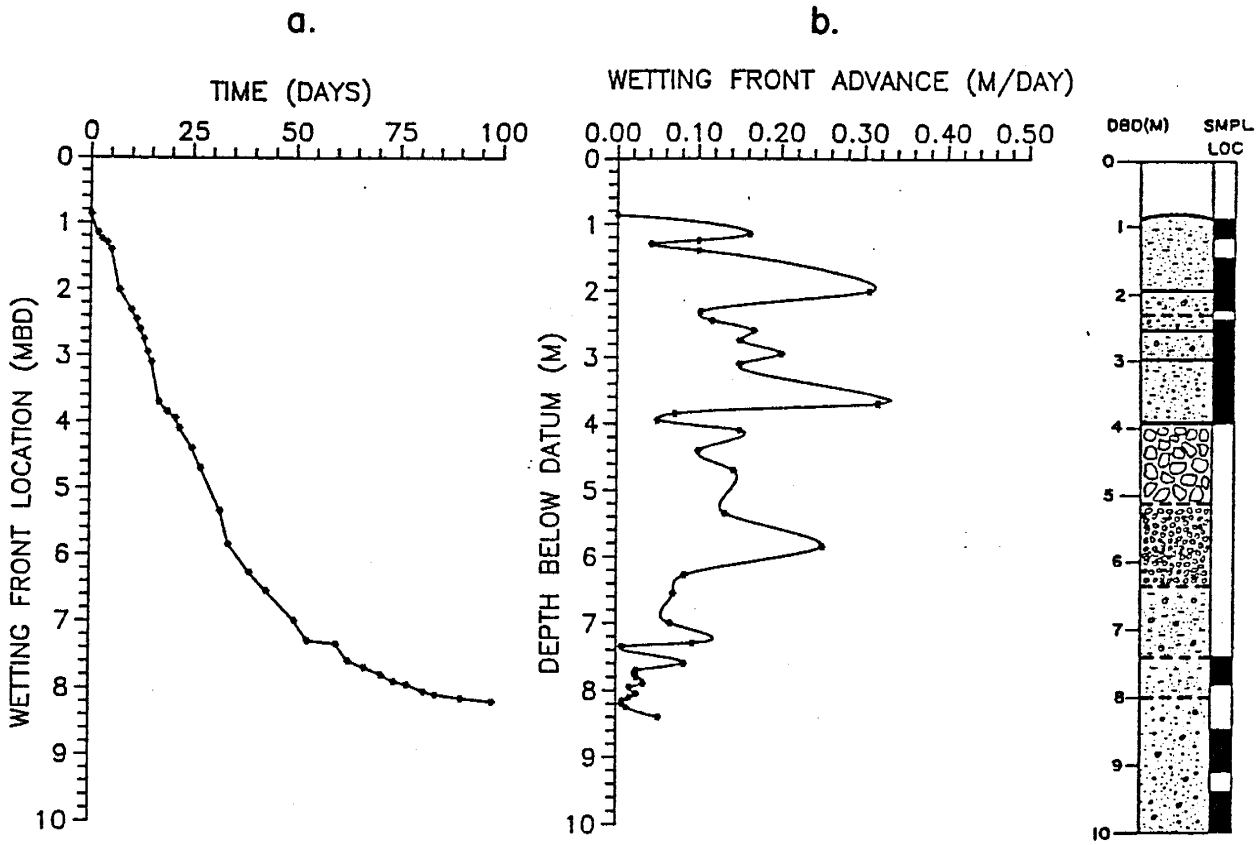

Figure 49. a) Wetting front location, b) rate of wetting front advance, and the geologic log for station 18-12.

Table 10. Average Rates of Wetting Front Advance*

Station	Depth Below Datum (m)	Rate of Wetting Front Advance (m/day)
15-15	0.86-6.15	0.182
	6.15-6.90	0.014
	6.90-7.80	0.129
	7.80-8.25	0.026
12-18	0.86-5.30	0.178
	5.30-6.52	0.058
	6.52-8.55	0.036
12-12	0.86-2.22	0.123
	2.22-3.95	0.050
	3.95-6.20	0.090
	6.20-6.60	0.020
18-18	0.86-3.60	0.226
	3.60-4.60	0.050
	4.60-5.60	0.016
18-12	0.86-5.85	0.147
	5.85-7.30	0.076
	7.30-8.20	0.020

* determined from slopes of wetting front location vs. time

The heterogeneity of the soil profile is apparent as water movement varies at each illustrated location (Figures 45-49). In the center of the field site at station 15-15, the wetting front location advanced fairly constantly for the first 30 days, decreased during the next 30 days, then increased again (Table 10). Moisture movement observed at stations 12-18 and 18-12, the northwest and southeast corners of the wetted area, had very similar wetting front advance rates to station 15-15 (Figures 45a,46a,49a). In the southwest corner of the wetted area at station 12-12, vertical moisture movement was always slower than in the center of the plot (Figures 45a,47a). At station 18-18, in the northeast corner of the irrigated plot, the location of the wetting front coincided with wetting front locations observed at station 15-15 for the first 12 days, then vertical moisture movement dramatically decreased through day 100 (Figures 45a,48a). In contrast to the fairly constant advance of the wetting front location (Figures 45a-49a), the rate of advance of the wetting front in discrete time intervals varied with depth by more than a factor of four (Figures 45b-49b).

The previous discussion has concentrated on the one-dimensional aspects of water movement. Looking at results of neutron logging outside the infiltration plot, the multi-dimensional nature of flow is apparent, as illustrated by the position of the wetting front for different times after infiltration began (Figure 50). After 80 days, the wetting front

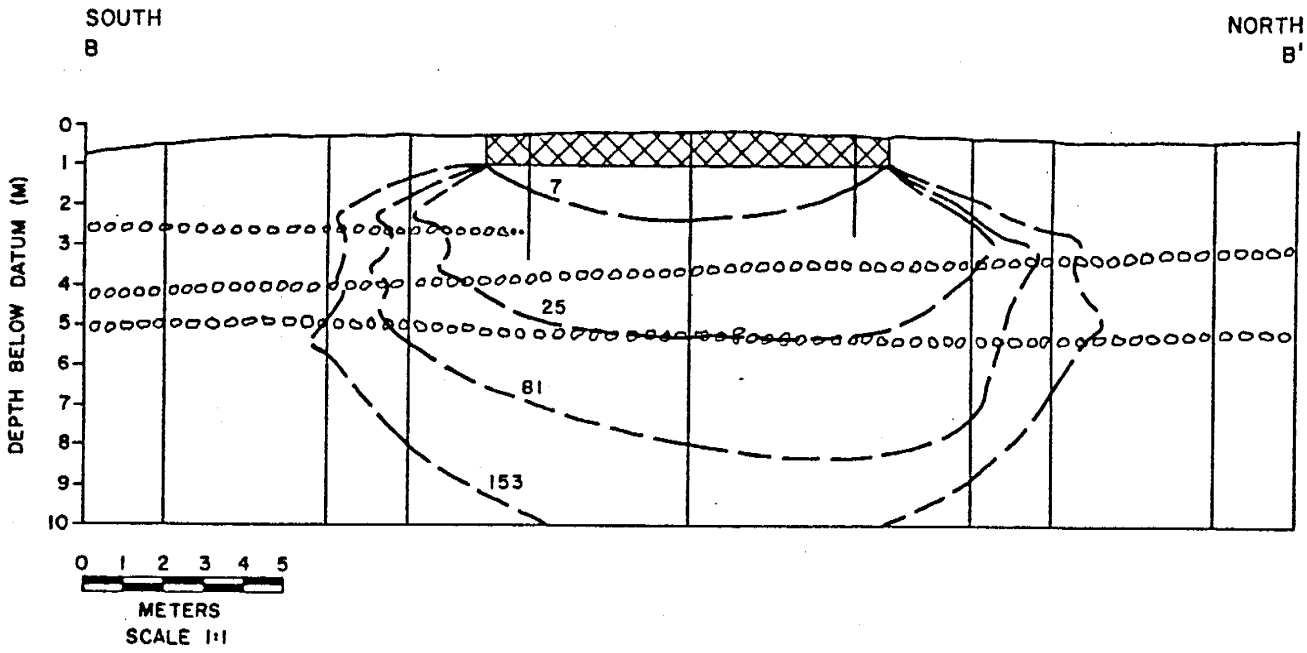

Figure 50. Wetting front locations after specified number of days after infiltration began.

had progressed approximately 7 meters vertically and 2 to 3 meters laterally from the edge of the irrigation plot.

6.4. STABILIZED MOISTURE CONTENT PROFILES

After 153 days of infiltration, the wetting front had progressed below the bottom of all center monitoring station neutron access tubes with the exception of station 18-18. The stabilized moisture content profiles represent conditions present beneath the irrigation plot after about 153 days of infiltration and approximately day 200 for station 18-18.

The stabilized moisture content profiles are very similar for all central stations (Figure 51). At the 3.5 meters depth, station 18-18 is about 5% drier than at the other station locations. On the average, moisture contents up to 38% are present to about 1.2 meters below datum, or about 0.30 meters below the emitters. These high moisture contents may reflect saturation of the thin sand layer below the emitters or effects of bentonite emplaced at the top of neutron access tube boreholes. The steady state moisture content beneath the emitters averages about 15% in the top 3 meters, and decreases to within 10 to 13% at depths to 9 meters below datum.

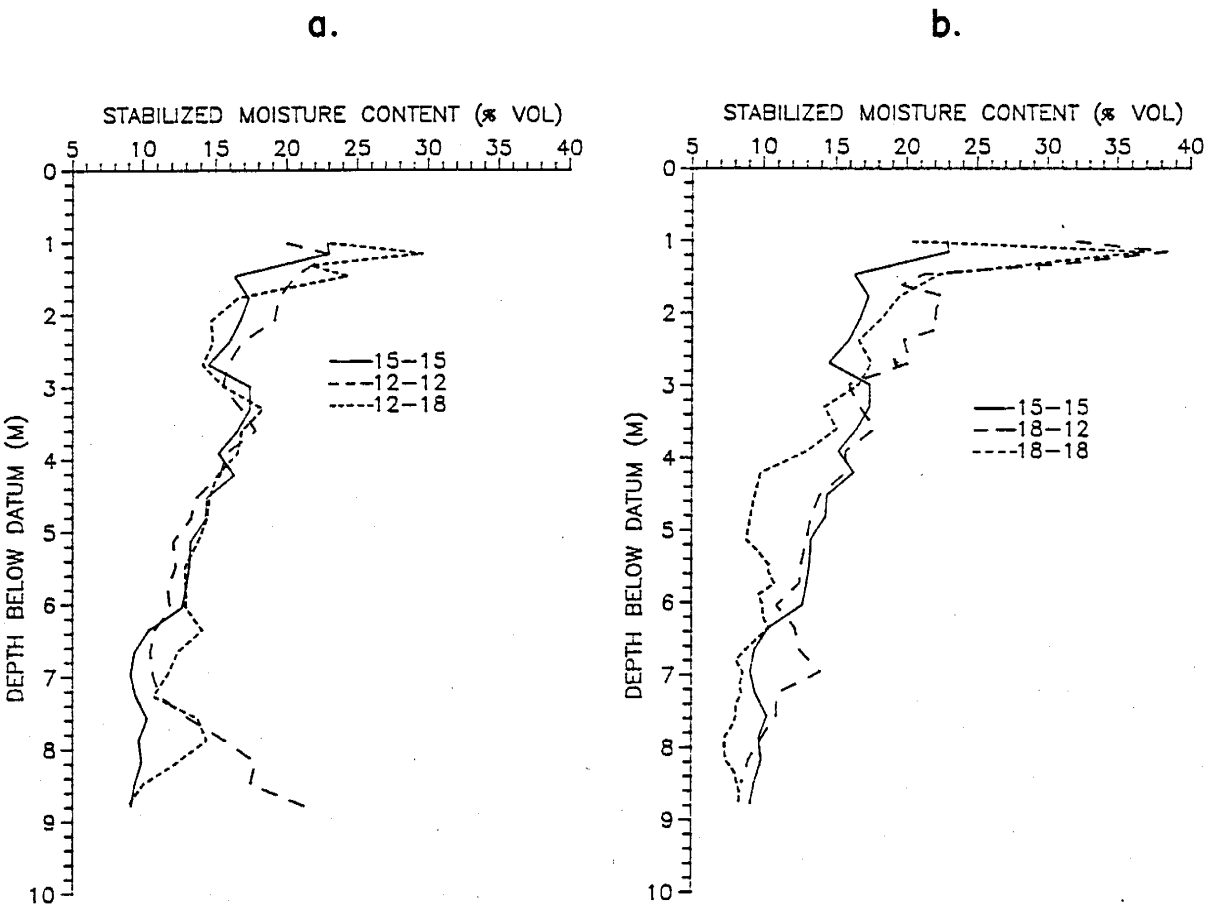

Figure 51. Stabilized volumetric moisture content beneath the irrigation plot after about 153 days of infiltration.

6.5. DISCUSSION

Several factors are pertinent to moisture movement observed at the field site. Stratification has a profound effect on vertical seepage movement. The initial and stabilized moisture content distributions also control the rates of water movement. The following discussion relates some moisture movement field observations to the geologic and hydrologic properties of the soil profile and to the controlled experimental factor, the seepage rate.

6.5.1. Stratification

Extreme changes in discrete rates of advance of the wetting front (Figures 45b-49b) often reflect geologic stratification in the soil profile. As Miller and Gardner (1962) point out, one expects the wetting front to slow as it reaches an interface where hydraulic properties differ markedly. The phenomena of textural change inhibiting downward movement through the profile is observed in the rates of wetting front advance beneath the wetted area. Pebble and cobble zones at depths of 3.6, 5, and 6.5 meters below datum at the center of the plot (station 15-15) do, in fact, temporarily impede the rate of wetting front advance (Figure 45). At the interface between a fine over coarse layer, apparently after or when fluid pressures are increased to the water-entry pressure of the lower layer, the wetting front moves rapidly through the coarse layer. Similar scenarios occur at station 12-18 at 3.0 ,4.5, and 6.5 meters below datum (Figure

46); station 12-12 at 6.25 meters below datum (Figure 47); station 18-18 at 4.0 meters and from 5.0 to 5.5 meters depth (Figure 48); and at station 18-12 at 4.0 and 5.5 meters below datum (Figure 49).

A significant decrease in the rate of advance of the wetting front advance occurred from days 30 to 60 at station 15-15 (Table 10). This may be attributed to both stratification and the leak which occurred in the irrigation system. The 14-fold decrease in advance rate coincides with the arrival of the wetting front at a coarse layer of pebbles located from 6.5 to 7.25 meters below datum (Figure 45). However, the decrease in advance may also be influenced by the leak which occurred from days 26 to 39. Neutron probe measurements indicated that the moisture contents behind the front remained stable during the leak, decreasing at most by one percent. After the leak was repaired, the rate of wetting front advance did not increase until 20 days later. The above results are evidence which suggests the leak is not the sole cause for inhibited downward movement of the wetting front. Stratification also controls the moisture movement.

The wetting front advance at station 18-18 is influenced by two cobble horizons present from 3.8 to 4.0 and 4.8 to 6.8 meters below datum. The cobbles are separated by a well-sorted, fine sand (Figure 48). The front is inhibited at about 3.8 meters, then a 12-fold increase in rate of wetting front advance occurred from 6 to 7 meters below datum, just below the lower cobble horizon.

When the wetting front is inhibited in downward movement, moisture may spread laterally across the top of the coarse horizon, as observed by Palmquist and Johnson (1962). Lateral flow components may be significant, especially at depths where large decreases in wetting front advance rate are observed. Such two-dimensional water movement may explain the general trend of decreasing wetting front advance rate with depth.

An average 2.5-fold decrease in the rate of wetting front advance occurs below 4 meters below datum after the wetting front entered the underlying fluvial sands (Figures 45b-49b).. It is expected that the rate of advance will slow with increasing depth in a profile which becomes more uniform and coarser with depth, which is the case at our field site.

6.5.2. Moisture Content

The wetting front advances more slowly than the average rate at station 12-12. There is no obvious stratigraphic control to inhibit vertical seepage movement at this location (Figure 47). However, the initial moisture content was the lowest in this corner (Figure 42), and the change in moisture content from initial to stabilized conditions is the largest (Figure 52). It is expected for the front to move more slowly under these circumstances (equation 7). There is no indication that the soil texture is finer in this location than in other locations within the irrigation plot based on the d_{10} grain size parameter (Figure 22) and visual geologic descriptions (Appendix B). There are no moisture retention curves from this location.

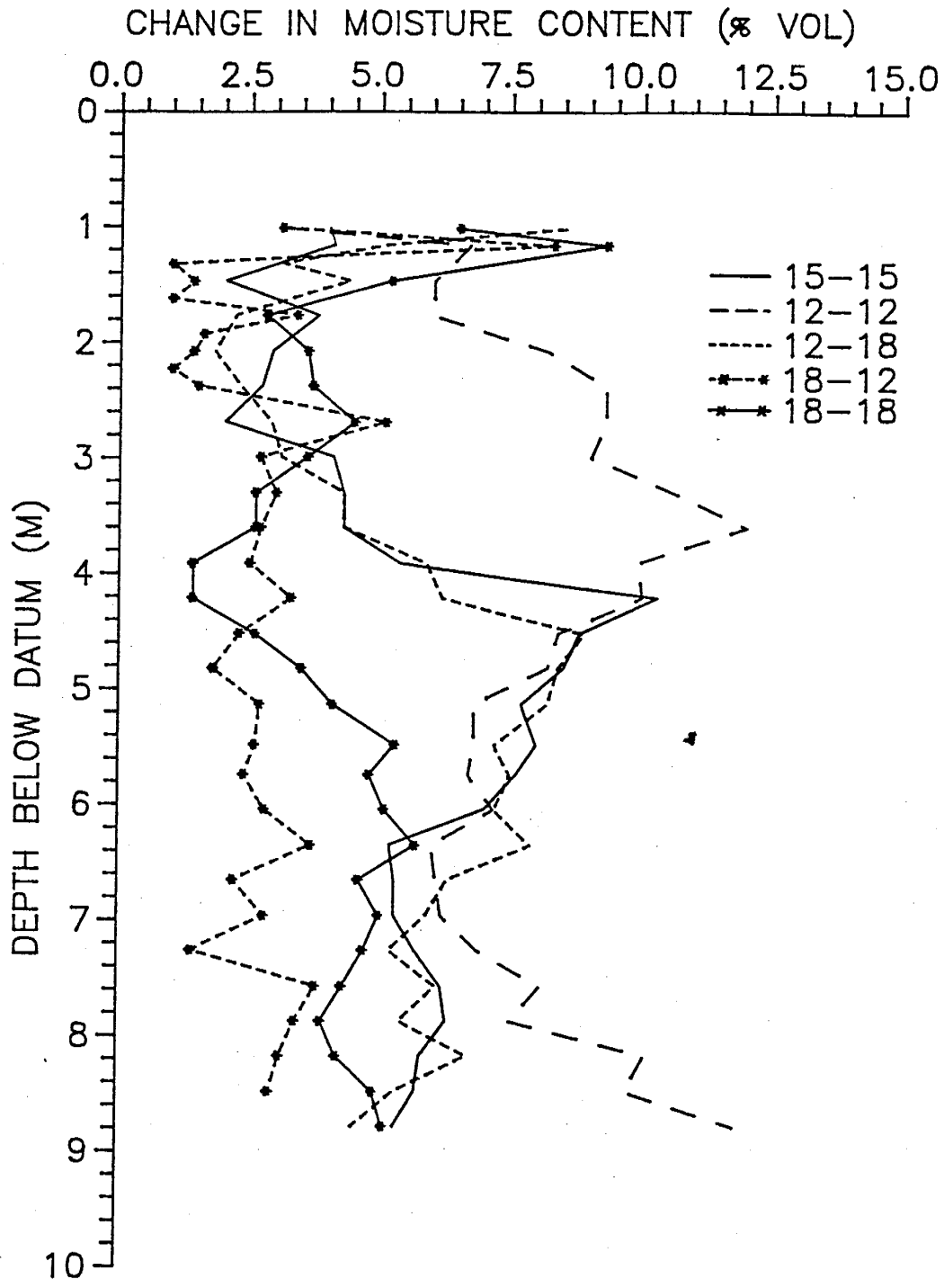

Figure 52. Change in volumetric moisture content observed beneath the irrigation plot after about 153 days of infiltration.

Warrick and others (1971) indicate that for a uniform one-dimensional flow field, the increase in moisture content behind the wetting front is approximately equal to the ratio of steady applied flux to the rate of wetting front advance. Applying this simple calculation, it is expected that the average moisture content would increase by 4.7% beneath the irrigation plot.

The observed increase in moisture content beneath the irrigation plot is quite variable (Figure 52). Excluding the outlier data of station 12-12, the average observed increase in moisture content is only about 3.5 percent to a depth of approximately 3.5 meters below datum. However, if data from station 12-12 are included, the observed average increase in moisture content of 4.6% is very close to the predicted average increase of 4.7%. Now, a one-dimensional model appears to be appropriate for predicting mean behavior. Sources of error in this simple analysis include hydraulic gradients different from unity, preferred paths of flow, insufficient numbers of logging stations, and errors in field calibration of the neutron probe.

7. ONE-DIMENSIONAL ANALYTICAL MODEL

The general modeling approach in this study only utilizes hydrologic data and moisture conditions prior to the experiment. The depth to the wetting front is predicted by the McWhorter and Nelson analytic model (1979) and compared to field observations for the first 60 days of infiltration. In this manner, we can evaluate the applicability of the model to a different site where post-infiltration data are not available. The analytical model is applied to three different soil profile conceptual models (Section 4.5), and the modeling results are discussed in this section. Depth to the wetting front predicted by the model is found in Appendix N.

7.1. MODEL INPUT PARAMETERS

Equations 6 and 7 are solved using program MNM.FOR. The parameters q, θ_s, θ_i, θ_r, K_s, and λ are required input. The three different mean flux rates, q, applied to the soil profile during the first 60 days of infiltration are utilized in the McWhorter and Nelson model (Figure 43).

The effect of the value of the pore size distribution index, λ, on the McWhorter and Nelson model is studied. The arithmetic mean and mode pore size distribution index, λ, are both used in

the modeling analysis. λ is calculated from the effective θ-ψ curves.

The sensitivity of the rate of wetting front advance to saturated hydraulic conductivity values is evaluated for the McWhorter and Nelson model. Saturated hydraulic conductivity has an important role in calculating the final moisture content (equation 6). Statistically, K_s is one of the most uncertain estimated parameters (Table 7). Varying the estimated K_s mean by plus or minus 50% is similar to adding or subtracting the variance (Table 3). A maximum (mean+50%), mean and minimum (mean-50%) K_s are considered. Table 11 summarizes the input parameters for each modeling run and the predicted final moisture contents.

7.2. RESULTS

The McWhorter and Nelson model assumes that infiltration occurs through the impoundment liner into a uniform foundation material. Therefore, only the one-layer conceptual model or flow through the first layer of a multi-layered system can be correctly applied to the McWhorter and Nelson model. The stratified nature of the soil at the field site indicates that the two- and five-layer conceptual models more accurately describe the flow domain. When a multi-layered conceptual model is applied, the modified McWhorter and Nelson model is used (see Section 2.3). The multi-layered conceptual models are studied in most detail.

TABLE 11. MCWHORTER AND NELSON MODEL (1979) INPUT PARAMETERS AND PREDICTED FINAL MOISTURE CONTENT

RUN	NUMBER OF LAYERS	POROSITY (cc/cc)	THETAi (cc/cc)	THETAr (cc/cc)	Ks (m/day)	Lambda (--)	Z (mbd)	q (m/day)	qt (days)	THETAf Predicted
STATION 15-15										
M1AL	2	0.374	0.140	0.128	17.76	0.68	3.6	8.06E-03	26.50	0.195
		0.334	0.055	0.052	13.03	1.72	10.0	4.86E-03	39.04	0.099
								7.85E-03	60.00	
M1AM	2	0.374	0.140	0.128	35.52	0.68	3.6	8.06E-03	26.50	0.188
		0.334	0.055	0.052	26.05	1.72	10.0	4.86E-03	39.04	0.092
								7.85E-03	60.00	
M1AH	2	0.374	0.140	0.128	53.28	0.68	3.6	8.06E-03	26.50	0.184
		0.334	0.055	0.052	39.08	1.72	10.0	4.86E-03	39.04	0.088
								7.85E-03	60.00	
M1ML	2	0.374	0.140	0.128	17.76	0.15	3.6	8.06E-03	26.50	0.282
		0.334	0.055	0.052	13.03	0.39	10.0	4.86E-03	39.04	0.165
								7.85E-03	60.00	
M1MM	2	0.374	0.140	0.128	35.52	0.15	3.6	8.06E-03	26.50	0.275
		0.334	0.055	0.052	26.05	0.39	10.0	4.86E-03	39.04	0.156
								7.85E-03	60.00	
M1MH	2	0.374	0.140	0.128	53.28	0.15	3.6	8.06E-03	26.50	0.272
		0.334	0.055	0.052	39.08	0.39	10.0	4.86E-03	39.04	0.151
								7.85E-03	60.00	
M5AM15	5	0.363	0.156	0.198	235.10	0.98	2.0	8.06E-03	26.50	0.219
		0.355	0.130	0.108	34.30	0.74	3.2	4.86E-03	39.04	0.165
		0.291	*0.085	0.055	74.40	1.03	4.7	7.85E-03	60.00	0.092
		0.323	0.055	0.044	23.50	1.11	6.4			0.097
		0.337	0.039	0.033	17.20	1.64	10.0			0.082
STATION 12-12										
M1212	2	0.374	0.093	0.128	35.52	0.68	4.2	8.06E-03	26.50	0.188
		0.334	0.051	0.052	26.05	1.72	10.0	4.86E-03	39.04	0.092
								7.85E-03	60.00	
STATION 12-18										
M1218	2	0.374	0.142	0.128	35.52	0.68	3.9	8.06E-03	26.50	0.188
		0.334	0.064	0.052	26.05	1.72	10.0	4.86E-03	39.04	0.092
								7.85E-03	60.00	

Table 11--continued

RUN	NUMBER OF LAYERS	POROSITY (cc/cc)	THETAi (cc/cc)	THETAr (cc/cc)	Ks (m/day)	Lambda (--)	Z (mbd)	q (m/day)	qt (days)	THETAf Predicted
AVERAGE										
MOL	1	0.314	0.096	0.108	43.8	0.88	10	8.06E-03	26.50	0.148
								4.86E-03	39.04	
								7.85E-03	60.00	
M2LAV	2	0.374	0.133	0.128	35.52	0.68	4.6	8.06E-03	26.50	0.188
		0.334	0.058	0.052	26.05	1.72	10.0	4.86E-03	39.04	0.092
								7.85E-03	60.00	
M5AMA	5	0.363	0.156	0.198	235.10	0.98	2.0	8.06E-03	26.50	0.219
		0.355	0.130	0.108	34.30	0.74	3.2	4.86E-03	39.04	0.165
		0.291	*0.085	0.055	74.40	1.03	4.7	7.85E-03	60.00	0.092
		0.323	0.055	0.044	23.50	1.11	6.4			0.097
		0.337	0.039	0.033	17.20	1.64	10.0			0.082

* adjusted to be less than predicted final moisture content

THETAi = initial moisture content
THETAr = residual moisture content
Ks = saturated hydraulic conductivity
Lambda = pore size distribution index
Z = maximum depth of layer
q = flux rate
qt = last day in flux rate period
THETAf Predicted = final moisture content predicted by the model for that layer

The modeling results are described in this section. First, the sensitivity analysis for the modified McWhorter and Nelson model in a two-layer system are discussed. Next, the wetting front location predictions for the one-, two-, and five-layer models are described.

7.2.1. Sensitivity Analysis

The pore size distribution index, λ, has a strong effect on wetting front location predictions (Figure 53). When the modified McWhorter and Nelson model is applied to the two-layer system, use of the modal λ results in depths to the wetting front underestimated at all times up to 50% compared to field observations at station 15-15. Conversely, application of the arithmetic mean λ results in wetting front locations which closely predict the observed depth to the wetting front for the first 8 days and from about 20 to 30 days. Then the front is overpredicted after 30 days of infiltration. By day 60 the depth to the wetting front predicted by the modified Mcwhorter and Nelson model applying the arithmetic mean λ is overestimated by almost 50% compared to field results. In view of the fact that the arithmetic mean λ results are the closest to observed results, at least at early time, the arithmetic mean λ is used for the remainder of the analytic modeling simulations.

Increasing the saturated hydraulic conductivity, K_S, by 50% of the mean value does not significantly improve the predicted depth to the wetting front results (Figure 54). The mean K_S and plus or minus 50% of the mean K_S were input to the modified McWhorter

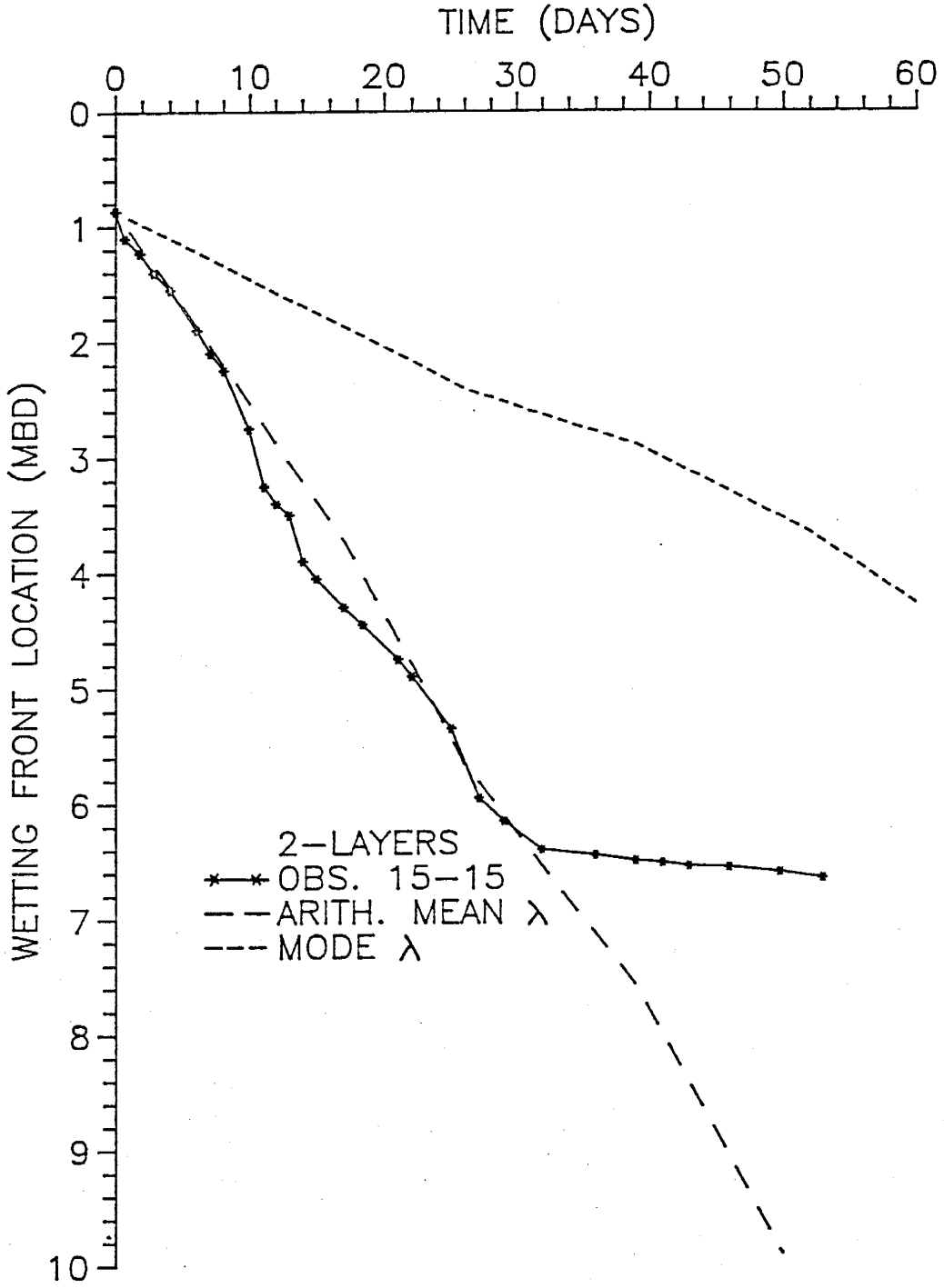

Figure 53. Wetting front locations predicted by the modified McWhorter and Nelson model in a two-layer system compared to observations at station 15-15. The arithmetic mean and mode λ values are used in calculations (Runs M1AM, M1MM).

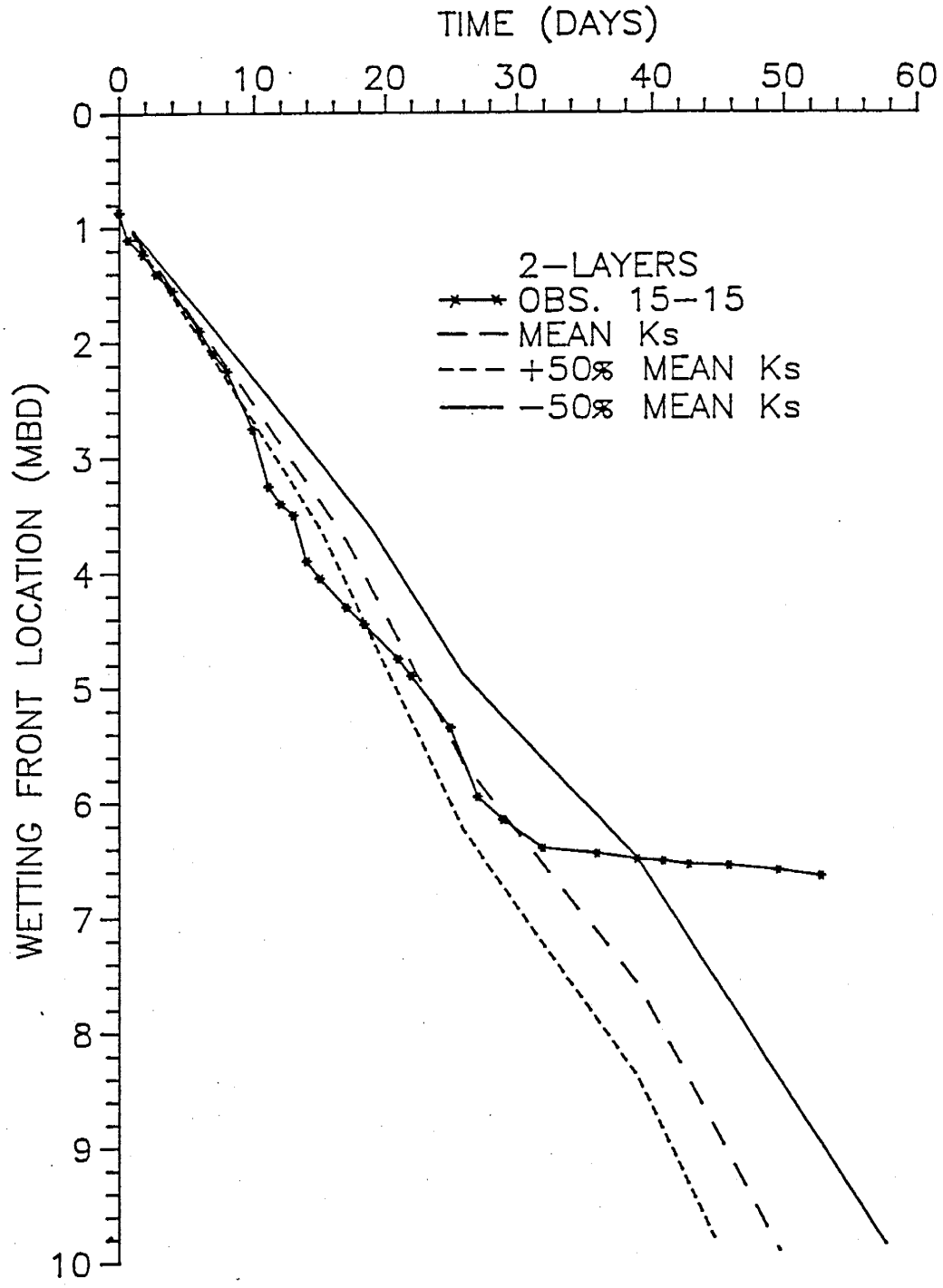

Figure 54. Wetting front locations predicted by the modified McWhorter and Nelson model in a two-layer system compared to observations at station 15-15. The arithmetic mean saturated hydraulic conductivity and the mean plus or minus 50% are used in calculations (Runs M1AL, M1AM, M1AH).

and Nelson model. For a two-layered system, when applying the largest K_s value, the modified model predicts the observed wetting front locations the most closely for about 20 days. But increasing K_s by 50% causes the model overestimation of the depth to the wetting front to begin to be significant after about 20 days, compared to 30 days using the arithmetic mean K_s. Considering the small improvement in predictions using the large K_s, the arithmetic mean is subsequently applied in further analysis.

7.2.2. One-Layer Model

The McWhorter and Nelson model closely predicts the mean observed wetting front location at early time in a homogeneous one-layer system. Based on wetting front location data averaged from the five central monitoring stations, the average wetting front locations observed beneath the irrigated plot at particular times are compared to the one-layer model predictions (Figure 55). The three different flux rates which occurred during the 60 day time period are reflected in three different rates of wetting front advance predicted by the one-layer model. The one-layer conceptual model predicts depths to the wetting front which agree with field observations until 18 days. After 18 days, the predicted wetting front location is overestimated compared to observations, with a difference of about 3 meters by day 60.

7.2.3. Two-Layer Model

The modified McWhorter and Nelson model closely predicts the mean depth to the wetting front for 22 days in a two-layer system (Figure 55). However, there is a tendency for underprediction, on

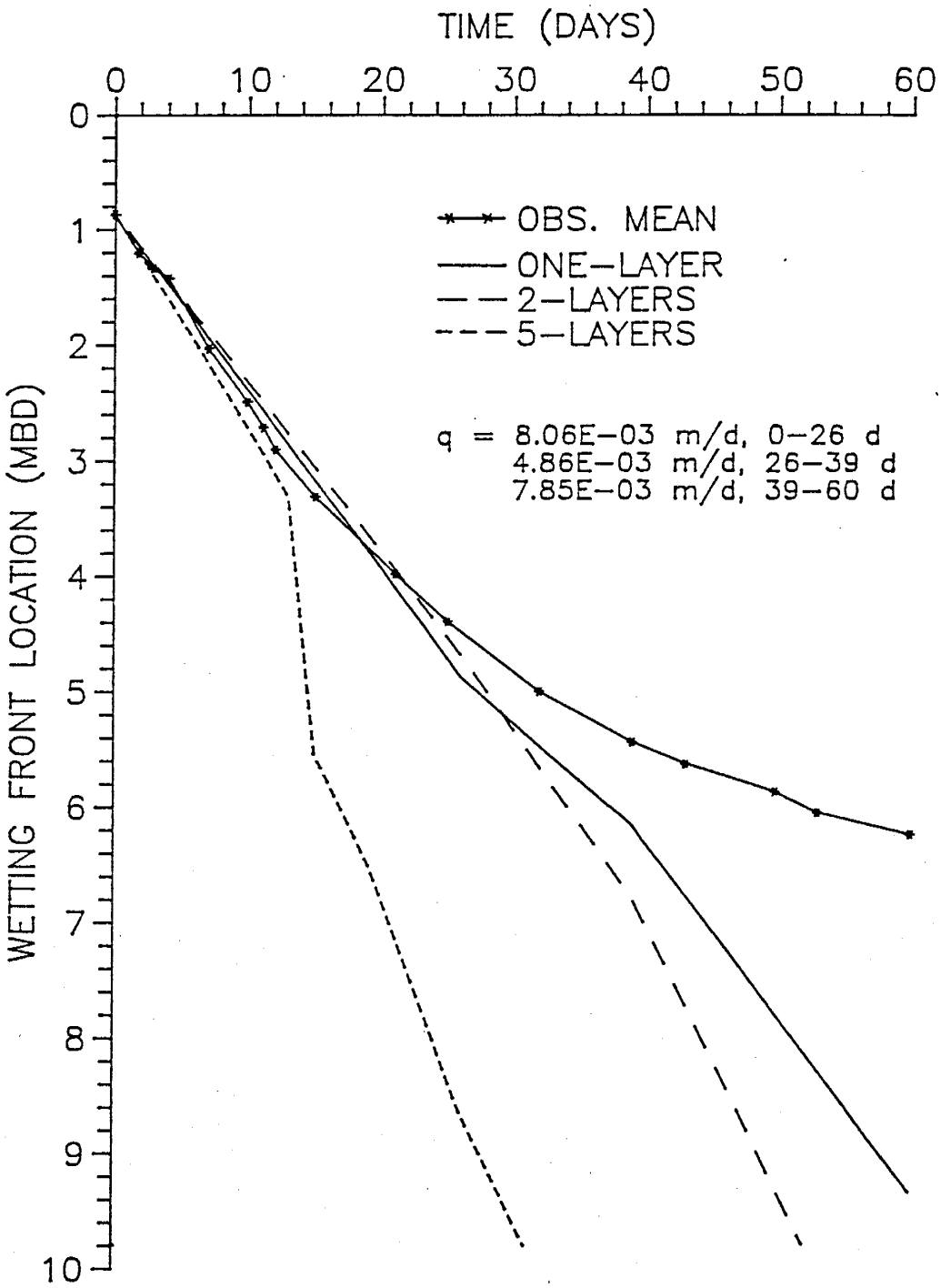

Figure 55. Wetting front locations predicted by the modified McWhorter and Nelson model in a one-, two-, and five-layer system compared to the mean wetting front locations observed beneath the central irrigation plot (Runs MOL, M2LAV, M5AMA).

the order of centimeters, at early time. After about 22 days, the mean observed wetting front advance begins to slow after reaching a depth of about 4 meters below datum. In contrast, the two-layer model predicts a fairly constant advance of the wetting front. As a result, the two-layer model overpredicts the depth to the wetting front on day 60 by several meters.

There is significant variation about the mean wetting front movement observed below the irrigation plot. When applying the two-layer conceptual model to individual locations within the irrigation plot, the results are different at each location (Figure 56). The wetting front is underpredicted by the analytical model by tens of centimeters through day 20 at station 12-12 and 15-15. Conversely, at station 12-18, the wetting front depth is overestimated by less than 10 centimeters until day 15. Overestimation at all locations at late time begins to occur at depths ranging from about 4 to 7 meters below datum. After 60 days of infiltration, the wetting front depth is overestimated at all locations by meters. Station 15-15, located in the very center of the irrigation plot is not a better indicator of the mean wetting front movement than other stations within the irrigation plot.

7.2.4. Five-Layer Model

The five-layer modified McWhorter and Nelson model predictions of the depth to the wetting front are overestimated by only a few centimeters for the first 12 days (Figure 55). After 12 days, the front location is severely overpredicted by several meters.

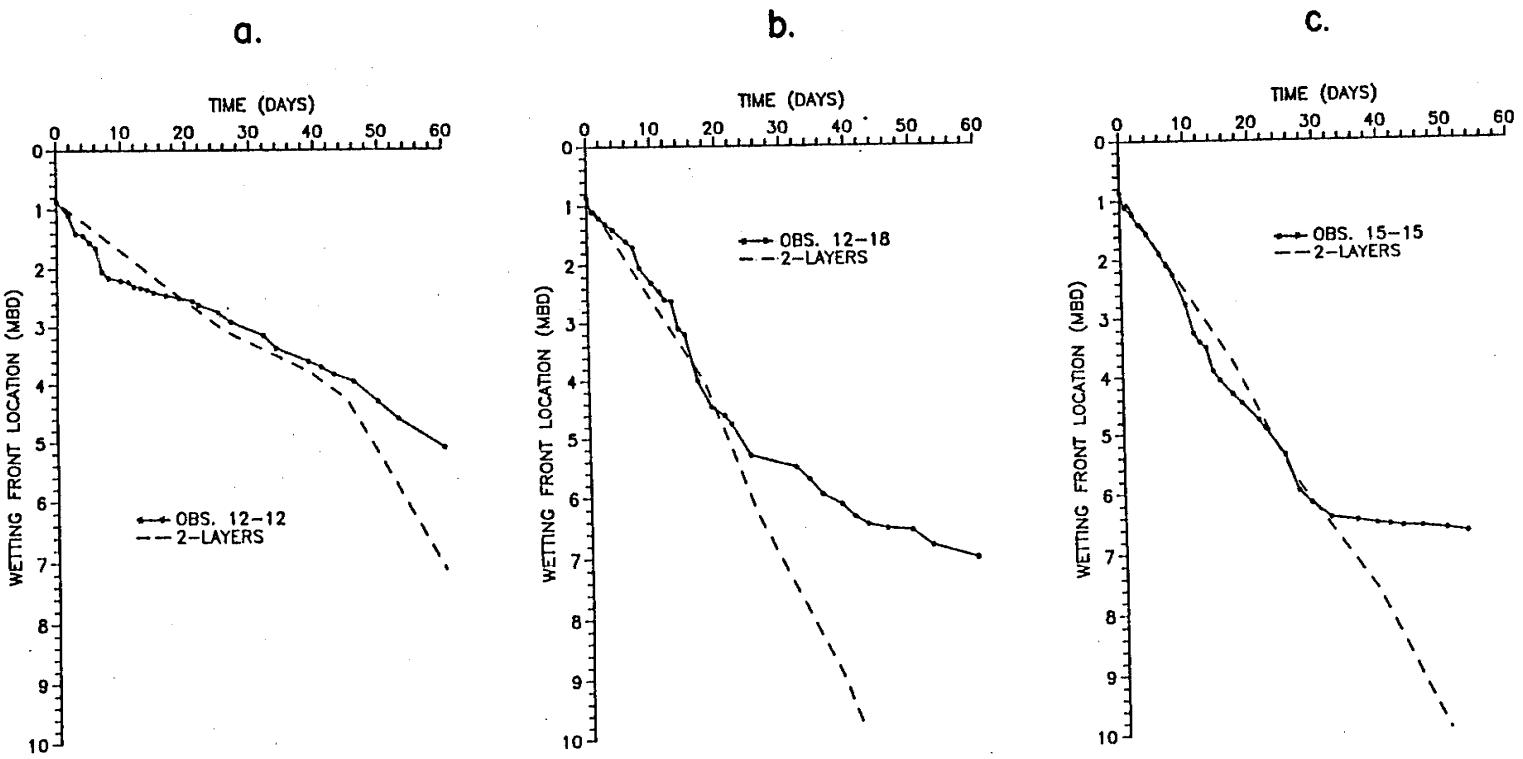

Figure 56. Wetting front locations predicted by the modified McWhorter and Nelson model in two-layer system compared to the wetting front locations observed at a) station 12-12, b) station 12-18, and c) station 15-15 (Runs M1212, M1218, M1AM).

By day 28, the five-layer model predicted the front had reached 10 meters below datum, while field observations indicate the front was actually about 4.4 meters below datum at this time.

7.3. DISCUSSION

The modified McWhorter and Nelson model predicts the observed depth to the wetting front very well at early time while the front moves through the upper 3 to 4 meters in the one-, two- and five-layer systems. All the modified model results tend to diverge from field observations after reaching the cobble zone located at about 4 meters below datum and subsequently entering the deeper coarse fluvial sand facies.

Although the McWhorter and Nelson model and modified McWhorter and Nelson model results do not compare well with late time field results, the models do function correctly. Siegel and Stephens (1980) found very good agreement between the McWhorter and Nelson model predictions for wetting front depth and numerical model results in an isotropic profile. Indeed, our two-layer modified McWhorter and Nelson model results are also very good in the first major textural layer through about 4 meters depth below datum at several locations (Figure 56). Similar modeling results are obtained for the mean wetting front movement to depths of 3 to 4 meters below datum using the one-, two-, or five-layer conceptual model (Figure 55). In the five-layer case, the predicted rate of advance of the wetting front increases in

comparison to the field observations at a depth of about 3.4 meters below datum. The wetting front had already entered the third layer of the five-layer model by that time (Table 8). The close agreement of observed and predicted wetting front locations through the first three layers of the five-layer model implies that the layered profile modification in the computer code MNM.FOR is reasonably accurate.

The modified McWhorter and Nelson model predicts that the wetting front advances at a faster rate in the deeper fluvial sands at depths below about 4 meters below datum. Theoretically, the accelerated advance of the wetting front after entering the coarser lower zone may be expected in unsaturated conditions. Under unit hydraulic gradient conditions, the pressure head will be constant with depth causing a discontinuity in moisture content across textural interfaces. A discontinuous moisture content profile implies different initial and final moisture content values for each layer. Therefore, the magnitude of the change in moisture content which occurs after infiltration will change from one layer to the next. The average stabilized moisture content observed in the field in the piedmont slope facies was about 17% (Figure 51). This moisture content corresponds to a negative pressure head of about 100 cm on the average piedmont slope moisture retention curve (Figure 30a). In the fluvial sand facies, 100 cm negative pressure corresponds to the region on the effective fluvial sand θ-ψ curve where $d\theta/d\psi$ approaches zero (Figure 30a), allowing a very small increase in moisture content when infiltration

occurs. With less pore space available to be filled with moisture, the wetting front will advance faster through the fluvial sand facies.

Moisture movement in the field beneath the irrigation plot is predicted with good accuracy by a one-dimensional analysis for the first 3 to 4 meters below datum. Observed wetting front locations in the field deviate from the modified McWhorter and Nelson model predictions beginning at about 4 meters below datum after about 20 days of infiltration. The deviation coincides with the arrival of the front at the first cobble zone and underlying fluvial sands. The vertical movement of the front in the field is impeded by stratification sequences of fine over coarse textured layers. Multi-dimensional processes such as lateral spreading control the moisture movement after the front reaches 4 to 5 meters below datum. The first indication of lateral spreading occurred in the field by day 25 when the front reached monitoring stations located a meter from the edge of the irrigation plot (Figure 50). According to the two-dimensional wetting front locations, significant lateral spreading began to occur in the field sometime between 7 and 25 days.

When multi-dimensional flow becomes significant, the one-dimensional analytical model of McWhorter and Nelson is a poor predictor of the field behavior. Our field observations are similar to Siegel and Stephens (1980) numerical simulation calculations of the wetting front location in an anisotropic profile. Siegel and Stephens found the McWhorter and Nelson

model overpredicts the depth to the wetting front under anisotropic conditions. Likewise, our results show the modified McWhorter and Nelson model overpredicts the wetting front location in a stratified profile.

There are problems with applying the modified McWhorter and Nelson model to a stratified profile, even if only one-dimensional occurred. The model does not account for the impedance of the wetting front at textural interfaces and assumes the front immediately enters the new layer and continues downward propagation. In reality, a certain amount of time is required for the pressure to build up at a fine over coarse interface before the front can enter the lower layer. Therefore, even if a one-dimensional analysis is appropriate, the modified McWhorter and Nelson model would overpredict the depth to the wetting front.

All three conceptual models predicted similar depth to the wetting front at early time. In some cases the one-layer conceptual model predictions are closer to observed results at early time than the two-layer model (Figure 55). At late time, the one-layer model results are the closest to the field observations. However, the observed wetting front locations are not appropriate for comparison with the model predictions at late time due to multi-dimensional flow components present at the field site. As more layers are added to the conceptual model, there is less uncertainty about the hydrologic properties and variability. Under one-dimensional flow conditions, it is expected for the five-layer model to estimate depth to the wetting front most

accurately. Due to multi-dimensional flow patterns observed at our field site, it is not possible to verify this hypothesis with the available data.

8. SUMMARY AND CONCLUSIONS

A field experiment was conducted to simulate seepage from a lined impoundment into a stratified soil in a semi-arid climate. Water was applied through a drip irrigation system at a flux rate of approximately $1x10^{-5}$ cm/sec over a 10m x 10m surface. The flux was about 100 times less than the mean saturated hydraulic conductivity of the soil profile. Moisture movement was monitored with neutron logging equipment in the 30m x 30m field site to depths up to 9 meters.

The soil is stratified, consisting of two major facies types. The upper unit, or piedmont slope facies, is comprised of red brown, silty sand and pebbles derived from Socorro Peak directly to the west. The piedmont slope facies is overlain by a fluvial sand facies; well sorted, tan, fine to coarse sands of ancestral Rio Grande River origin. Difficulties were encountered in collecting soil samples due to the stoney nature of the field site. As a result only a limited number of samples were obtained below about 3.5 meters below datum where the first major cobble zone is located.

Geologic properties identified in the field hydrologic properties of the soil were determined in the laboratory. Effective moisture retention characteristics and unsaturated hydraulic conductivity curves were calculated to represent each

layer of interest. Parameters of fit to moisture retention data, α and n_v, have a strong effect on the slope of the K-θ curve. The fit parameters α and n_v are neither normal or log normally distributed, based on fractile diagram analysis of 68 piedmont slope facies samples.

Field observations of the wetting front movement directly beneath the irrigation plot indicate that stratification tends to inhibit downward vertical movement of the moisture movement. There is significant variation in observed moisture movement between each of the five monitoring stations within the irrigation plot. After 60 days of infiltration, the wetting front had progressed 6 meters vertically and 2 to 3 meters laterally away from the edge of the irrigation system.

The McWhorter and Nelson (1979) one-dimensional analytical solution was used to predict the depth to the wetting front below the irrigation plot. The model was modified to account for stratification. To simplify model input, the stratified soil was represented as a one-and two-layer system based on geologic characteristics, and as five-layers based on hydrologic properties. The analytical solution fairly accurately predicts the mean wetting front location for the first 20 days of infiltration to about 4 meters depth for all three conceptual models. After about 20 days the front location is overpredicted by as much as 50%. Close agreement between the McWhorter and Nelson model predictions and field observations of the wetting front depth beneath the irrigation plot indicate that one-dimensional flow

dominates at early time. After about 20 days, multi-dimensional flow such as lateral spreading appears to dominate in the field and the analytic model fails to accurately predict moisture movement. Clearly, it is not appropriate to use a one-dimensional model for multi-dimensional flow processes in the vadose zone.

9. RECOMMENDATIONS FOR FUTURE WORK

It is apparent that more detailed site characterization is necessary. The small soil core samples (100 cc) are not always representative of the average hydrologic properties of the layer sampled, due to small scale variability within the major layer. Ideally, a trench at least 4 meters deep which cut across the field site would enable two-dimensional geologic mapping of the strata. Ring samples should be collected at regular, closely spaced intervals from the trench walls. The cobble zones should be studied in more detail and perhaps soil samples of the matrix material from those zones collected.

van Genuchten has a more updated analytical model for approximating the unsaturated hydraulic conductivity (RETC.FOR) which allows the data points to be weighted. This would be useful in our study because there is no data available in the dry range from about 300 to 15000 centimeters negative pressure. The 15 bar moisture content is the only data available at very high negative pressures. Moisture retention data from the hanging columns and pressure plate should be studied to determine if the new code calculates significantly different results than the current analysis.

Some interesting statistical studies are possible using the limited number of samples currently available. More study of the

α and n_v parameter distributions, as well as other hydrologic properties would be useful for determining model input. A geostatistical kriging and variogram analysis would also be helpful in site characterization and determining the best model input value.

In situ saturated and unsaturated hydraulic conductivity tests should be conducted at the field site, in both facies types. More tests are necessary in the upper piedmont slope facies due to higher variability. These results should be compared to laboratory determinations, and eliminate need for calculating effective moisture retention characteristics and effective unsaturated hydraulic conductivity curves. Such field tests should be incorporated with the trench excavation.

The validity of using mean α, n_v, θ_s, θr, and K_s to calculate an effective unsaturated hydraulic conductivity relationship requires more study. The simplicity of this approach is appealing, but it has not been proven whether the effective curves describe actual field conditions.

10. REFERENCES

Asseed, M., and D. Swartzendruber, 1975, Water infiltration into uniform and stratified soils II. Experimental evaluation of an approximate theory, Libyan J. of Agric., 4: 129-140.

American Society for Testing and Materials, 1987, Annual Book of ASTM Standards, Soil and Rock; Building Stones; Geotextiles, 4(4.08): 115-123.

Aylor, D.E., and J-Y. Parlange, 1973, Vertical infiltration into a layered soil, Soil Sci. Am. J., 37: 673-676.

Bachman, G.O., and H.H. Mehnert, 1978, New K-Ar dates and the late Pliocene to Holocene geomorphic history of the central Rio Grande region, New Mexico, Geol. Soc. Am. Bull., 89:283-292.

Baldwin, B., 1963, Part 2, Geology, IN Geology and water resources of the Santa Fe area, New Mexico, eds. Spiegel, Z. and B. Baldwin, USGS Water Supply Paper, 1525: 21-89.

Baldwin, B., 1956, The Santa Fe Group of north-central New Mexico, IN NM Geol. Soc. Guidebook, Seventh Annual Field Conference, Southeastern Sangre de Cristo Mountains, 115-121.

Bear, J., 1972, Dynamics of Fluids in Porous Media, American Elsevier Publ. Co., NY.

Betson, R.P., 1984, Ground-Water Transport Studies Phase II, Design and Cost Estimates, Tennessee Valley Authority, Office of Natural Resources and Economic Development Branch, Rpt. RP2485-05.

Bouwer, H., 1969, Infiltration of water into nonuniform soil, J. Irrig. and Drainage Div. Am. Soc. Civil Eng., 102(IR4): 451-461.

Brooks, R.H., and A.T. Corey, 1966, Properties of porous media affecting fluid flow, J. Irrig. and Drainage Div. Am. Soc. Civil Eng., 92(IR2): 61-88.

Brooks, R.H., and A.T. Corey, 1964, Hydraulic Properties of Porous Media, Hydrology Paper No. 3, Colorado State University, Ft. Collins, CO, 24 p.

Bryan, K., 1938, Geology and ground-water conditions of the Rio Grande depression in Colorado and New Mexico, Regional Planning, Part VI-Upper Rio Grande, Natl. Res. Comm., 1: 197-225.

Bryan, K., and F.T. McCann, 1937, The Ceja del Rio Puerco, a border feature of the Basin and Range province in New Mexico; Part 1, stratigraphy and structure of New Mexico, Journ. Geology, 45: 801-828.

Bucks, D.A., and F.S. Nakayama, 1985, Guidelines for maintenance of a trickle irrigation system IN Drip/Trickle Irrigation in Action, Proceedings of the Third International Drip/Trickle Irrigation Congress, Nov. 18-21, Fresno, CA, ASCE, 119-126.

Bybordi, M., 1968, Moisture profiles in layered porous materials during steady state infiltration, Soil Sci., 105: 379-383.

Chamberlain, R.M., 1985, personal communication on 12/2/85, Economic Geologist, New Mexico Bureau of Mines, Socorro, NM.

Chamberlain, R.M., 1980, Cenozoic stratigraphy and structure of the Socorro Peak volcanic center, central New Mexico, New Mexico Bureau of Mines and Mineral Resources, Open-file Rpt. 118, 2 vol, 495 p.

Chapin, C.E., R.M. Chamberlain, G.R. Osburn, D.L. White, and A.R. Sanford, 1978, Exploration framework of the Socorro geothermal area, New Mexico IN New Mexico Geol. Soc. Spec. Publ., 7: 114-129.

Childs, E.C., and M. Bybordi, 1969, The vertical movement of water in stratified porous materials 1. Infiltration, Water Resour. Res., 5: 446-459.

Chu, S.T., C.A. Onstad, and W.J. Rawls, 1986, Field evaluation of layered Green-Ampt model for transient crust conditions, Transactions of the Amer. Soc. Ag. Eng., 29(5): 1268-1277.

Crosby, J.W., D.L. Johnstone, C.H. Drake, and R.C. Fenton, 1968, Migration of pollutants in a glacial outwash environment, Water Resour. Res., 4(5): 1095-1114.

Crosby, J.W., D.L. Johnstone, and R.L. Fenton, 1971, Migration of pollutants in a glacial outwash environment 2., Water Resour. Res., 7(1): 204-208.

Dane J.H., 1980, Comparison of field and laboratory determined hydraulic conductivity values, Soil Sci. Soc. Am. J., 44: 228-231.

DeBrine, B., Z. Spiegal, and D. Williams, 1963, Cenozoic sedimentary rocks in Socorro Valley, New Mexico, Guidebook of the Socorro Region, New Mexico, 14th Field Conference, New Mexico Geol. Soc., 123-131.

Denny, C.S., 1940, Tertiary geology of the San Acacia area, New Mexico, J. of Geology, 48: 73-106.

Green, W.H., and G.A. Ampt, 1911, Studies in soil physics 1. The flow of air and water through soils, J. Agric. Sci., 4: 1-24.

Gutjahr, A., 1988, personal communication on 6/6/88, Professor, Math Department, New Mexico Tech, Socorro, NM, 6/6/88.

Hawley, J.W., F.E. Kottlowski, W.S. Strain, W.R. Seager, W.E. King, and D.V. LeMone, 1969, The Santa Fe Group in the south-central New Mexico border region IN Border Stratigraphy Symposium, New Mexico Bureau of Mines and Mineral Resources Circ. 104, 52-76.

Hayden, F.V., 1869, First, second, and third reports of the United States Geological Survey of the Territories for the years 1867, 1868, and 1869.

Hendrickx, J.M.H., P.J. Wierenga, M.S. Nash, and D.R. Nielson, 1986, Boundary location from texture, soil moisture, and infiltration data, Soil Sci. Soc. Am. J., 50(6): 1515-1520.

Hillel, D., 1980a, Fundamentals of Soil Physics, Academic Press, New York, 413 p.

Hillel, D., 1980b, Applications of Soil Physics, Academic Press, New York, 385 p.

Hillel, D., and W.H. Gardner, 1970, Transient infiltration into crust topped soils, Soil Sci., 109: 410-416.

Idike, F.I., C.L. Larson, D.C. Slack, and R.A. Young, 1980, Experimental evaluation of two infiltration models, Am. Soc. Ag. Eng. Transactions, 1428-1433.

Johnson, T.M., K. Cartwright, and R.M. Schuller, 1981, Monitoring of leachate migration in the unsaturated zone in the vicinity of sanitary landfills, Groundwater Monit. Rev., Fall: 55-63.

Kempthorne, O., and R.R. Allamaras, 1986, Errors and variability of observations IN Methods of Soil Analysis Part 1, 2nd Edition, ed. A. Klute, Am. Soc. of Agron. Inc, Soil Sci. Soc. Am., Madison, WI, 1-31.

Kieft, T., 1986, personal communication on 12/2/86, Asst. Professor, Biology Department, New Mexico Tech, Socorro, NM.

Klute, A., and D.F. Heerman, 1978, Water movement in uranium mill tailings profiles, Science and Education Administration, Ft. Collins, CO, U.S. Dept. of Commerce, PB-291 688, 81 p.

Kool, J.B., J.C. Parker, and M.Th. van Genuchten, 1985, ONESTEP: A nonlinear parameter estimation program for evaluating soil hydraulic properties from one-step outflow experiments, Virginia Agric. Exp. Station Bull 85-3.

Kottelowski, F.E., 1958, Geologic history of the Rio Grande near El Paso IN Franklin and Hueco Mountains: West Texas Geol. Soc. Guidebook, 46-54.

Larson, M.B., and D.B. Stephens, 1985, A comparison of methods to characterize unsaturated hydraulic properties of mill tailings, Proc. Seventh Symposium on Management of Uranium Mill Tailings, Low Level Waste and Hazardous Waste, Fort Collins, CO.

Machette, M.N., 1978, Geologic map of the San Acacia quadrangle, Socorro County, New Mexico, USGS Geological Quadrangle Map, GQ-1415, scale 1:24,000.

Mattson, E.D., 1988, Field Simulation of Waste Impoundment Seepage, Unpublished Masters Independent Study, New Mexico Tech, Socorro, NM, in press.

McWhorter, D.B., and J.D. Nelson, 1979, Unsaturated flow beneath tailings impoundments, J. Geotech. Eng. Div. Am. Soc. Civil Eng., 105(GT11): 1317-1334.

McWhorter, D.B., and D.K. Sunada, 1977, Ground-Water Hydrology and Hydraulics, Water Resources Publications, Littleton, CO, 290 p.

Miller, D.E., 1963, Lateral flow as a source of error in moisture retention studies, Soil Sci. Soc. Am. Proc., 27: 716-717.

Miller, D.E., and W.H. Gardner, 1962, Water infiltration into stratified soil, Soil Sci. Soc. Am. Proc., 26: 115-118.

Moore, I.D., and J.D. Eigel, 1981, Infiltration into two-layered soil profiles, Am. Soc. Agric. Eng. Trans., 24(6): 1496-1503.

Mualem, Y., 1984, Soil anisotropy of unsaturated soils, Soil Sci. Soc. Am. J., 48: 505-509.

Mualem, Y., 1976, A new model for predicting the hydraulic conductivity of unsaturated porous media, Water Resour. Res., 12(3): 513-522.

Palmquist, W.N., and A.I. Johnson, 1962, Vadose flow in layered and non-layered materials, USGS Prof. Paper, 450-C: C142-C143.

Parlange, J.Y., 1972, Theory of water movement in soils: 8. One-dimensional infiltration with constant flux at the surface, Soil Sci., 114(1): 1-4.

Parsons, A.M., 1988, 9I-KB Laboratory Analysis Notebooks: Volumes I,II,III, New Mexico Tech, Socorro, NM.

Ragan, D.M., 1973, Structural Geology, An Introduction to Geometrical Techniques, 2nd Ed., John Wiley and Sons, New York, p. 19.

Routson, R.C., W.H. Price, D.J. Brown, and K.R. Fecht, 1979, High level waste leakage from the 241-T-106 tank at Hanford, Rockwell Intl. Rpt. RHO-ST-14, Richland, WA, 37 p.

Siegel, J., and D.B. Stephens, 1980, Numerical simulation of seepage beneath lined ponds, Proc. Symposium on Uranium Mill Tailings Management, Ft. Collins, CO, Nov. 24-25, 219-232.

Stephens, D.B., and S. Heerman, 1988, Dependence of anisotropy on saturation in a stratified sand, Water Resour. Res., 24(5): 770-778.

Stephens, D.B., 1988, personal communication on 3/10/88, Assc. Professor, Hydrology Program, New Mexico Tech, Socorro, NM.

Stephens, D.B., and K. Rehfeldt, 1985, Evaluation of closed-form analytical models to calculate hydraulic conductivity in a fine sand, Soil Sci. Soc. Am. Proc., 49: 12-19.

Stephens, D.B., L.W. Gelhar, and S. Young, 1984, Field Experiment to evaluate dispersion in unsaturated media (abs), EOS, Am. Geop. Union, 65(16): 206.

U.S.Geological Survey, 1979, Socorro Quadrangle, New Mexico-Socorro Co., 7.5 Minute Series, Scale 1:24,000.

Vachaud, G.A., P. de Silans, P. Balabanis, and M. Vauclin, 1985, Temporal stability of spatially variable measured soil water probability density function, Soil Sci. Soc. Am. J., 49(4): 822-828.

van Genuchten, M.Th., 1980, A closed-from equation for predicting the hydraulic conductivity of unsaturated soil, Soil Sci. Soc. Am. J., 44: 892-898.

Vomocil, J.A., 1965, Porosity IN Methods of Soil Analysis, Part 1, 1st Edition, ed. C.A. Black, Am. Soc. of Agron. Inc., WI, 299-314.

Wang, J.S.Y., and T.N. Narasimhan, 1988, Correlation of characteristic parameters of unsaturated materials IN International Conference and Workshop on the Validation of Flow and Transport Models for the Unsaturated Zone, Inn of the Mountain Gods, Ruidoso, NM, May 22-25.

Ward, A., L.G. Wells, and R.E. Phillips, 1983, Characterizing unsaturated hydraulic conductivity of western Kentucky surface mine spoils and soils, Soil Sci. Soc. Am. J., 47: 847-854.

Warrick, A.W., 1974, Time-dependent linearized infiltration. 1. Point Sources, Soil Sci. Soc. Am. J., 38: 383-386.

Warrick, A.W., J.W. Biggar, and D.R. Nielson, 1971, Simultaneous solute and water transfer for unsaturated soil, Water Resour. Res., 7: 1216-1225.

Warrick, A.W., and D.R. Nielson, 1980, Spatial variability of soil physical properties in the field IN Applications of Soil Physics, ed. D. Hillel, Academic Press, New York, 319-344.

Wright, H.E., 1946, Tertiary and Quaternary geology of the lower Rio Puerco area, New Mexico, Geol. Soc. Am. Bull., 57: 383-456.

Yeh, J.T.-C., and L.W. Gelhar, 1983, Unsaturated zone in heterogeneous soils IN The Role of the Unsaturated Zone in Radioactive and Hazardous Waste Disposal, ed. J.W. Mercer and others, Ann Arbor Science, Ann Arbor, MI.

Zaslavsky, D., 1964, Theory of unsaturated flow into a nonuniform soil profile, Soil Sci., 97(6): 400-410.